

**Elucidation of the Cellular and Molecular Events Associated with Bovine Uterine  
Development and Disruptive effects of Tamoxifen**

by

Meghan Lynn Peters Davolt

A thesis submitted to the Graduate Faculty of  
Auburn University  
in partial fulfillment of the  
requirements for the Degree of  
Master of Science

Auburn, Alabama  
August 1, 2015

Keywords: uterine development, multispectral imaging, digital image processing, cow,  
progesterone receptor, estrogen receptor

Copyright 2015 by Meghan Lynn Peters Davolt

Approved by

Robyn R. Wilborn, Chair, Associate Professor of Clinical Sciences  
Frank F. Bartol, Co-Chair, Alumni Professor of Anatomy, Physiology, and Pharmacology  
M. Daniel Givens, Alumni Professor of Pathobiology

## **Abstract**

Development of the bovine uterus begins prenatally and is completed postnatally with the formation of endometrial glands. Adenogenesis, uterine gland formation, is steroid hormone-sensitive and is required for proper uterine development and function. Uterine glands produce histotroph, secretions which are essential for conceptus development, recognition and maintenance of pregnancy, and placental and fetal growth. Exposure of developing uterine tissues to steroids, including estrogens and progestins, can alter patterns of uterine development such that uterine endometrial structure and function are compromised in the adult. Disruption of estrogen receptor alpha (ESR1) and progesterone receptor (PR) -mediated organizational events in ruminants can induce such effects. However, little is known about mechanisms regulating bovine endometrial development.

Studies described here were designed to define cellular and molecular events associated with postnatal bovine endometrial histogenesis and cytodifferentiation. Multilabel immunohistochemistry (IHC), multispectral imaging (MSI) and digital image processing (DIP) were used to detect, capture and extract qualitative and quantitative data for multiple targeted signals associated with specific endometrial proteins, including transcription factors, and endometrial cell proliferation simultaneously in single uterine tissue sections.

In study one, for purposes of technical validation, uterine samples from a single Holstein heifer obtained on postnatal day (PND) 40, treated with 5'bromo-2-

deoxyuridine (BrdU) five days prior to euthanasia, were used to establish and validate imaging protocols. Single- and multilabel IHC protocols were evaluated in uterine cross-sections. Images were captured using MSI, and wavelength-specific data were extracted and analyzed using DIP tools. Resulting image data were compared qualitatively and quantitatively for transcription factors including ESR1 and PR forms-A, -B (PR), as well as for markers of cell proliferation Ki67 and BrdU. On PND 40 both endometrial luminal epithelium (LE) and glandular epithelium (GE) were observed. Nascent glands extended into the underlying stroma (ST) as coiled tubular structures. Both transcription factors (ESR1 and PR) and cell proliferation markers (Ki67 and BrdU) were identified in LE and GE and, to a lesser extent, in ST. Transcription factor (ESR1 and PR) expression was higher ( $P < 0.01$ ) in epithelium than in stroma. Results obtained using protocols for multilabel and single-label IHC were comparable, particularly for targeted transcription factors. Thus, multilabel IHC, combined with MSI and DIP technologies, can be employed to identify, capture and analyze multiple targets of interest simultaneously in single bovine uterine tissue sections.

In study two, bovine uterine histoarchitecture as well as temporospatial patterns of PR expression and cell proliferation (marked by BrdU labeling) were evaluated in Holstein heifers from birth (PND 0) to PND 42 using validated IHC, MSI and DIP technologies. Uteri were obtained from four heifers each day on PND 0, 7, 14, 21, 28, 35, and 42. Nascent GE was present on PND 0 as defined histologically by shallow epithelial invaginations or buds penetrating underlying ST. From PND 7 to 14 epithelial buds elongated into tubular structures and developed into coiled structures by PND 21,

extending through the ST and approaching the stromal-myometrial junction by PND 42. Overall, endometrial PR expression was greater ( $P < 0.0001$ ) in the epithelial than in the stromal compartment. Epithelial PR expression (LE and GE) was greatest on PND 0, waned thereafter to PND 21 and increased again to PND 42 ( $P < 0.0001$ ). Patterns of endometrial cell proliferation, reflected by BrdU labeling, differed with age between epithelial and stromal compartments (Cell x Age,  $P < 0.0001$ ). At birth, BrdU labeling index (LI = percent labeled cells) was higher in stroma than in epithelium. This relationship was also observed on PND 14 and 42. Otherwise, BrdU LI was higher in epithelium than in stroma. Epithelial BrdU LI increased from PND 0 to PND 14 and decreased gradually thereafter to PND 42. Results reflect histoarchitectural changes similar to those observed for postnatal endometrial histogenesis in other ungulate species.

Study three examined the role of ER-mediated events in the developing prepubertal bovine uterus and endometrial adenogenesis as evaluated on PND 120. Here, tamoxifen (TAM), a mixed-function ER agonist/antagonist and selective estrogen receptor modulator (SERM), was used as a tool to alter normal ER signaling patterns in prepubertal uterine tissues. Holstein heifers were given either TAM (3 ml/kg BW/day, i.m.) or vehicle alone ( $N = 7-8$  heifers/group) from PND 28 to PND 120 when tissues were collected.

Compared to controls on PND 120, effects of TAM on endometrial histoarchitecture were varied and pronounced. Where control tissues contained regularly dispersed, coiled tubular endometrial glands throughout intercaruncular stroma and extending to the endometrial-myometrial interface. Uterine gland genesis in TAM-treated heifers was generally inhibited and irregular. While endometrial thickness was

not affected, gland penetration depth was reduced ( $P < 0.05$ ) in TAM-treated heifers. Moreover, effects were endometrial zone (superficial vs deep) – specific. Generally, uterine gland cross-sectional area was greater ( $P < 0.05$ ) in TAM than in control groups. Cyst-like uterine glands were seen regularly in TAM-treated animals. Effects of TAM on endometrial cell proliferation as reflected by BrdU LI were pronounced in deep endometrium. Generally, BrdU LI was reduced ( $P < 0.05$ ) in TAM-treated heifers, particularly in deep stromal tissues. Treatment with TAM altered patterns of ESR1 expression without marked effects on PR. On PND 120, expression of both ESR1 and PR was most pronounced in epithelium. Similar to patterns observed for BrdU LI, TAM treatment generally reduced ( $P < 0.05$ ) ESR1 signal and LI in the endometrium.

Overall, results: (1) provide evidence for the utility of IHC, in combination with MSI and DIP, for evaluation of bovine endometrial development; (2) indicate that, as observed in other ungulate species, endometrial histogenesis occurs, to a large extent, postnatally in the cow; (3) support the idea that neonatal bovine uterine tissues are likely to be progestin-sensitive from birth; and (4) show that organizational events associated with postnatal endometrial development involve ER-mediated signaling events. The latter observation is based on results obtained from evaluation of the effects of TAM on uterine development.

## **Acknowledgments**

I would first like to thank my mentors Dr. Robyn Wilborn and Dr. Frank “Skip” Bartol for your combined insight, encouragement, and assurance there was a computer science student within me. I have enjoyed the challenge of learning new techniques and exploring different technologies to better understand cellular and molecular events associated with development of the female reproductive tract. This unique collaboration between clinical science and biomedical research provided opportunities to explore and develop my interests in developmental biology and veterinary medicine; I thank you both for that.

In appreciation for the invaluable lab skills and love of teaching, I thank Ms. Anne Wiley. I could not imagine a better supporter to have in my corner nor a better expert to learn from.

To Dr. Steven Ellis, I extend my most sincere gratitude. As a teacher, a mentor and a collaborator I thank you, and will continue to push the boundaries of programming, pipelines, and image processing.

To my lab counterparts (at Auburn U., Virginia Tech, Clemson U. and Rutgers U.), Dori Miller, Alejandro Silva, Hannah Tucker, Kathleen Ferio, Hank Bignel and Meredith Camp, thank you for assistance and friendship all the way through. Special thanks to Kimberly Roberts and Katie Brennan for your eagerness to learn and get involved.

Last but not least, I would like to thank my friends and family, Alabama has been quite an adventure. To my Oma, Gloria Peters, your continued love and encouragement means the world to me. To my parents Connie and Steven Davolt as well as my brother Michael, thank you for your encouragement and support throughout my entire endeavor, no matter how long it took.

## Table of Contents

<b>Abstract.....</b>	<b>ii</b>
<b>Acknowledgments.....</b>	<b>v</b>
<b>List of Tables.....</b>	<b>x</b>
<b>List of Figures .....</b>	<b>xi</b>
<b>List of Abbreviations .....</b>	<b>xiii</b>
<b>Introduction.....</b>	<b>17</b>
<b>Chapter 1: Review of the Literature .....</b>	<b>19</b>
<i>1.1 The Cow .....</i>	<i>19</i>
<i>1.2 The Female Reproductive Tract.....</i>	<i>20</i>
1.2.1 Basic Anatomy and Histology .....	20
<i>1.3 Uterine Development .....</i>	<i>22</i>
1.3.1 Prenatal organogenesis .....	23
1.3.2 Postnatal morphogenesis .....	25
<i>1.4 Mechanisms regulating postnatal uterine morphogenesis .....</i>	<i>28</i>
1.4.1 Epithelial-Stromal interactions .....	28
1.4.2 Hox and Wnt genes.....	30
1.4.3 Growth factors .....	32
1.4.4 Ovarian regulation of postnatal morphogenesis.....	34
<i>1.5 Uterine function .....</i>	<i>40</i>
1.5.1 Maternal recognition of pregnancy.....	40
1.5.2 Uterine Capacity .....	41
<i>1.6 Developmental Programing and the Lactocrine hypothesis .....</i>	<i>42</i>
<i>1.7 Perinatal Disruption of Uterine Development .....</i>	<i>44</i>
1.7.1 Reproductive effects of early steroid exposure in ruminants.....	45

1.7.2 Selective Estrogen Receptor Modulators (SERMs) .....	49
<b>1.8.1 Principles .....</b>	<b>53</b>
<b>1.8.2 Immunolabeling Methods and Applications .....</b>	<b>55</b>
<b>1.8.3 Limitations .....</b>	<b>58</b>
<b>1.9 Multispectral Imaging.....</b>	<b>58</b>
<b>1.9.1 Principles .....</b>	<b>59</b>
<b>1.9.2 Applications and Benefits.....</b>	<b>61</b>
<b>1.9.3 Limitations .....</b>	<b>63</b>
<b>1.10 Digital Image Processing.....</b>	<b>64</b>
<b>1.11 Summary and Implications .....</b>	<b>65</b>
<b>Chapter 2: Establishment and Validation of Multispectral Imaging Technology to the Studies of Bovine Reproductive Tract Development .....</b>	<b>67</b>
2.1 Abstract.....	67
2.2 Introduction .....	69
2.3 Materials and Methods .....	70
2.4 Results.....	74
2.5 Discussion.....	77
2.6 Aknowledgements.....	78
<b>Chapter 3: Coordinated Changes in Postnatal Bovine Uterine Histoarchitechture and Progesterone Receptor Expression .....</b>	<b>95</b>
3.1 Abstract.....	95
3.2 Introduction .....	96
3.3 Materials and Methods .....	97
3.4 Results.....	101
3.5 Discussion.....	103
3.6 Aknowledgements: .....	106
<b>Chapter 4: Tamoxifen Affects Pre-pubertal Bovine Endometrial Development.....</b>	<b>118</b>
4.1 Abstract.....	118
4.2 Introduction .....	120
4.3 Materials and Methods .....	121

<i>4.4 Results.....</i>	124
<i>4.5 Discussion.....</i>	127
<i>4.6 Acknowledgements.....</i>	131
<b>Appendix A.....</b>	Error! Bookmark not defined.
<i>Immunohistochemistry .....</i>	<b>Error! Bookmark not defined.</b>
<b>Appendix B.....</b>	Error! Bookmark not defined.
<i>Multispectral Imaging of Uterine Tissues.....</i>	<b>Error! Bookmark not defined.</b>
<i>Spectral Library Set Up .....</i>	<b>Error! Bookmark not defined.</b>
<i>Spectral Unmixing IM3 Files to Component Data Files.....</i>	<b>Error! Bookmark not defined.</b>
<b>Appendix C.....</b>	Error! Bookmark not defined.
<i>Digital Image Analysis: CellProfiler<sup>TM</sup> Analyses of Fluorescent Signals.....</i>	<b>Error! Bookmark not defined.</b>
Technology Establishment and Validation .....	<b>Error! Bookmark not defined.</b>
Bovine Endometrial Development .....	<b>Error! Bookmark not defined.</b>
<i>Digital Image Analysis: CellProfiler<sup>TM</sup> Analyst.....</i>	<b>Error! Bookmark not defined.</b>
TAM: rule filter included with additional cell compartments identified manually	<b>Error! Bookmark not defined.</b>
<b>Appendix D.....</b>	Error! Bookmark not defined.
<i>Aperio® ePathology Solutions.....</i>	<b>Error! Bookmark not defined.</b>
<b>Appendix E.....</b>	Error! Bookmark not defined.
<i>VisioPharm® image analysis and stereology software .....</i>	<b>Error! Bookmark not defined.</b>

## **List of Tables**

<b>Table 1.</b> <i>Primary Antibodies</i> .....	81
<b>Table 2.</b> <i>Secondary Antibodies</i> .....	82
<b>Table 3.</b> <i>Filter Cube Sets</i> .....	84
<b>Table 4.</b> <i>Primary Antibodies</i> .....	109
<b>Table 5.</b> <i>Primary Antibodies</i> .....	133

## List of Figures

<b>Figure 1.</b> Experimental Design .....	80
<b>Figure 2.</b> Primary Antibody Validation.....	83
<b>Figure 3.</b> MSI Process.....	85
<b>Figure 4.</b> CellProfiler <sup>TM</sup> Image Analysis Process. ....	86
<b>Figure 5.</b> Comparison of PR (-A, -B forms) and ESR1 Immunostaining Procedures in Developing Bovine Endometrium.....	Error! Bookmark not defined.
<b>Figure 6.</b> Comparison of BrdU and Ki67 Immunostaining Procedures in Bovine Endometrium. ....	88
<b>Figure 7.</b> Compartment-specific Expression of ESR1, PR (-A, -B forms), and Co-localization of ESR1+PR. ....	89
<b>Figure 8.</b> Compartment-specific Localization of BrdU, Ki67, and Co-localization of BrdU+Ki67. ....	90
<b>Figure 9.</b> Cross-validation Accuracy Plot for ESR1-, PR- and ESR1+PR-positive cells. ....	91
<b>Figure 10.</b> Effects of IHC-labeling Procedure on Cross-validation Accuracy Plot for ESR1- and PR-positive Cells.....	92
<b>Figure 11.</b> Effects of IHC-labeling Procedure on Cross-validation Accuracy Plot for BrdU- and Ki67-positive Cells. ....	93
<b>Figure 12.</b> Cross-validation Accuracy Plot for ESR1+PR- and BrdU+Ki67-positive Cells. ....	94
<b>Figure 13.</b> Experimental Design .....	108
<b>Figure 14.</b> MSI Process.....	110
<b>Figure 15.</b> CellProfiler <sup>TM</sup> Image Analysis Process .....	111
<b>Figure 16.</b> Effects of Postnatal Age on Endometrial Histoarchitecture.....	112

<b>Figure 17.</b> Effects of Postnatal Age on Endometrial Labeling Patterns of PR (-A, -B forms) and BrdU.....	113
<b>Figure 18.</b> Effects of Postnatal Age on Endometrial Labeling Indices of PR protein and BrdU	115
<b>Figure 19.</b> Effects of Postnatal Age on Endometrial Expression of PR protein.....	116
<b>Figure 20.</b> Cross-validation Accuracy Plots for PR-, BrdU- and PR+BrdU-positive Cells.....	117
<b>Figure 21.</b> Experimental Design .....	132
<b>Figure 22.</b> MSI Process.....	134
<b>Figure 23.</b> Use of VisioPharm Software to Quantify Endometrial Glandularity in Bovine Endometrium.....	135
<b>Figure 24.</b> Endometrial Histoarchitecture affected by TAM .....	136
<b>Figure 25.</b> TAM affects Gland Morphogenesis .....	137
<b>Figure 26.</b> Compartment-specific Localization of BrdU.....	138
<b>Figure 27.</b> TAM affects Compartment-specific Expression of PR protein (-A, -B forms).....	139
<b>Figure 28.</b> TAM affects Compartment-specific Expression of ESR1 .....	140

## **List of Abbreviations**

ESR1: estrogen receptor alpha

PR: progesterone receptor

IHC: immunohistochemistry

MSI: multispectral imaging

DIP: digital image processing

PND: postnatal day

BrdU: 5'bromo-2'deoxyuridine

LE: luminal epithelium

GE: glandular epithelium

ST: stroma

TAM: tamoxifen

SERM: selective estrogen receptor modulator

ml: milliliters

kg: kilograms

BW: body weight

i.m.: intramuscular

ER: estrogen receptor

FRT: female reproductive tract

MD: Müllerian Ducts

C: caruncles

IC: intercaruncular

WD: Wolffian Duct

UGS: urogenital sinus

SRY: sex determining region Y

Sox9: sex determining region Y box 9

FGF: fibroblast growth factor

AMH or MIS: anti-müllerian hormone

GD: gestation day

ECM: extracellular matrix

GAG: glycosaminoglycans

AB: Alcian Blue

MMP: matrix metalloproteinases

TIMP: tissue inhibitors of metalloproteinases

*Hox*: homeobox genes

FZD: frizzled receptors

SFRP: secreted FZD-related protein

HGF: hepatocyte growth factor

IGF: insulin-like growth factor

MAPK: mitogen-activated protein kinase

NOR: norgestomet

EB: estradiol- $17\beta$  benzoate

OVX: ovariectomy

E2:  $17\beta$ -estradiol

ERE: estrogen response elements

αERKO: ESR1-knockout

EV: estradiol-17 $\beta$  valerate

P4: progesterone

CL: corpus luteum

PGF2a: prostaglandin F2 alpha

MRP: maternal recognition of pregnancy

IFNT: interferon tau

OXTTR: oxytocin receptor

UGKO: uterine gland knock out

EDC: endocrine disrupting compounds

mg: milligrams

TBA: trenbolone

PE: P4 and EB combination

SRM: selective receptor modulator

SEARM: selective estrogen activity receptor modulator

SARM: selective androgen receptor modulator

SPRM: selective progesterone receptor modulator

SPPARM: selective peroxisome proliferator activated receptor modulator

ICI: Imperial Clinical Industries

GAPDH: glyceraldehyde 3-phosphate dehydrogenase

Ig: immunoglobulin

OCT: optimum cutting temperature

FFPE: formaldehyde-fixed paraffin-embedded

HIER: heat-induced epitope retrieval

ABC: avidin-biotin complex

PAP: peroxidase anti-peroxidase

LSAP: labeled-streptavidin peroxidase

LCTF: liquid crystal tunable filter

Qdots: Quantum dots

UV: ultraviolet

CP: CellProfiler<sup>TM</sup>

CPA: CellProfiler<sup>TM</sup> Analyst

i.v.: intravenous

PCNA: proliferating cell nuclear antigen

s.q.: subcutaneous

## **Introduction**

Mammalian reproductive success requires proper organizational and functional development of the female reproductive tract, including the uterus. Unlike other organs, uterine wall development is completed postnatally with the formation of endometrial glands through the process of adenogenesis. Glandular secretions, or histotroph, are composed of a variety of factors including cytokines, enzymes, hormones, transport proteins and growth factors that are important for pregnancy recognition, conceptus survival, development and maintenance of pregnancy throughout gestation. Disruption of uterine development during organizationally critical periods, often during early neonatal life, can have lasting effects on tissue form and function, and result in infertility in the adult.

In the cow, as in other ruminants, the adult uterine mucosa or endometrium is populated by raised, aglandular caruncles surrounded by intercaruncular endometrium containing glands. Bovine endometrial development begins prior to birth, with evidence of glandular buds by about 250 days of gestation in the bovine fetus [1]. As in other species, proliferation of nascent glandular epithelium is primarily a postnatal process, occurring between birth and three months of age [1, 2]. Exposure of the developing endometrium to steroids, such as progestins and estrogens, can alter patterns of uterine development with lasting effects on structure and function of adult uterine tissues as seen in cows [2-4], sheep [5, 6], and pigs [7-9]. Disruption of ESR1- and PR-mediated uterine

organizational events in ruminants can induce such effects [3, 4, 10-12]. However, cellular and molecular mechanisms of bovine endometrial development remain unclear.

Work presented here was conducted to elucidate cellular and molecular events associated with bovine endometrial development. Previous work in the sheep [5, 6, 13-15] provided an important reference with regard to both patterns of endometrial development and consequences of steroid hormone- disruption of endometrial adenogenesis in ruminants.

Experiments presented here were designed to: i) establish and validate methods of multiple antigen detection and extraction of quantitative data from bovine uterine tissues using MSI and DIP technologies; ii) describe changes in histoarchitecture, temporospatial patterns of PR expression and cell proliferation in neonatal bovine uteri at regular intervals from birth (postnatal day = PND 0) to PND 42; and, using TAM, a SERM administered from PND 28 – PND 120, iii) determine if postnatal estrogen receptor (ER)-mediated events are involved in bovine endometrial morphogenesis as reflected by changes in uterine histoarchitecture, cell proliferation, and cell compartment-specific expression of ESR1 and PR on PND 120.

## **Chapter 1: Review of the Literature**

### **1.1 The Cow**

The dairy cow, *Bos taurus*, is the primary source of dairy products for human consumption [16]. A ruminant, the cow has a bicornuate uterus, single uterine body, single cervix, and moderately developed uterine horns [17]. The cow is a polyestrous, non-seasonal breeder that can have multiple estrous cycles throughout the year regardless of day length [17]. Holstein heifers reach puberty at 8-9 months of age. Puberty is synonymous with first behavioral estrus (heat), first ovulation, and the ability to conceive. Estrous cycle length, the time between one estrus and the next, is 21 days in the cow [17]. Estrus, the period of sexual receptivity, can range from 1-2 days in length, and standing heat can occur anytime within a 24 hour window during that period [17]. The cow is typically monotocous, carrying a single calf for a gestation period of approximately nine months (280 days). Like all mammals, pregnancy in primiparous dairy cattle establishes conditions necessary for mammogenesis and lactogenesis. Reproductive efficiency in dairy cattle, defined as the capacity to become pregnant shortly after giving birth and to produce live calves, is essential for dairy productivity, defined by lifetime milk production.

With tremendous selection pressure placed on milk production, the dairy industry has reported an associated and severe decline in cow fertility [16]. Consequently, it is important to define genetic, developmental, physiological and environmental factors

affecting fertility in the adult cow [16]. Included here is a need to understand mechanisms regulating development of the female reproductive tract. Relatively little is known about endocrine, cellular and molecular mechanisms that regulate pre- and postnatal development of the uterine endometrium in the cow. Much of what we do know is a result of studies using other animal models, including the sheep [5, 6, 10, 13-15, 18-23] and pig [7, 8, 24-28]. This review will focus on summarizing endocrine, cellular, and molecular mechanisms that regulate uterine development, and will discuss sources and consequences of uterine developmental disruption with emphasis placed on ungulate species.

## **1.2 The Female Reproductive Tract**

The female reproductive tract (FRT) is derived from the embryonic Müllerian ducts (MDs), which give rise to the infundibula, oviducts, uterus, cervix and anterior vagina [17]. While genetic potential for uterine competence and reproductive success is established at conception, factors affecting adult uterine competence remain poorly defined for cattle. However, studies from ungulate species, including the cow [3, 4, 29-31] and sheep [5, 11, 32, 33], as well as rodents [34-40], indicate that success of the program of organizational events supporting endometrial histogenesis and cytodifferentiation during perinatal life can determine adult uterine capacity to function [2].

### **1.2.1 Basic Anatomy and Histology**

The FRT is a tubular organ consisting of distinct cellular layers surrounding a central lumen. By cross-section the wall of the FRT consists of cells that compose tunics, or layers, including the mucosa or endometrium, muscularis or myometrium, and outer

serosa or perimetrium [17]. The tunica mucosa surrounds the lumen and consists of epithelium and connective tissue composing the lamina propria which is encased in layers of muscle making up the tunica muscularis. Finally, the outer most layer, tunica serosa, consists of a simple squamous epithelial covering. Antero-posterior patterning during development results in histologically distinct FRT zones defined as the oviducts (uterine tubes), uterus, cervix and anterior vagina.

The oviducts, or uterine tubes, are physically separated from the ovaries by the ovarian bursa and function to accept, transport, and protect ovulated oocytes as well as to support sperm transport and capacitation in preparation for fertilization [17]. Divided into three zones, the infundibulum is most proximal to the ovary, followed posteriorly by the ampulla and isthmus, which communicates with the uterine lumen at the utero-tubal junction. The lumen of the oviduct is surrounded predominantly by simple, pseudostratified columnar epithelium with varying populations of ciliated and secretory cells [41]. Loose connective tissue of the lamina propria support the overlying epithelium. Characteristic of the ampulla, near the ovarian end, layers of the tunica mucosa fold into the lumen creating a labyrinth of primary and secondary folds [41]. In most mammals, fertilization occurs in the ampulla [17]. Moving distally, toward the utero-tubal junction and isthmus, primary and secondary folds wane and populations of ciliated cells decrease [41]. This area provides an environment for sperm to congregate prior to fertilization. Sheets of inner circular and outer longitudinal smooth muscle fibers compose the tunica muscularis. The presence of the tunica muscularis develops in the cranio-caudal direction, approaching the uterus such that, in the fimbriae of the infundibulum, very few muscle fibers are present. In the ampulla, distinct inner circular

and outer longitudinal layers are apparent, and in the isthmus the muscular layer is thicker than the mucosal layer [41]. Finally, simple squamous epithelium of the tunica serosa covers the combined cellular tunics and the tubular organ is encased in a layer of mesothelium.

The uterus is both functionally and histologically unique to the FRT [17]. The endometrium consists of simple or pseudostratified columnar epithelium lining the lumen with supporting layers of dense and loose connective tissue, stratum compactum and spongiosum, respectively [41]. Elastic fibers are present in loose connective tissue near the layers of smooth muscle that defines the myometrium. In ruminants, areas of endometrium develop into caruncles (C), raised aglandular structures with rich vascularity that serve as specialized attachment sites for fetal placental cotyledons [1, 13]. Uterine glands are found in intercaruncular (IC) areas, and extend from the lumen to the inner circular layer of the myometrium [1, 13]. These simple or branched tubular glands are lined by simple columnar epithelium with sub-populations of ciliated cells [41]. Complex networks of uterine glands present in the adult endometrium are absent or rudimentary in the neonate. Inner circular and outer longitudinal smooth muscle layers surround the endometrium. The FRT is supported in the pelvis by the broad ligament. Extensions of the broad ligament support the ovaries (mesovarium), oviducts (mesosalpinx), and uterus (mesometrium).

### **1.3 Uterine Development**

During development of the FRT the uterus undergoes both organizational and functional transformation that begins prior to birth and is completed during neonatal life in most mammals [2, 12, 42]. Fetal development and fusion of the paramesonephric

ducts provide early uterine form, whereas neonatal influences affect tissue-specific transformation of the uterine wall. Normal development of the uterus requires appropriate genetic, molecular, cellular, and morphological events in order to insure that tissues of the uterine wall are organized to function properly in support of reproduction [42].

### **1.3.1 Prenatal organogenesis**

Prenatal uterine development requires appropriate formation, patterning and fusion of the paramesonephric ducts (MDs). During vertebrate embryogenesis, the FRT develops as part of the urogenital system, which is derived from the intermediate mesoderm during gastrulation [42-44]. The urogenital system includes paired structures of the renal and reproductive systems that includes the kidneys, gonads and connecting tubular structures [45, 46]. The male reproductive system is derived from the mesonephric, or Wolffian ducts (WDs), while most structures of the FRT, including the uterus, are derived from the MDs. Primordial germ cells, from the intermediate mesoderm, migrate to the genital ridge and promote differentiation of the coelomic epithelium. Formation of the MDs begins as small invaginations from localized, thickened coelomic epithelium, or Müllerian plaques [47]. These form tubular structures that extend caudally, most likely guided by paracrine signaling from the WDs [48]. Paired tubules of the developing MDs then fuse with the dorsal wall of the urogenital sinus (UGS), which is derived from endoderm. Fusion of the MDs and WDs with the UGS forms the sinovaginal bulbs, or projections of epithelial cords into the UGS. Prior to sexual differentiation the embryo is considered phenotypically bipotential, consisting of both male and female primitive reproductive structures regardless of genetic sex [42].

Sex determination and ultimate progression or regression of WDs or MDs in males and females is dependent on genetic sex in mammals as determined at fertilization [49-51]. Aside from genetic abnormalities, XY chromosomes result in testis development in the male, while XX chromosome pairings result in female internal and external reproductive tissue development [52]. Mammalian female gametes do not have a Y chromosome. Thus, the genotype of sperm (X-bearing vs Y-bearing) determines the genetic sex (XX vs XY) of the embryo. In normal males the Y chromosome contains a sex determining region Y (SRY). Expression of the SRY gene leads to production of the SRY protein which, in turn, acts to up-regulate expression of transcription factors sex determining region Y box 9 (Sox9) and fibroblast growth factor-9 (FGF-9) [42]. These factors increase the expression of anti-müllerian hormone (AMH or MIS) to precipitate regression of the MDs and development of the male reproductive tract [53]. Before sexual differentiation, activity of Sox9 and FGF-9 are equivalent to other factors involved in the progression of female phenotype, such as members of the Wnt family of signaling molecules [42]. In the absence of the Y chromosome bipotential gonads become ovaries and the absence of SRY protein activity fails to stimulate male promoting transcription factors. Thus, the scales are tilted to allow progression of the female phenotype. The WDs regress and MDs persist, forming the primitive structures of the FRT (oviducts, uterus, cervix and anterior vagina). The remaining structures, posterior vagina and vestibule, are derived from both MDs and UGS tissues. Tissue-specific changes follow with development and differentiation of uterine and vaginal epithelium, and organization of appropriate histoarchitecture.

Morphology of the FRT varies greatly between species [44, 54, 55]. In particular, the gross structure of the uterus is dependent on the degree to which the MDs fuse during development [54]. In rodents and marsupials, limited fusion of the MDs results in a duplex type uterus consisting of two separate uterine bodies, two cervices and a common vaginal opening to the exterior. In opossums, the anterior vagina is split into two separate canals that lead to complementary cervical bodies [17]. Anatomy of the female opossum is further complemented by the pronged or forked male penis. Other animals, like the rabbit, have a less complex vaginal morphology with a common vaginal opening and complementary single internal vaginal canal [17]. The bicornuate uterus, common to domestic animals, has characteristic uterine horns connected to a small common uterine body that communicates with a single cervix. Uterine horn length is highly developed in the sow, bitch and queen, moderately developed in ruminants (cow, ewe and goats), and poorly developed in the mare as a result of partial MD fusion. In primates, including humans, nearly complete MD fusion results in formation of a simplex uterus that consists of a single uterine body lacking uterine horns. Morphological variations within species (often aberrant) do occur [54].

### **1.3.2 Postnatal morphogenesis**

At birth in most mammals the uterus consists of a simple layer of epithelium supported by undifferentiated mesenchymal tissue. In rodents, domestic animals and humans, development of tissue-specific histoarchitecture is completed postnatally [2, 8, 55, 56]. Radial patterning establishes specific uterine cell compartments that include the endometrium, myometrium and perimetrium. Morphogenetic events including; 1) organization and stratification of stroma; 2) differentiation and growth of smooth muscle

layers; and 3) coordinated development of endometrial glands occur sequentially during neonatal life. Timing of these events is species-specific and dependent on the stage of uterine development at birth [34, 44, 46, 57-61].

### ***1.3.2.1 Gland genesis and function***

Endometrial glands are tubular structures lined by simple columnar epithelium, and develop through processes of bud formation, tubulogenesis, coiling and branching morphogenesis within the uterine endometrium [56]. At birth, the uterine wall is devoid of uterine glands in most mammals including rodents [62], sheep [13] and pigs [8]. Initially, uterine luminal epithelia form small invaginations or buds that penetrate the underlying stroma slightly. During neonatal life, endometrial glands grow out from the lumen toward the myometrium. In ruminants, uterine glands continue to coil and branch within the IC area. Ultimately, the uterus reaches functional maturity and is therefore able to receive and respond to signals from the developing conceptus and support pregnancy [2, 56]. The timing of gland development or adenogenesis, and completion of uterine wall development varies among species. However, phases of development are similar [56].

Information pertaining to the timing of uterine gland development in the cow is limited to a single publication by Atkinson et al. [1]. As early as gestation day (GD) 201, small areas of invaginated epithelium within the IC area were observed. By GD 265, further development of glandular buds into underlying, superficial ST was observed. At birth, prominent raised aglandular caruncles were present on the luminal surface. Uterine development by PND 90 was pronounced, as indicated by the presence of coiled,

branched uterine glands extending from the luminal surface to the stromal-myometrial interface [1].

Endometrial glands are essential for uterine function. Glandular epithelia produce factors including cytokines, growth factors, transport proteins, hormones and enzymes [56], all of which are components of histotroph. Studies in rodents and ruminants, showed that endometrial glands and their products are required to establish and maintain pregnancy [32, 38].

From an historical perspective, the idea that the uterus supplies nourishment to the growing fetus reaches back to Hippocrates (460-370BC). It was suggested by students of Hippocrates that the fetus physically nursed the maternal cotyledons, or ‘uterine paps’ *in utero* [63]. The thought was that, as the fetus grew and uterine volume increased, pressure from the uterus stimulated the mammary glands to produce milk. At this time, a direct anatomical connection from the breasts to the uterus was envisioned (incorrectly). Aristotle (384-322BC) negated this theory based on anatomical evidence. However, the concept persisted through drawings from Leonardo DaVinci (1452-1519AD) and Andreas Vesalius (1514-1564AD). It was William Harvey (1578-1657AD) who recognized that fetal nourishment came from the uterus and not from the mammary glands. Walter Needham (1631-1691AD) also argued Hippocrates’ theory, claiming that ‘uterine milk’ could be squeezed from the endometrium and that this was unique to the uterus and did not originate elsewhere [64]. In the late nineteenth century the terms embryotroph and then histotroph and hemotroph were coined to describe substances needed for conceptus survival and fetal development, either from secretions of the uterine endometrium (histotroph) or directly from blood (hemotroph).

Research in rodents [38], sheep [11, 33] and cows [3] illustrates how the absence of uterine glands in adults, a condition induced through inhibition or disruption of gland development during early neonatal life, can have lasting effects on uterine function and compromise reproductive performance.

#### **1.4 Mechanisms regulating postnatal endometrial morphogenesis**

Postnatal endometrial morphogenesis requires continuous integration of endocrine, cellular and molecular events in order to transform layers of undifferentiated cells into an organized, functionally competent uterine wall capable of supporting and maintaining pregnancy [56]. Shortly after parturition, the neonatal uterine wall undergoes morphological changes that require specific communication between cell compartments and components of the extracellular matrix (ECM). Differentiation and growth of GE requires specific changes in tissue microenvironment such that molecular factors driving and conditions supportive of these processes are in place. Specific cellular and molecular mechanisms driving endometrial adenogenesis are beginning to be defined. Nevertheless, much still remains to be understood [2, 19, 32, 42, 56, 65]. Aspects of such organizationally important mechanisms are described below.

##### **1.4.1 Epithelial-Stromal interactions**

Postnatal morphological changes in the uterus that lead to the histologic maturation of the uterine wall are dependent on cell-cell and cell-ECM interactions [2, 66]. Evidence from elegant tissue recombination studies in mice showed that epithelial differentiation and development is dictated by underlying mesenchyme, while epithelium functions to regulate organizational events of underlying stroma and differentiation of the myometrium [43, 67, 68]. The uterus differs from the vagina structurally and

functionally. Notably, uterine epithelium consists of simple cuboidal/columnar cells, while vaginal epithelium is of the stratified squamous type. When perinatal murine uterine and vaginal epithelia were recombined with either vaginal or uterine stroma (homotypic and heterotypic combinations), epithelial grafts assumed the cell phenotype associated with the paired stromal tissue, regardless of the origin of the epithelium [67, 68]. Mechanisms associated with epithelial-stromal communication and stromal-driven differentiation of the epithelium remain unclear, however recent work [39, 42, 69, 70] indicates changes in the microenvironment may be mediated by intrinsic growth factor systems as well as mediators of ECM composition.

Initial development of GE from LE and appearance of glandular buds within the uterine stroma may occur as a result of epithelial differentiation and site-specific alterations in the basal lamina, as indicated by data for sheep and pigs [11, 19, 28]. While cell proliferation, indicated by IHC analyses, is apparent in GE at the tips of growing glands, cytodifferentiation and mesenchymal remodeling events are likely dependent on tissue microenvironment [19, 28]. Alterations in the basal lamina may direct local patterns of gene expression affecting cellular responsiveness and migration, thereby facilitating initial penetration of nascent GE into the underlying stroma and continued growth of uterine glands [13, 71].

The ECM provides a supporting matrix and conduit for signals regulating epithelial-stromal interactions governing endometrial development, including uterine gland formation. Components of the ECM such as glycosaminoglycans (GAGs) can have direct and indirect effects on cell behavior and function by mediating interactions of growth factors or other morphogens with target cells [2, 8]. Clear patterns of GAG

distribution in relation to uterine gland growth and development were reported for the pig and sheep [8, 10, 28, 71]. Using alcian blue (AB) histochemistry, increased GAG accumulation at the epithelial-stromal interface and subadjacent stroma was illustrated in areas of structural stability such as around the necks of growing glands. In contrast, decreased AB staining was observed in areas of high morphogenic activity at the tips of growing glands, suggesting high GAG turnover [10, 28]. Modulators of ECM composition, such as matrix metalloproteinases (MMPs) and their inhibitors (TIMPs), can affect the nature of physical and chemical interactions at the epithelial-stromal interface. In fact, accelerated glandular development was reported in uteri of mice lacking the gene for TIMP-1 [72]. Many MMPs and TIMPs were identified in the developing murine uterus [73], and expression of both MMP-2 and -9 was documented in murine and porcine models of endometrial gland development [74]. Together, data indicate that alterations in the tissue microenvironment play a key role in coordination and control of cell behaviors affecting differentiation, proliferation and migration.

#### **1.4.2 Hox and Wnt genes**

Postnatal uterine morphogenesis requires appropriate regional expression of members of the homeobox (*Hox*) and *Wnt* gene families [2, 42, 65]. Information regarding temporospatial expression patterns for *Hox* and *Wnt* genes during FRT development comes primarily from murine studies [60, 66, 68, 75], with few studies in ungulate species [14, 76]. Mammalian *Hox* genes and their products regulate tissue identity and organization along the anterior-posterior body axis. Prenatally, *Hoxa-9*, -10, -11, -13 and *Msx1* gene expression is uniform along the murine MD. However, by postnatal day 10 in the mouse *Hox* gene expression is regionally limited such that *Hoxa-9*

is expressed in the oviducts, *Hox-10*, *-11* and *Msx1* are expressed in the uterus, *Hoxa-11* and *-13* are expressed in the cervix, and *Hoxa-13* is expressed in the anterior vagina [77].

Members of the *Wnt* signaling pathway act through cell surface frizzled (FZD) receptors to control a variety of developmental processes including embryonic patterning, cell proliferation and differentiation [78-80]. From a recent study in sheep, the expression of six *Wnt* genes (*Wnt-2*, *-2B*, *-4*, *-5a*, *-7a* and *-11*) and two *Wnt* receptors (FZD-2, -6 and co-receptor LRP6) was localized in the neonatal ovine uterus via *in situ* hybridization [76]. Results showed cell compartment-specific expression patterns whereby *Wnt-7a* and *-11* were localized in LE, *Wnt-5a* in GE, and *Wnt-2b* in stroma. Receptors FZD-2, and -6, and co-receptor LRP-6 were identified in all uterine cells [76]. Further, secreted FZD-related proteins (SFRPs), which are *Wnt* antagonists, were abundant in aglandular caruncular tissue on PND 7-56, and absent in IC areas at birth. From elegant gene mutation studies in mice, disruption of *Hoxa-10* and *Hoxa-11* genes (normally expressed in the uterine stroma) resulted in partial or complete anteriorization of the uterus to an oviductal morphology [81, 82]. Similarly, disruption of *Wnt-5a* and *Wnt-7a* signaling resulted in altered patterns of MD growth (and eventual lethality) [60, 83]. However, postnatal effects of *Wnt-5a* and *Wnt-7a* disruption included development of a uterus devoid of glands [60]. Together, results from rodent and ungulate studies indicate that there is cell compartment-specific expression of *Wnt* genes and their receptors, and that these expression patterns support potential paracrine and autocrine signaling mechanisms involving epithelial and stromal cell compartments. In addition, results of engineered ‘loss-of-function’ studies [60, 81-83] showed that regional

expression of and signaling by *Hox* and *Wnt* gene products are required for MD segmentation and postnatal uterine morphogenesis, including endometrial adenogenesis.

#### **1.4.3 Growth factors**

Epithelial-stromal communication involves autocrine and paracrine-acting growth factor signaling systems to support epithelial differentiation, proliferation, and branching morphogenesis in epitheliomesenchymal organs including the uterus [2, 84]. Interactions between growth factors and their receptors can involve components of the ECM, which can have effects on ligand presentation and alterations in cell surface receptor complexes, as alluded to above [42].

Stromal-derived growth factors such as fibroblast growth factor (FGF), hepatocyte growth factor (HGF), and insulin-like growth factor (IGF) were implicated in endometrial gland development and morphogenesis [11, 20-23]. All three growth factor systems activate mitogen-activating protein kinase (MAPK) pathways [85, 86]. Literature ([20, 22, 23]) highlights FGF-7, FGF-10, HGF, IGF-1 and IGF-2 as key regulators and mediators of epithelial proliferation, differentiation and glandular morphogenesis in the endometrium. Expressed primarily in the mesenchyme, FGF-7 is a paracrine-acting growth factor that stimulates epithelial proliferation and differentiation, while FGF-10, originally discovered in developing lung mesenchyme, elicits bud formation and has a potential role in branching morphogenesis [87]. These activities are mediated by epithelial FGF receptor, FGFR2iib, a single-pass transmembrane receptor with tyrosine kinase activity [88]. HGF also functions in a paracrine-acting manner to mediate epithelial-stromal interactions that regulate mitogenic, motogenic and morphogenic activities of LE and GE via the epithelial receptor Met [85, 89]. Like FGF

and HGF, IGF-1 and IGF-2 support uterine growth, cell proliferation and differentiation through paracrine mechanisms mediated through IGF receptor, IGF-1R [20, 90].

Reports on the developing ovine uterus indicated that stromal FGF-7, FGF-10, HGF, IGF-1, IGF-2 and their epithelial receptors (FGFR2iib, Met and IGF-1R respectively) are present in the endometrium [11, 20, 21]. *FGF-7* was present in all uterine cells from PND 1-56, whereas *FGF-10* and *HGF* mRNA was relatively low from PND 1-21 and increased from PND 21-56 [20]. This period is recognized to be associated with coiling and branching activity of nascent uterine glands in the ovine endometrium [13]. Epithelial receptors *FGFR2iib* and Met (or gene product *c-met*) were localized to the LE and GE in both ovine [20, 21] and murine [89] models of uterine development. Results from *in situ* hybridization studies showed that *IGF-1* expression was localized in the IC area of the ovine endometrium proximal to nascent and growing glands, whereas *IGF-2* was expressed in both areas (IC and C) of the endometrial stroma, with particular abundance surrounding growing glands on PND 21-42 [20]. Consistently, *IGF-1R* was localized to LE and GE, and was also found in surrounding stroma at the tips of growing glands.

Exposure of developing ovine endometrium to norgestomet (NOR; synthetic progestin) from birth (PND 0), or estradiol-17 $\beta$  benzoate (EB) after PND 14, disrupted patterns of postnatal uterine development and growth factor expression [11, 14]. Exposure to EB reduced the number of uterine glands and disrupted patterns of *FGF-7*, *FGF-10*, *HGF* and *IGF-1* and -2 mRNA expression in comparison to controls without affecting cell proliferation [14]. In contrast, exposure to NOR from birth resulted in complete gland ablation and selective disruption of the expression of growth factor

ligands and their receptors [21]. Interestingly, exposure to NOR reduced *FGFR2iiib* mRNA expression in uterine epithelium (LE and GE), without affecting stromal ligands FGF-7 and FGF-10 [21]. While *c-Met* expression was similar to that of control groups, *HGF* expression was reduced in IC stroma of NOR-treated animals [21]. As a result of studies in sheep [14, 20-23], and other species [85, 87, 89] it is clear that HGF, FGF and IGF signaling systems play a role in regulation of epithelial cell behaviors, and function to support the communication network of epithelial-mesenchymal interactions involved in endometrial gland development.

#### **1.4.4 Ovarian regulation of postnatal uterine development**

Prenatal FRT development is not thought to be affected by fetal ovarian activity. Thus, processes associated with prenatal FRT development are ovary-independent. This concept was demonstrated by Alfred Jost through classic experimental work with rabbits [91]. Postnatal organizational events in the uterus, including endometrial adenogenesis, are also unaffected by ovarian factors for a period of time during neonatal life, as illustrated by rodent [92], pig [24] and sheep [71] studies. Patterns of uterine growth in neonatal gilts ovariectomized at birth, reflected by uterine wet weight and endometrial thickness, did not differ from those observed for ovary-intact controls until after PND 60 [24]. However, effects of ovariectomy (OVX) at birth were pronounced between PND 60 and 120, when growth of the uterus was marked in ovary-intact gilts [24]. Interestingly, patterns of endometrial adenogenesis between birth and PND 120 were unaffected by OVX at birth. Similarly, in neonatal ovine uteri, where significant gland genesis occurs between birth and PND 56, bilateral OVX at birth did not affect endometrial histogenesis as evaluated on PND 14 [71]. However, effects of OVX on

PND 7 reduced uterine weight and the number of coiled and branched uterine glands as evaluated on PND 56 [6, 15, 18]. These results, illustrate a time- and process-specific influence of ovarian factors on endometrial gland development, particularly coiling and branching morphogenesis, as opposed to initiation of gland development in the sheep. Contributing factors were presumed to originate from growing antral follicles present on the ovaries at PND14, with candidate factors suggested to include members of the activin-follistatin system, as well as IGF1 and IGF2 [18]. Thus, while some organizational events associated with uterine growth and development may not require ovarian support shortly after birth, other aspects of postnatal uterine growth and development, particularly more advanced processes of adenogenesis, depend on the ovaries and their products.

#### ***1.4.4.1 Estrogen and Estrogen Receptor***

Estrogens are involved in regulation of cell growth and differentiation, and have effects on many target tissues, including the reproductive tract. In the female, the steroid hormone estradiol-17 $\beta$  (E2) is produced primarily by the ovaries and is synthesized from testosterone through actions of the aromatase enzyme. Lack of E2 production due to inhibition of aromatase did not affect uterine histogenesis or processes associated with endometrial adenogenesis in sheep [6] or rodents [93]. Circulating estrogens are present in the neonatal sheep at birth and change during phases of endometrial development. Serum E2 levels are relatively high on PND 1, increase from PND 14 to PND 28, and fall to PND 48 and PND 56 [19]. As mentioned above, daily subcutaneous injections of aromatase inhibitor (CGS-20267) given to neonatal sheep from birth to PND 55 reduced levels of circulating E2, particularly between PND 5 and PND 13, when glandular

epithelium transitions from bud invaginations to elongated tubular structures [6].

However, treatment of ewes with CGS-20267 did not affect uterine development or endometrial adenogenesis [6] as seen on PND 14 and PND 56.

Estrogen-induced effects on epithelial proliferation, differentiation and gland development are mediated through ligand binding with ERs. Like other steroid hormone receptors, ERs are ligand-activated transcription factors. Genomic effects of E2 are mediated through nuclear ESR1 and ESR2 (formerly ER $\alpha$  and ER $\beta$ ). Non-genomic effects of E2 are regulated through a recently described membrane-associated ER [94]. Classic ligand-binding of E2 causes receptor dimerization, translocation to promotor regions within the cell nucleus, and interaction with estrogen response elements (EREs) upstream from target genes [95]. Although nuclear ESR1 and ESR2 are widely distributed among target tissues, ESR1 is predominantly present in the uterus [95-97]. The absence of ESR1 in the murine ESR1-knockout ( $\alpha$ ERKO) model, disrupts normal mitotic stimulation of epithelial, stromal and muscle cells resulting in infertile mice with hypoplastic uteri where all cell types are present in reduced numbers [40]. In the absence of ESR2, female  $\beta$ ERKO mice are fertile and show no deficiencies in FRT development [98]. Like E2, presence or expression of ESR1 is not a requirement for uterine organogenesis, but is required for normal growth and histogenesis of the uterine wall.

At birth, murine uterine epithelium is devoid of ESR1 and displays restricted expression in underlying stroma [99]. Similarly, ESR1 expression in IC epithelium is undetectable in the ovine uterus at birth, but is present in stroma [19]. Mouse studies showed that paracrine stimulation from the stroma induces epithelial proliferation and ESR1 expression in nascent glandular buds [100, 101]. In the pig, expression of ESR1 is

a unique marker of nascent glandular epithelial differentiation [24, 25]. In sheep, ESR1 is evident in LE by PND 1 and becomes relatively more abundant by PND 7, particularly in growing glands [19]. Evidence from mouse [102], pig [24, 25] and sheep [6, 19] studies indicates that ESR1 expression in GE increases as glands emerge and develop.

ER-mediated events associated with neonatal uterine wall development vary between species. In the pig, daily injections of estradiol-17 $\beta$  valerate (EV) from birth advanced uterine development as reflected by endometrial adenogenesis and increased proliferation of epithelium in early postnatal life [24, 25]. By contrast, treatment of ewe lambs with EV from birth reduced uterine weight and endometrial thickness, decreased *ESR1* expression in all uterine cells, and inhibited gland development on PND 14 and 56 [6, 19]. Interestingly, treatment of sheep with the ER-antagonist EM-800 from birth had little effect on uterine growth and development, and resulted in only marginal reduction of gland numbers in neonatal ovine uteri on PND 56 [6, 19]. The ER-antagonist ICI 182,780 was antiuterotrophic when administered to gilts from birth [24, 25]. These effects were pronounced on PND 14. Treatment of gilts with ICI 182,780 during the proliferative phase of endometrial development (PND 7-14) reduced endometrial thickness and epithelial proliferation [24, 25]. Similarly, when the window of treatment with ER-antagonist was adjusted to encompass the normal period of gland development in mice (PND 10-14), uterine growth and development were inhibited, as reflected by decreased uterine weight and reduction in ESR1 in all uterine cells [103]. Collectively, observations indicate that ER-mediated regulation of endometrial development in the neonate is broadly conserved, although roles of such mechanisms in this process are species-specific.

#### **1.4.4.2 Progestins and Progesterone Receptor**

Progesterone (P4), the ‘hormone of pregnancy’, is the primary steroid hormone product of corpora lutea (CLs), which develop from cells of the postovulatory ovarian follicle and serve as a principle source of P4 throughout gestation. Progesterone is also made in abundance by placental tissues in ruminants [104-106] and other mammals [17, 107]. This is true for the cow [105] and, particularly, for the ewe [106]. By consequence, circulating levels of progesterone remain high in maternal circulation throughout gestation, defining an important aspect of the endocrine environment in which conceptus and fetal development take place.

Progestins inhibit many actions of estrogens, particularly on uterine epithelium and gland development. Uterine tissues obtained at hemihysterectomy on PND 14 from ewe lambs treated with NOR from birth displayed endometrial histology characteristic of PND 0, as reflected by the absence of uterine glands [10]. After removal of the progestin ‘brake’ to gland genesis on PND 13, evaluation of uterine tissues from the same animals following hysterectomy on PND 26 revealed evidence of nascent GE in IC endometrium and increased proliferation of nascent GE as marked by  $^3\text{H}$ -thymidine incorporation [10]. Thus, in the neonatal ewe, progestin is antiadenogenic and withdrawal of the progestin block to adenogenesis is permissive to this process [10]. Similarly, daily treatment with P4 beginning on PND 2 inhibited uterine gland development and decreased LE proliferation in mice on PND 20 [108]. Treatment with P4 inhibited E2-induced epithelial proliferation in murine tissue recombinations, illustrating specific signaling through stromal PR on epithelial ESR1 [109]. Treatment with NOR after PND 14 in sheep, inhibited endometrial adenogenesis with reduced *ESR1* mRNA and protein

expression in uterine epithelium on PND 28 [21]. Although cell proliferation was unaffected on PND 28 in NOR-treated sheep, negative effects of NOR on epithelial differentiation and adenogenesis were clear [21].

Progestin activity is mediated through the progesterone receptor (PR; a long B form and truncated N-terminal A form), the product of a single gene [110]. A member of the steroid hormone/nuclear receptor superfamily, signal transduction through PR requires ligand-binding for receptor dimerization and transcriptional effects to occur. Unlike ERs, PR is present in the endometrium at birth in mice [65], dogs [111], and sheep [19]. Female mice lacking PR showed defects in all reproductive tissues, including uterine hyperplasia and the inability to ovulate [112]. Inhibitory effects of P4 on E2-induced epithelial DNA synthesis occur through stromal [109] and epithelial PR [113]. Estrogen down-regulates PR expression in uterine epithelium, primarily through effects on the stroma [36]. In 2011, Li et al. reported a unique P4-induced, basic helix-loop-helix transcription factor, Hand2, as a critical regulator of epithelial-stromal communication in the uterus [114]. Hand2, which is uniquely present in the stroma, inhibits production of many FGFs that act as paracrine mediators of estrogen inducible mitogenic activity. A murine conditional Hand2 knockout, *Hand2<sup>d/d</sup>*, was created to eliminate Hand2 expression in PR-positive cells of the adult uterus. In mice lacking Hand2, uterine stromal FGF production was uninhibited, resulting in continued stimulation of uterine epithelial proliferation, ER-signaling pathways, and subsequent failure of embryo implantation [114]. Although incomplete, reports in the sheep [19, 21], cow [2] and mouse [101] provide evidence of potential for cell-compartment specific PR- and ESR1-signaling during critical periods of postnatal development in the uterus.

## **1.5 Uterine function**

Normal uterine development is essential for reproductive success in the adult. The bovine uterus is responsible for production of prostaglandin F2-alpha (PGF2 $\alpha$ ), the luteolytic signal, transport and maturation of spermatozoa, recognizing and receiving developing embryos, providing an embryotrophic environment for their development and survival, and providing the contractile force necessary for delivery of the fetus and placenta at parturition [17, 115]. These functions are supported by the uterine endometrium and myometrium. Here, aspects of uterine endometrial function associated with establishment and maintenance of pregnancy are discussed.

### **1.5.1 Maternal recognition of pregnancy**

Establishment of pregnancy requires active dialogue between a competent conceptus and receptive maternal endometrium. In cattle, nearly all embryonic loss occurs between days 8 and 16, prior to maternal recognition of pregnancy (MRP) on day 16 [116]. In ungulates, MRP is the process by which the developing conceptus communicates its presence, via the maternal endometrium, in order to inhibit luteolysis and insure an ovarian source of P4 from the CL. This is necessary to insure maintenance of an embryotrophic uterine environment [117]. Uterine receptivity, the window during which the endometrium is optimally receptive to biochemical signals from and physical interactions with the developing conceptus, are orchestrated molecularly and cellularly at the conceptus-endometrial interface [118].

Evidence of complex, temporospatial regulation of the maternal endometrial transcriptome associated with preparation for implantation, MRP and maintenance of pregnancy in the cow is now clear [119-121]. Up until day 16 post-estrus/mating,

endometrial gene expression profiles are similar between pregnant and cyclic cows, indicating that the uterus defaults to expect and prepare for impending pregnancy [121].

In the presence of a viable conceptus, interferon-tau (IFNT), produced by mononuclear cells of the trophectoderm, signals to the adult endometrium as necessary to prevent PGF $2\alpha$ -induced luteolysis. In ruminants, IFNT serves to establish and maintain pregnancy. In the adult endometrium, IFNT inhibits expression of both ESR1 and oxytocin receptors (OXTR) in the epithelium of the endometrial glands to prevent normal patterns of uterine PGF $2\alpha$  production [122]. Insuring an adequate source of P4 supports conceptus development and conceptus-derived IFNT production in cattle [123]. The capacity of maternal uterine endometrial tissues to recognize and integrate local conceptus and systemic endocrine signals determines the fate and course of pregnancy.

### **1.5.2 Uterine Capacity**

Establishment of pregnancy alone does not guarantee continued successful conceptus development and survival. Traditionally, uterine capacity is defined for litter-bearing species, such as the pig, as the ability of the uterus to support the maximal number of fetuses and carry those fetuses to term [124]. For monotocous species such as the cow, uterine capacity can be defined as the ability of the uterus to provide an optimal environment for conceptus and fetal development as reflected by production of healthy, viable offspring.

While factors affecting uterine capacity continue to be defined, it is clear that disruption of uterine development during neonatal life can compromise adult uterine function. In sheep, treatment with NOR for eight weeks from birth inhibited uterine gland development and produced adult uteri lacking endometrial glands, a condition

defined as the uterine gland knockout (UGKO) phenotype [2, 125]. To determine effects of gland ablation on uterine capacity, UGKO ewes were bred to intact rams [5]. In comparison to normal control ewes in which an 80% pregnancy rate was recorded, pregnancy was never detected in UGKO ewes. Whereas similar numbers of hatched blastocysts were present in both control and UGKO groups nine days after mating [5], conceptus development was retarded in UGKO ewes 14 days post-mating [33]. Results of UGKO studies established that uterine glands and, by inference, their secretions are necessary to support conceptus development and pregnancy [5, 11, 32].

In pigs, treatment with EV from birth advanced uterine histogenesis in the neonate [26, 126]. To evaluate effects of neonatal EV treatment on litter size, normal control and neonatally EV-exposed adult gilts were bred to intact boars and conceptus numbers were evaluated on pregnancy day 45 [126]. Neonatal treatment with EV reduced conceptus numbers as compared to control groups. Taken together, results from sheep and pig studies indicate that disruption of postnatal uterine development can have lasting effects on uterine capacity in adult ungulates.

## **1.6 Developmental Programming and the Lactocrine hypothesis**

Developmental programming was defined as “*the response of the developing organism to an insult during a specific critical time window that results in altered developmental trajectory of which phenotypic effects persist in the adult*” [127]. Potential challenges facing developing neonates can reflect effects of nutritional, environmental, and maternal factors. Regardless of the insult or organ system in question, fundamental principles of developmental programming include the ideas that: 1) critical windows must exist such that developing tissues are vulnerable; 2) programming has

permanent effects; 3) programming involves structural changes in important organs; 4) compensation by the fetus [or neonate] or efforts to rescue the phenotype following a challenge can cause consequences themselves; and 5) effects of programming may be passed on through generations [128].

Critical windows of uterine development exist such that an insult during a defined period of time has the potential to alter uterine developmental trajectory in the neonate, causing long-term effects in adult uterine tissues and compromised reproductive function or infertility. Neonatal exposure to progestins in sheep [2, 5] and mice [101] during critical windows of development inhibited formation of uterine glands, and produced a UGKO phenotype and infertility in adults [2, 101]. Similarly, disruption of uterine gland development in the neonatal pig by treatment with EV or ICI 182,780 affected the developmental program and trajectory of endometrial tissues [25] and compromised uterine capacity in neonatally EV-exposed adults [26, 126].

Epigenetics can play a critical role in developmental programming of the uterus. Epigenetic effects are often defined as conditions that affect patterns of gene expression without affecting nucleic acid sequence. Phenotypic changes induced by early exposure to developmentally disruptive conditions can have epigenetic origins. Canonical examples include changes in gene function through histone modifications or DNA methylation [129]. For example, aberrant activation or repression of ER [14] and PR [21] signaling during neonatal life in sheep results in reduced uterine expression of members of the FGF, HGF, and IGF systems and disruption of uterine gland development. Exposure of the developing endometrium to challenges during critical windows of

development can originate from natural sources as well, including environmental and maternal sources, such as milk.

Milk acts as a natural conduit through which bioactive factors are conveyed from mother to offspring during neonatal life [57]. Communication of bioactive factors from mother to offspring as a specific consequence of nursing was defined as lactocrine communication [130]. Based on data for the pig, the lactocrine hypothesis, as first proposed by Bartol et al. [57], states that bioactive factors in first milk or colostrum affect events associated with FRT and, particularly, uterine development during early neonatal life with potential for lasting effects in the adult. Consistently, imposition of a lactocrine-null state from birth by feeding neonatal gilts porcine milk replacer instead of colostrum altered events associated with FRT development, inhibiting both uterine and cervical histogenesis [131, 132]. The same conditions also dysregulated events associated with development of the neonatal testis [133]. Data indicating that lifetime fecundity, reflected by live litter size over four parities, was reduced in adult sows that consumed minimal amounts of colostrum on their day of birth (PND 0), provided evidence of long-term lactocrine effects on uterine programming [134]. Current research aims to identify specific components and factors in milk that can have such dramatic effects on development and function of the reproductive tract.

## **1.7 Perinatal Disruption of Uterine Development**

Exposure to natural hormones or xenobiotics during perinatal life can have lasting effects on reproductive efficiency in the adult [2, 59, 65]. Specific or ‘critical’ time periods exist during development when the FRT is susceptible to disruption [65, 135]. Work involving rodents showed that treatment with estrogens, progestins, or androgens

early in life can cause uterine lesions and suppress fertility in adulthood [38, 108, 136-138]. Natural or synthetic compounds that disrupt development by altering endocrine-related events are classified as endocrine disrupting compounds (EDCs) [2, 59]. EDCs mimic actions of other endocrine-acting compounds, and have the potential to alter epigenetic processes and developmental programming by affecting normal, hormone receptor-mediated signaling events [129, 139]. All tissues and organs that depend upon hormone/ligand-mediated receptor signaling to support a normal developmental program and trajectory, including the FRT, are potential targets for EDCs.

### **1.7.1 Reproductive effects of early steroid exposure in ruminants**

Exposure of the developing endometrium to steroids can alter patterns of uterine development with long-term effects on the structure and/or function of adult uterine tissues. The most dramatic example of this is the ovine UGKO phenotype mentioned previously. The ovine UGKO phenotype is defined by the absence of endometrial glands in the adult uterus [2, 21]. The UGKO model is a valuable tool with which to study effects of the endometrium and uterine glands on ovarian cyclicity, conceptus development and pregnancy [5].

In the United States, growth-promoting steroids and steroidal compounds are used routinely to enhance growth rates, feed efficiency and lean muscle mass in beef steers and heifers [2, 140]. Replacement beef heifers require proper management to insure successful productivity. It is advantageous to producers for heifers to reach puberty at a younger age [141]. Historically, female beef calves intended for use as breeding replacements were given implants containing the estrogenic compound zeranol alone (36mg; Ralgro®, Schering-Plough Animal Health Corp., Union, NJ), or a combination of

P4 (100mg) and EB (10mg) (Synovex-C®; Zoetis, Fort Dodge Animal Health, Fort Dodge, Iowa) [2-4, 30, 140, 142, 143]. Such practices, while often not recommended under labeled protocols, were implemented with the idea that ‘if normal growth is good, enhanced growth is better’, and that advantages in growth parameters would translate to advantages in aspects of reproductive performance, particularly where calving ease at parturition was concerned. Although such treatments often did improve feed efficiency and increase muscle mass, they often reduced reproductive efficiency in replacement heifers, as described below.

Effects of postnatal exposure to any bioactive compound on the developing FRT depend on dosage, duration of exposure, and age at first exposure. Several studies involving zeranol [29-31] showed adverse effects on pregnancy rate, age at onset of puberty, uterine growth and development, and follicular dynamics when beef heifers were treated before one month of age [2, 4]. This suggested a window of developmental vulnerability to estrogenic EDCs. Heifers implanted with zeranol at birth, PND 100, 200 (approximate age at weaning), and again at PND 300 had reduced pregnancy rates as compared to non-treated controls [30]. Over the course of the study nearly 73% of zeranol-implanted heifers had a recorded pregnancy over the entire breeding season. However, by the end of the trial 37.5% of those heifers had lost pregnancies, while all control heifers remained pregnant [30]. Interestingly, 12/19 heifers exposed to zeranol and not determined pregnant by the end of the trial were also acyclic at the beginning of breeding season, illustrating a delay in onset of puberty by 21-45 days. Likewise, treatment with a variety of estrogenic compounds including zeranol, trenbolone acetate (TBA), E2, or a combination of zeranol, TBA and E2 for one year, beginning at PND 84,

had variable but consistent negative effects on uterine wet weights [31]. Zeranol exposure from birth reduced pre- and postpubertal uterine diameter, as well as the size of the largest follicle without affecting the total number of follicles when compared to controls [30]. These data describe antiuterotrophic effects of postnatal exposure to estrogenic compounds, and suggest possible lesions to the hypothalamo-pituitary-gonadal axis as well. When heifers were treated with zeranol from PND 0-300, incidences of abortion were observed between 25-45 days of gestation, suggesting that treatment caused uterine lesions affecting conceptus-endometrial interactions [30].

Effects of neonatal exposure to both P4 and EB, as found in the growth-promoting implant Synovex-C®, were related to age at first hormone exposure [2-4]. To determine effects of P4 and EB (PE) exposure on the bovine uterus as delivered by the Synovex-C implant, crossbred beef heifers were assigned at birth to one of four treatment groups, defined by age at first PE exposure. Heifers ( $n = 5$  per group) were exposed to PE from approximately 200 days beginning on PND 0, PND 21, PND 45, the earliest age recommended for administration of Synovex-C to heifers intended for breeding replacement, or were left untreated to serve as controls. All heifers were allowed to reach puberty and uteri were obtained from adult heifers during diestrus. No differences were found in plasma P4 concentrations or body weights at slaughter between treated and untreated control heifers [3]. Regardless of treatment, neonatal exposure to PE reduced uterocervical wet weight by 35%, myometrial area by 23%, and endometrial area by 27% as compared to untreated controls [3]. Endometrial gland density was reduced by 65% in heifers treated with PE from birth, and 22% and 33% when PE exposure began at PND 21 or 45. Thus, the magnitude of this affect was related directly to age at first PE

exposure [3]. Compared to untreated controls, uterine fluid protein content was reduced in neonatally PE exposed animals [3]. Together, results indicated that neonatal PE exposure induced uterine hypoplasia, endometrial aplasia and altered uterine protein content in cyclic adult heifers exposed chronically to PE beginning on or before PND 45 [2, 3]. All effects observed in adult heifers were most pronounced when exposure began at birth. Results indicate that bovine uterine tissues are organizationally sensitive to PE within 45 days of birth [2, 3], defining a potentially critical window for developmental events that may be P and/or E sensitive.

Subsequently, a study was conducted to define a critical window of bovine endometrial development. Crossbred beef heifers were assigned to one of five groups at birth (groups 1-5; n = 5-6 heifers per group). Heifers in groups 1-3 received a single PE implant at birth, while heifers in groups 4-5 served as untreated controls. On PND 21, all heifers were laparotomized, uteri were measured, and PE implants were removed from calves in group 1 creating a group of adult tissues in which exposure to PE was limited to 21 days from birth. In addition, heifers in groups 2 and 5 were hemihysterectomized creating subgroups in which short-term PE exposure could be evaluated. Uteri were collected at slaughter during diestrus at 26 months of age [2]. Antiuterotrophic effects were evident by PND 21. Neonatal exposure to PE reduced uterine horn length as well as uterine volume [2]. Heifers in groups 2 and 5 displayed the extreme effects of neonatal PE exposure. Nascent endometrial glands were present in both PE-treated and untreated control tissues on PND 21. However, uterine glands in PE-treated animals were prematurely branched and apoptotic in appearance on PND 21 when compared to those observed in controls [2]. Chronic PE exposure reduced or eliminated uterine glands in

neonatally PE-exposed adults [2]. Still, all heifers displayed estrus cycles of normal duration, including calves in group 2 where endometrial glands were few or absent [2]. These data were interpreted to indicate that endometrial glandular epithelium may not be a requirement for normal cyclicity, and that normal cyclicity may not be a precise or an accurate indication of endometrial integrity. Exposure to PE exceeding 21 days is required to produce extreme negative effects on uterine weight and endometrial glandularity as reported in that study [2]. Results support the existence of a critical window of developmental sensitivity to steroidal compounds progesterone and estradiol benzoate between birth and PND 21.

Postnatal exposure to steroids and steroid-like compounds can have specific, extreme and lasting effects on the adult bovine endometrium that could alter the embryotrophic potential of the uterine environment [2, 144]. Effects of neonatal exposure as observed in the adult are more profound when initiated shortly after birth, when processes of endometrial cell proliferation and differentiation peak [65]. Studies focused in the cow [2-4, 30], sheep [10, 11, 145], pig [7, 25-27], and other animals [26, 57, 101, 126] showed that postnatal exposure to endocrine disrupting compounds can be used to create unique and extreme adult uterine phenotypes.

### **1.7.2 Selective Estrogen Receptor Modulators (SERMs)**

Selective estrogen receptor modulators (SERMs) interact with ERs to activate or repress gene transcription. Unlike estrogens and anti-estrogens, which illicit agonistic and antagonistic affects, respectively, SERM activity can be species-, tissue-, cell- and gene-specific [146]. Defined as non-steroidal, SERMs typically lack the canonical estrogen structure yet possess the tertiary structure required for ligand binding to the receptor. As

reviewed above, estrogens (and SERMs) signal through classic ligand binding to ERs located within target cell nuclei. Once activated, ERs undergo conformational changes and recruit other activated ERs to create dimers which, in turn, interact with EREs in promoter regions of responsive genes to regulate transcription [147]. The unique, mixed agonist-antagonist action of SERMs is complex. Currently three mechanisms are proposed to explain these actions, including: (1) varying concentrations of ER isoforms, ESR1 and ESR2; (2) changes in ER conformation following ligand binding; and (3) availability of co-regulatory proteins to effect the promotion or regression of target gene transcription [147]. The therapeutic potential and effectiveness of SERMs depends on their degree of estrogenic or antiestrogenic effects on target and non-target tissues [148]. Other categories of selective receptor modulators (SRMs) include selective estrogen activity receptor modulators (SEARM), selective androgen receptor modulators (SARM), selective progesterone receptor modulators (SPRM), and selective peroxisome proliferator activated receptor modulators (SPPARM) [149].

#### ***1.7.2.1 Tamoxifen***

Tamoxifen (TAM), a SERM, was discovered in the early 1970's by a group of reproductive endocrinologists at Imperial Clinical Industries (ICI) Pharmaceutical Division (now AstraZeneca) led by Dr. A. L. Walpole [150]. Originally intended for use as a post-coital contraceptive, antiestrogenic effects of TAM in rats did not translate to humans. In fact, treatment with TAM induced ovulation in subfertile women [151]. This observation was intriguing to the developing field of breast cancer research in that it suggested that TAM could have therapeutic value as an antiestrogen [151]. Preliminary studies were conducted in the mid-1970s testing TAM as a potential treatment for breast

cancer. Treatment of postmenopausal women with TAM produced effects similar to those obtained with other antiestrogens and, more importantly, showed improved side effect profiles in comparison to high-dose estrogens or androgens [152]. These results served as a springboard to development of TAM as a treatment for breast cancer. In following years, studies were conducted to test effects of long-term TAM treatment for this purpose in ER-positive and –negative, pre- and postmenopausal patients [153]. Results indicated that ER-negative patients were unaffected by TAM treatment for 1, 2 or 5 years, while ER-positive patients treated with TAM for 2 or 5 years exhibited cancer survival advantages [153]. However, when patients were treated with TAM for 10 years or more, results showed an increase in tumor reoccurrence as well as harmful side effects including endometrial cancers and prevalence of blood clots [154]. In 1992, a full placebo-controlled, randomized clinical trial began in the United States. Out of 13,800 high-risk pre- and postmenopausal patients, data indicated a 50% reduction of breast cancer in TAM-treated women [155]. In 1998, the FDA approved TAM for reduction of breast cancer risk in pre- and postmenopausal women [150].

Mixed agonist/antagonist activities of TAM can illicit tissue-, cell-, and gene-specific effects within species [146, 156, 157]. In women, TAM competitively antagonizes ERs in mammary tissue [158]. However, in the uterus TAM is estrogenic and linked to uterine hyperplasia and endometrial cancer [158-160]. Estrogenic effects of TAM can also be beneficial, as seen with osteoclast inhibition, and in treatment for osteoporosis [150]. TAM exerts estrogen-like effects in rat uteri, as shown by treatment with TAM at PND 1-5 or 10-14, a critical window of developmental sensitivity to steroids. Histological results illustrated delayed uterine gland development when mice

were exposed to TAM at PND 1-5 or 10-14. These effects persisted to PND 26 and 60, respectively [161]. Results in rats, similar to those observed in mice treated with E2 on PND 1-5, indicated delayed uterine gland genesis and infertility in adults [162]. Assuming antiestrogen effects of TAM, Robertson et al. [163] treated adult sheep with a single injection of TAM four weeks after OVX. Uteri and liver samples were obtained 24 hours later in order to evaluate whether TAM would affect E2-regulated changes in gene expression [146, 163]. Unexpectedly, treatment with TAM mimicked E2 effects in the uterus, where endometrial *ER*, *PR*, *glyceraldehyde 3-phosphate dehydrogenase* (GAPDH) and *c-fos* expression increased [146, 163]. Collectively, studies reinforce the importance of evaluating TAM effects in target species. Nevertheless, this SERM may be useful in studies designed to identify ER-mediated uterine organizational events.

## **1.8 Multilabel Immunohistochemistry**

Immunohistochemistry (IHC) is a fundamental tool used widely in the fields of diagnostic pathology and translational research to localize agents or antigens in tissue [164-167]. The principles of immunohistochemistry come from the fields of immunology, histology, and chemistry [168]. This technique was first described by Albert Coons in the early 1940's, who used a conjugated fluorescein anti-pneumococcal type III antibody to detect murine liver cells positive for the disease [169]. Visualization of desired antigens within tissue depends upon the interaction between antibodies and antigens *in situ*. Typical practice uses single IHC techniques to visualize one antibody-antigen interaction. However, this protocol limits the number of antigens or proteins that can be studied in a single cell or tissue section [165]. In order to study the relationship between two or more targets (i.e. proteins, gene products, cell signaling molecules etc.) a

method for visualization of multiple antibody-antigen interactions must be employed.

Following is an overview of the principles, labeling methods, applications and limitations of multilabel IHC.

### **1.8.1 Principles**

IHC is centered upon the use of antibodies to detect specific antigens within tissues [168]. Antibodies are produced through the immunization of different animal species against a purified antigen, which can result in monoclonal or polyclonal varieties [167]. Antibodies can be of different immunoglobulin (Ig) classes, although most of those used in IHC are IgGs. However, IgA and IgM classes are also used.

Immunoglobulins are composed of a pair of constant heavy chains and branched pairs of variable light chains bound by disulphide bonds in the shape of a “Y” [168]. Paratopes, located on the tip of the variable light chains, bind to selective epitopes of the desired antigens located in tissue [168, 170]. The antibody-antigen interaction is highly dependent on the specificity of the antibody, the receptivity of the tissue and the presence and epitope availability of the antigen itself. For these reasons, a special focus on preparation of the tissue is important.

Factors affecting the outcome of IHC protocols begin at the time of tissue collection. From tissue excision to microscopic visualization, the mechanical and chemical steps involved can affect the quality, processing, quantitation, and repeatability of IHC imaging and analysis dramatically [168, 171, 172]. Once tissue is excised, fixation is essential in order to preserve cell morphology and tissue architecture. Tissue should be immersed in the chosen fixative solution immediately after excision. Both aldehyde- and alcohol-based fixatives are common in histology and IHC protocols.

Aldehyde-based solutions such as neutral buffered formalin, formaldehyde and paraformaldehyde stabilize cell constituents [168, 173] by creating methylene cross-bridges between the formalin and available uncharged reactive amino groups (-NH or -NH<sub>2</sub>) [174, 175]. Alcohol-based fixatives (i.e. ethanol or methanol) are non-cross-linking solutions that rely on dehydration properties to break hydrogen bonds and turn the tertiary structure of proteins effectively ‘inside-out’ in order to preserve epitope binding sites [168, 174]. Other fixative solutions include mercurials (B-5 or Zenker’s), oxidizing agents (permanganate, dichromate) and picric acid (Bouin’s solution). After fixation, the tissue sample is embedded in a paraffin or resin material to mechanically stabilize the tissue so that sections (3-6µm) can be cut using a microtome.

For tissue samples or antigens that do not react well to aldehyde- or alcohol-based fixatives, methods of ‘snap-freezing’ tissues using liquid nitrogen are an option. Frozen tissues are embedded in optimum cutting temperature (OCT) medium, stored at -80C and sectioned using a cryostat. While this method may be well suited for some tissues, antigens and circumstances (e.g. biopsy), morphological visualization with frozen sections is typically poor in comparison to formalin-fixed paraffin-embedded (FFPE) tissues.

After sectioning, tissues are treated with a solution to remove the embedding material and subjected to optional antigen retrieval protocols. Antigen retrieval enhances antibody-antigen binding by methods of enzymatic or heat-induced procedures designed to reverse adverse effects of fixation and embedding [176]. Methods of heat-induced epitope retrieval (HIER) introduced by Shi et al. [177] were based on the chemical reactions between cross-linking fixatives (i.e. formaldehyde) and proteins in tissue.

HIER methods can partially reverse adverse effects of fixation with high temperature solutions [178]. Common theories concerning how HIER methods of antigen retrieval ‘reverse’ effects of fixation are discussed elsewhere [178-180]. Many theories focus on the reversal of fixative solutions through the breaking of methylene cross-bridges in tissues treated with formaldehyde-based solutions and rehydrating or ‘re-naturation’ of epitope conformation in tissues fixed with alcohol-based solutions [181]. After antigen retrieval, blocking agents are applied to tissues to prevent non-specific primary antibody binding. At this point, tissues are ready for immunolabeling procedures discussed below.

### **1.8.2 Immunolabeling Methods and Applications**

As a cornerstone in both pathology and basic research, IHC has the potential to serve many purposes. In diagnostics, IHC is often used to identify abnormal cells and/or specific markers indicative of cell behaviors associated with disease or dysfunction [165, 166]. Similarly, applications of IHC in basic research focus on evaluation of the distribution and localization of various cellular and/or molecular targets within a tissue section as they relate to effects of a treatment or other imposed condition (e.g. age or environment).

With proper tissue preparation, different visualization methods are available and dependent upon tissue type and desired sensitivity [166]. In general, the antibody-antigen interaction cannot be seen by light or fluorescent microscopy unless the reaction is labeled with a reporter molecule. Reporter molecules can be attached to primary, secondary or tertiary antibodies, common reporters include enzymes, metals, and a variety of fluorescent compounds [168].

Detection methods are classified as direct or indirect [168]. Direct detection (labeling) employs a ‘one-step’ application of a single antibody conjugated to a reporter molecule, such as an enzyme or fluorophore, to produce a color where the antibody and tissue antigen interact [182, 183]. This method is rarely used due to limits of sensitivity, and minimal if any signal amplification potential [166, 168]. Indirect labeling is more complicated and involves a layer of unlabeled primary antibodies reacting with tissue antigens followed by a layer of labeled secondary antibodies to react with the layer of unlabeled primary antibodies. This two-step method was first proposed by Coons et al. [169] in response to the need for greater assay sensitivity. Common enzyme (or chromagen) –based, indirect methods include use of the avidin-biotin complex (ABC), peroxidase anti-peroxidase (PAP) system, and labeled-streptavidin peroxidase (LSAP) methods [168]. Selecting a detection method should be based upon the tissue type and desired sensitivity of the assay.

Information gained from single-target IHC methods is limited to a single protein [165], whereas direct and indirect methods of multilabel IHC are designed to reveal multiple targets in the same tissue using chromagen- or fluorescent-based approaches [172]. In order to identify and label multiple unique tissue antigens, detection methods (direct or indirect) must be applied in sequence or simultaneously [165]. These methods are based on primary antibodies chosen for dissimilar animal species, Ig isotype and subclass, conjugate or concentration [164]. Complex and time-consuming, sequential methods of multilabel IHC allow for development of one antibody-antigen reaction to be completed before a second or third (or even fourth) antibody-antigen reaction is applied [165]. In contrast, simultaneous labeling methods call for all desired primary antibodies

to be applied as a cocktail in one step. After incubation, all matched secondary antibodies are also applied as a cocktail for detection of targeted primary antibodies *in situ*. Chromagen-based multilabeling protocols rely on visual contrast between appropriately labeled tissue antigens and their mixed color when co-localized *in situ* [165, 172].

In 1968, Paul Nakane demonstrated the use of multiple chromagen-based stains in rat pituitary tissue using peroxidase-labeled antibodies to detect thyrotropic hormone, luteinizing hormone, and GH [184]. While many chromagen color combinations are possible with IHC, “*only two combinations have been proven sufficient for direct visualization of the unique and mixed color labels*” [183], red-blue and turquoise-red. Compared to chromagen-based staining [182, 185], immunofluorescence offers a greater spectral range of fluorochrome reporters, the ability to conjugate fluorochromes directly to antibodies (primary or secondary), and higher optical and spatial resolution [186, 187]. For these reasons, fluorescent-based multilabeling is the preferred reporting system for the identification of unique and/or colocalized multiple targets within single tissue sections.

Multilabel IHC expands applications of traditional staining methods and conserves tissue reserves in the process. Visualizing two or more tissue antigens in a single tissue section can reveal information generally hidden with single-staining IHC of sequential tissue sections [186, 188]. This advantage of multilabel methods over traditional histological methods allows research scientists and pathologists alike to address questions regarding cell behavior and phenotype due to the unique or

colocalization of antigens [189]. These advantages are only heightened by the continued development of spectral imaging and compatible imaging techniques, discussed below.

### **1.8.3 Limitations**

Multilabel IHC rivals traditional methods of single staining. Success of either technique depends on direct visualization of the antibody-antigen reaction, which is made possible by the reporter. However, multilabel techniques require careful selection and compatibility of several primary and reporter-conjugated secondary antibodies. Key limitations of multilabeling include primary antibody availability, cross-reactivity of selected antibodies and antibody validation [190]. Commercial production of antibodies can make primary antibodies, along with detailed information about the selected antibody, host species, Ig isotype and subclass, species and tissue reactivity, and even selected images and relevant literature, attractive and readily available. However, all purchased antibodies should be validated ‘in house’ or in the lab to insure specificity and reactivity of the antibodies to targets of interest [167]. The field lacks a standardized method of antibody validation. Consequently, IHC protocols and, unfortunately, results, can vary between labs [191, 192]. In this light, there is a need to standardize IHC in research and diagnostics [191, 192]. Advances in imaging technologies such as spectral imaging and DIP will allow IHC to evolve from protocols for qualitative ‘special staining’ to validated, quantitative protocols applicable in research and diagnostics.

## **1.9 Multispectral Imaging**

Spectral imaging is an important part of microscopy and is particularly useful for visualization and measurement of multiple signals produced through IHC protocols. Multispectral imaging (MSI) integrates spectral and spatial methods of imaging to

acquire qualitative and quantitative image data across the electromagnetic spectrum [193]. Using MSI, information is collected such that a spectrum is provided at each pixel. Consequently, the resulting data set is more similar to a three-dimensional cube than to a two-dimensional picture. Image data can be visualized and unique signals can be measured separately or in combination, in the case where signals are colocalized within a single cell or cellular compartment. This is achieved by ‘spectrally unmixing’ or extracting and separating individual signals from one another through advanced image processing methods and associated algorithms [186, 193]. This section will focus on the principles, applications and limitations of MSI, and provide basic information for users of the Nuance FX MSI system and contributing elements (Perkin Elmer; Waltham, MA, USA).

### **1.9.1 Principles**

MSI is based upon the combination of spectroscopy and imaging to allow the collection of data at multiple wavelengths across the electromagnetic spectrum, in the visible to near-infrared range [193]. This section will focus on liquid crystal tunable filter (LCTF) -based MSI systems as found in the Nuance FX [194] used for experimentation described herein.

MSI involves the combination of imaging and spectroscopy in order to acquire spectrally resolved images at varying wavelengths across a spectrum of interest. While combining different methods to acquire information is straightforward in theory, MSI requires the pairing of a dispersive component with an imaging system [193]. For this reason, different scanning methods including: (1) wavelength-scan methods, (2) spatial-scan methods, (3) time-scan methods and (4) whole-spectrum methods are applicable.

Wavelength-scan methods, as used with variable filter LCTF-based systems, measure each image one wavelength at a time. The LCTF-based system transmits a narrow-band wavelength by applying a varying voltage on a polarizable liquid crystal mounted between two linear polarizers [193]. This type of variable filter is beneficial because it is small in size, low power, highly stable, and can be set to transmit light across a range of wavelengths from visible to near-infrared [187]. Regardless of scanning method, MSI generally measures emission (or transmission) from the sample. However, excitation spectra can also be measured [195-197].

Datasets generated using MSI are large and complex. Indeed, such datasets are too complex to be visualized and analyzed by the human eye and require further digital processing. The goal of image processing is to extract or separate various signals of interest in order to evaluate them independently [198]. This can be accomplished through use of algorithms based upon spectral information, imaging information or both. Two types of algorithm methods are discussed here, including linear decomposition and similarity mapping. More detailed and extensive reviews of this topic can be found elsewhere [193].

Linear decomposition or ‘spectral unmixing’ is based on the assumption that there is a proportional linear relationship between the measured signal color and the concentration of that color in the targeted sample [198]. The linear decomposition algorithm separates each signal and, by consequence, enables measurement of the concentration of each fluorochrome at each pixel when presented alone or colocalized with another signal. A similarity mapping algorithm is used in cases where the interaction between signal and tissue, as may occur in chromagen-based histological

stains, is complex and the different components contributing to the spectrum cannot be resolved [198]. By comparison, linear decomposition identifies each color component of the spectrum prior to image acquisition and applies identified ‘spectral profiles’ to the experimental sample. In contrast, a similarity mapping algorithm evaluates the extent of similarity of each spectrum identified within the sample to a reference spectrum [193, 198]. These algorithms are often embedded into software that accompanies imaging systems and, more often than not, require only the click of a button to engage.

Once image sets are captured and processed by spectral unmixing, wavelength-specific data can be visualized in a variety of ways. The most common way to view all stained or labeled targets simultaneously is in the composite image, in which each target is assigned a color. This provides both spatial and spectral information about the sample. However, the composite image does not allow quantitation of individual target signals. Data from component images are used to quantitate signals associated with individual targets. In these grey-scale images, signal intensity is directly proportional to the amount of each target.

### **1.9.2 Applications and Benefits**

MSI is a tool best used to capture, evaluate and quantify spatial and spectral information of single or multiple signals in IHC preparations. This technology can be applied to a variety of imaging approaches including fluorescent and bright field microscopy, live-cell, and non-invasive *in vivo* imaging [165, 186-189, 199]. Thus, image collection and analysis can be performed at the cell, tissue, and whole-animal level [188]. Unlike other imaging methods such as confocal microscopy, where multiple

images are collected at red, green, and blue wavelengths and combined in a z-stack, MSI collects spectral data from individual targets at specific wavelengths simultaneously.

Fluorescent imaging of FFPE tissue is often confounded by interfering autofluorescence, which can reduce detection of fluorochromes and be easily mistaken for target signal [165, 186]. Separating colors into individual channels depends on the quality of fluorochrome or reporter emission spectra. For this reason many researchers use Quantum Dots (Qdots; Invitrogen Life Technologies, Grand Island, NY, USA) and/or secondary antibodies of the AlexaFluor® series (Invitrogen Life Technologies, Grand Island, NY, USA). Important properties of these systems include narrow emission band widths, photo stability, large Stokes shifts, and a wide range of reagents covering the visible to near-infrared spectrum [165]. Autofluorescence is present across the entire visible and near-infrared spectrum. However, such confounding signal is typically brightest at ultraviolet (UV)- and blue wavelengths [186]. Collagens, red blood cells, and neuronal constituents present in the tissue will also contribute to high or bright autofluorescence [186, 189]. For wavelength-specific quantitation, signals must be captured and measured without the interference of background autofluorescence, elimination of autofluorescence is challenging [186, 187, 192].

MSI can eliminate concerns associated with autofluorescence by accounting for the spectral profile associated with autofluorescence itself. Spectral profiles, or wavelength-specific channels can be turned on or off at the discretion of the operator in order to highlight signals of interest while removing interfering signals [187, 189]. In fluorescent microscopy, setting the autofluorescence channel to black removes autofluorescence present in the image across the sampled spectrum digitally. This increases contrast or

signal-to-noise ratio and provides a better picture of the true signal, particularly in situations where the emission spectra of autofluorescence and targeted signal(s) overlap [187, 189]. Using these procedures, MSI allows visualization of multiple signals in separate cell compartments and/or colocalized signals without the interference of autofluorescence.

### **1.9.3 Limitations**

Despite the wide range of applications and imaging modalities available to support MSI, this technology is not without obstacles. Using MSI to identify one or many targets requires corresponding unique reporters and additional post-processing in order to extract desired data [189, 192]. When IHC is involved, collection of multiple target signals from a given tissue type requires specific, tissue-compatible primary and corresponding secondary antibodies [182, 200]. Depending on tissue type and species of origin there may be a small or vast array of primary antibodies available. These must be chosen carefully to ensure that selected reagents do not cross-react inappropriately with one another. This requires selection of antibodies from different host species and Ig subtypes [183]. For example, addressed properly, two primary antibodies generated against different murine antigens can be applied to the same tissue section and individual targets can be imaged simultaneously if the Ig subtypes of the primary antibodies differ. This allows for different, fluorescently labeled Ig subtype-specific secondary antibodies to be matched and paired appropriately [183, 185, 200].

Time is a factor for any MSI application. Depending on the type of detector and IHC protocol, image acquisition may take up to several minutes per field, limiting throughput and potentially causing photobleaching and/or phototoxicity in a sample

[192]. Post processing time is also significant. While some imaging systems are equipped with software to handle spectral unmixing of captured image data, many are not [186]. Consequently, raw data must be exported for further processing by specific DIP software.

## 1.10 Digital Image Processing

Advancements in biological imaging technology have pushed manual visualization and qualitative scoring to the breaking point. Users are turning to computer-assisted analysis in order to digest and evaluate the massive volume of information now available with automated digital imaging [201]. Digital image analysis or DIP software packages are used to evaluate biological phenotypes quantitatively and reliably [166, 201]. Advantages of DIP include objectivity and the speed at which large amounts of image-based data can be analyzed [201-204].

Imported MSI images are more than two-dimensional pictures. The detector or digital camera is affixed to a microscope, as explained above. When an image is collected, the detector divides the field of view into a grid of pixels digitally and the intensity of each signal in each pixel is assigned a numerical value [198, 201]. Digital image processing uses that grid of numerical values to extract biologically relevant information related to signal intensity. There are many DIP tools including ImageJ, CellProfiler<sup>TM</sup> (CP) and CellProfiler<sup>TM</sup> Analyst (CPA) [204], VisioPharm, and MATLAB, to name a few. Some, such as ImageJ and CellProfiler<sup>TM</sup>, are open-source free-ware, while others are not. In general, DIP software uses a common work flow composed of commands that allow for cell compartment or sub-compartment identification, determination of foreground or signal over background, and extraction of

quantitative image features that can range from whole animal, tissue, cell population or individual cell-by-cell measurements [204].

### **1.11 Summary and Implications**

The uterus is an essential reproductive organ in female mammals. Reproductive success is defined, to a large extent, by the functional capacity of the uterine endometrium to recognize, support and maintain an embryo throughout pregnancy [2]. While the genetic potential for reproductive success, including uterine functionality, is established at conception, phenotypic potential for reproductive success is determined, to a significant extent, developmentally. In this light, developmental determinants of uterine capacity are encountered postnatally [2, 12, 56, 65] and may be defined by the success of organizational events governing morphogenesis and cytodifferentiation of the endometrium and formation of endometrial glands.

Little is known regarding mechanisms regulating these processes in the cow [1]. Postnatal endometrial adenogenesis requires continual, coordinated epithelial-stromal communication to provide the necessary autocrine and paracrine signaling mechanisms [35, 36, 100]. Uterine glandular secretions are functionally important for conceptus development and maintenance of pregnancy. Disruption of uterine development during neonatal life can result in altered adult uterine morphology and function, as reported for the cow [3, 30], sheep [5, 11, 15, 21, 32, 205], and pig [25-27]. In these ungulate species, endometrial morphogenesis involves steroid hormone-sensitive events that are beginning to be defined. However, effectively nothing is known about early postnatal endometrial histogenesis in the cow, whether the neonatal bovine endometrium expresses PR or ER,

or the extent to which early uterine organizational processes may be sensitive to disruption by exposure to SRMs.

Here, objectives of study one involved establishing and validating methods for multilabel fluorescent IHC, image capture using MSI, and data analysis using DIP software for evaluation of neonatal bovine uterine tissues. Objectives of study two were to apply both standard histological and newly validated IHC and imaging protocols to describe bovine endometrial histogenesis between birth and PND 42, and associated temporospatial patterns of cell proliferation and PR expression in these tissues. Objectives of study 3 were to determine effects of TAM exposure between PND 28 and PND 90, when bovine uterine tissues are still developing, on patterns of endometrial development, cell proliferation and both PR and ESR1 expression in tissues obtained on PND 120.

## **Chapter 2:**

### **Establishment and Validation of Multispectral Imaging Technology to Enable Studies of Bovine Reproductive Tract Development**

#### **2.1 Abstract**

Development of the bovine uterus begins prenatally and is completed postnatally with formation of endometrial glands. Disruption of this process during neonatal life can reduce adult uterine capacity to support pregnancy. However, little is known about mechanisms regulating bovine endometrial development. With a goal of defining molecular and cellular events associated with bovine endometrial histogenesis and cytodifferentiation from birth (postnatal day 0 = PND 0), objectives here were to establish methods for immunohistochemical (IHC) localization of progesterone receptor (PR-A, -B forms) and estrogen receptor (ESR1), as well as two markers of cell proliferation, Ki-67 and 5'bromo-2-deoxyuridine (BrdU), in developing bovine endometrium using multispectral imaging (MSI). For purposes of technical validation, uterine tissue was obtained from a single Holstein heifer treated with BrdU (5mg/kg BW/day, i.v.) for five days prior to euthanasia on PND 40. Tissue was fixed in 4% (w/v) paraformaldehyde, embedded in Paraplast-plus®, sectioned (6 $\mu$ m) and subjected to antigen retrieval in citrate buffer (pH 6). An indirect, non-amplified, multilabel IHC method was employed using primary antibodies chosen based upon target specificity, host species and immunoglobulin subtype. Matched, AlexaFluor®-labeled secondary antibodies (Invitrogen Corporation; Carlsbad, CA) were used to produce target-specific fluorescent signals. All tissue sections were counterstained with POPO-1 to reveal

nuclear DNA. Fluorescent staining for cytokeratin 8 (CK8) was used to distinguish epithelium from stroma in image analyses. The Nuance FX MSI system (Caliper Life Sciences; Hopkinton, MA) was used to capture quantifiable image data at specific wavelengths from as many as four unique fluorescent signals simultaneously. Fluorescent signals were analyzed using CellProfiler<sup>TM</sup> ([www.cellprofiler.com](http://www.cellprofiler.com)). Spectrally unmixed target signal intensities were compared between stromal and epithelial cell compartments on a within-tissue basis after extraction of compartment-specific regions of interest from single- and multilabeled tissue sections. Data were subjected to analyses of variance to identify technical sources of variation. Images generated using multilabel IHC and MSI procedures were equivalent, qualitatively and quantitatively, to those obtained using single-labeling procedures. Using MSI, quantifiable, wavelength-specific data were extracted from spectrally unmixed images generated from multilabeled tissues. Automated analyses permitted rapid evaluation of unique and colocalized fluorescent signal intensities and/or labeling indices for ESR1, PR, Ki-67 and BrdU in stromal and epithelial cell compartments. Relative signal intensity for ESR1, PR and colocalized ESR1+PR was higher ( $P<0.005$ ) in epithelium than stroma. Labeling indices for these transcription factors were also greater ( $P<0.05$ ) in epithelium than stroma. Labeling indices for cell proliferation markers, BrdU and colocalized BrdU+Ki67, were greater ( $P<0.05$ ) for epithelium than for stroma. Establishment and validation of multilabel IHC and MSI procedures for qualitative and quantitative analysis of multiple fluorescent signals in single tissue sections sets the stage for studies designed to evaluate patterns of neonatal bovine endometrial development at cellular and molecular levels.

## 2.2 Introduction

Development of the bovine uterus begins prenatally and is completed postnatally [1]. Endometrial adenogenesis, or uterine gland formation, involves a series of molecular changes that are driven by stromal-epithelial interactions. Bovine glandular morphogenesis occurs in the intercaruncular (IC) areas of the endometrium. While nascent glands are first observed at about 250 days of gestation in the cow [1], proliferation of nascent uterine glands is largely a postnatal process, occurring between birth and 3 months (90 days) of age [2, 3]. Exposure of the developing endometrium to steroid hormones, including progestins and estrogens, can alter patterns of uterine development with long-term effects on the structure and function of adult uterine tissues as seen in cows [2-4], sheep [5], and pigs [7]. Disruption of ESR1- and PR-mediated uterine organizational events in ruminants can induce such effects [2].

Traditional methods of IHC require multiple serial sections of a tissue in order to assess the spatial relationship between two or more targets [183]. By contrast, multilabel IHC allows visualization of two or more tissue antigens in a single tissue section. This can reveal information generally hidden with single-staining IHC of sequential tissue sections [186, 188]. Multispectral imaging (MSI) is a tool best used to capture, evaluate and quantify spatial and spectral information of single or multiple signals in IHC preparations. This technology has been applied to a variety of imaging approaches including fluorescent and chromagen methods of staining tissue sections [165, 186, 187].

Here, studies were conducted to establish: 1) methods for localization of multiple, targeted antigens within single neonatal bovine tissue sections using IHC; and 2) MSI protocols for acquisition of qualitative and quantitative image data from

immunofluorescently labeled uterine tissues. Validation of MSI protocols were accomplished by evaluating single- vs. multilabeling IHC procedures using targeted transcription factors including the progesterone receptor (PR-A, -B forms) and estrogen receptor (ESR1), as well as markers of cell proliferation, Ki-67 and BrdU.

### **2.3 Materials and Methods**

#### *Animals and Tissues*

Animal and tissue handling procedures complied with the guide for Care and Use of Agricultural Animals and were approved by the Institutional Agricultural Animal Care and Use committee of the Clemson University System Agricultural Experiment Station (Animal Use Protocol ARC2007-013). Uterine tissue was obtained from a single Holstein heifer treated with BrdU (5mg/kg BW/day, i.v.) for five days prior to euthanasia on PND 40 (Figure 1). Tissue was excised, immediately fixed in 4% paraformaldehyde and embedded in Paraplast-plus® (Fischer Scientific; Atlanta, GA). Parrafin blocks were transferred to laboratories at Auburn University, Auburn, AL to continue preparation and downstream analyses. Uterine tissues were sectioned at 4-6 µm thick and mounted on VWR Superfrost®Plus microscope slides (VWR International, LLC; Radner, PA).

#### *Immunofluorescent Staining*

Uterine cross-sections were deparaffinized in Hemo-De® (Scientific Safety Solvents; Keller, Texas) and rehydrated through a graded alcohol series into distilled water. Tissues were then subjected to heat-induced antigen retrieval for 15 min in citrate buffer (pH 6) allowed to cool for 15 min and then a blocking solution of 10% non-immune goat serum in phosphate-buffered saline (PBS) was applied to all tissue sections at room temperature for 20 min. Primary antibodies were applied to tissue sections

individually or as a cocktail using an indirect, non-amplified, simultaneous immunohistochemical method and allowed 1 hour incubation at room temperature. For validation purposes, tissue sections were labeled with one of two primary antibody combinations; (1) mouse anti-human PR-A and -B forms (hPRa 2+hPRa 3, 1:100, 200ug/mL), mouse anti-bovine ESR1 (C-311, 1:100, 200ug/mL) and rabbit anti-bovine CK8 (polyclonal, 1:50) or (2) mouse anti-BrdU (BMC 9318, 1:100, 50ug/500ul), rabbit anti-human Ki67 (SP6, 1:100) and mouse anti-human CK8 (1E8, 1:100) or labeled with a single primary antibody directed against the same targets.

To establish and validate methods for simultaneous immunohistochemical localization of multiple antigens within single tissue sections, labeling patterns and signal intensity data were compared for targets (ESR1, PR-A and -B, Ki67, and BrdU). Targets were applied individually (Single-) and in combination with 2 or more targets (Multi-). Primary and secondary antibodies used were selected based upon immunoglobulin (IgG)-specificity and paired accordingly. Primary antibodies (Table 1) were commercially produced and previously validated by collaborators [206]. Secondary fluorescent antibodies from the AlexaFluor® series (Table 2) were chosen and paired with primary antibodies. Fluorescent labeling was specific to targeted antigens, alone and in combination, this was determined by eliminating only the primary antibody of interest in each primary-secondary antibody pairing, data not shown [207]. Primary antibody IgG-specific labeling was validated by replacing the primary antibody with non-specific IgG from the appropriate host in the applied cocktail. Image results show the absence of fluorescent labeling specific to each host IgG that was used (Figure 2). Spectrally unmixed composite images depicting target-specific labeling patterns were compared.

Slides were incubated at room temperature for 1 hour with corresponding cocktail of matched AlexaFluor®-labeled fluorescent secondary antibodies: goat anti-mouse 488, goat anti-rabbit 546, and goat anti-mouse 594 (1:400; Table 2). Slides were then incubated for 15 min at room temperature with POPO<sup>TM</sup>-1 iodide (1:10, Invitrogen Corporation; Carlsbad, CA), a blue nuclear counterstain dye, coverslipped using VectaShield Mounting Medium for fluorescence (Vector Laboratories, INC.; Burliname, CA), and housed overnight at 4C in a humidified chamber void of light.

#### *Multispectral Imaging (MSI)*

Fluorescently labeled neonatal bovine endometrial cross-sections were imaged in one session using a Nuance FX MSI system (Caliper Life Sciences, Hopkinton, MA) affixed to a Molecular Machines and Industries (MMI) CellCut Workstation using a Nikon TE-2000U inverted microscope (MMI, Haslett, MI). For purposes of validation, a total of 10 images of both mesometrial and anti-mesometrial endometrium were captured from five non-sequential sections. Raw, unmixed images were captured at fixed exposure times every 10nm throughout the spectral range, 420-720nm. This system captured emission wavelength-specific images of fluorescent signals *in situ* using long-pass emission filter cubes optimized for the specific signals listed in Table 3; POPO<sup>TM</sup>-1 , A488, A546, and A594 (Chroma Technology Corp., Bellows Falls, VT). To distinguish each target signal, image data were spectrally unmixed to produce component images based on a spectral library of emission wavelengths using Nuance FX software (illustrated in Figure 3). Development of the spectral library involved preparation and collection of wavelength-specific data from tissue sections treated uniquely with anti-PR, anti-CK8 or anti-ESR1 primary antibodies and matched secondary antibodies (A488 or

A546 or A594), or that were stained with POPO-1<sup>TM</sup> alone. Negative controls included the omission of primary antibodies, resulting in a total lack of corresponding immunoreactivity. Procedures permitted removal of autofluorescence and collection of wavelength-specific data from all captured images [208].

*Digital Image Processing (DIP) and identification of endometrial cell compartments*

Exported wavelength-specific data were analyzed using CellProfiler<sup>TM</sup> and CellProfiler<sup>TM</sup> Analyst (CP and CPA; [www.cellprofiler.com](http://www.cellprofiler.com)) (Figure 4). Using this DIP software, a series of steps were defined in order to establish automated identification of epithelium and stromal cell compartments. Each wavelength-specific channel corresponded to a specific targeted antigen. CK8, an epithelial-specific structural marker, was used as a mask to highlight epithelium (intensity threshold range 0.00-1.0 relative intensity units; RIU) for purposes of technical validation. Images were captured such that only epithelial and stromal compartments appeared in the field of view. Therefore, all cells not masked by CK8-specific signal were defined as stroma by default and masked accordingly, revealing only cells of the epithelium. All objects in a field were identified using a nuclear counterstain (POPO-1<sup>TM</sup>) based upon measurement ranges of object size (20-150 pixels in diameter) and relative intensity (0.0-1.0 RIU). Merged objects were distinguished using relative intensity calculations.

With the DIP protocol established, data collected for each nuclei in epithelial and stromal cell compartments included: (1) mean signal intensity indicative of applied primary antibody targets, expressed in MIU (MIU x 103); and (2) target labeling index (LI), defined as the percentage of cell nuclei in a given compartment determined to express target at or above a signal threshold (A488, A546 and A594). The signal

threshold used in LI calculations was determined empirically for epithelium and stroma by means of machine-learning algorithms developed using CPA [201]. Factors considered included measures of secondary antibody (A488, A546, and A594) intensity and objectively excluded other factors such as object shape, size, and texture. Procedures enabled identification and scoring of 13,617 epithelial cells and 13,812 stromal cells as being single-target positive (ESR1-, PR-, BrdU- or Ki67-positive), double-target positive (ESR1+PR- or BrdU+Ki67- positive) or negative for single- and double-target combinations.

#### *Statistical Analyses*

All quantitative image data were subjected to analyses of variance using General Linear Models (GLM) procedures in Statistical Analysis Software system (2009-10; SAS) to evaluate technical sources of variation [209]. Analyses considered main effects of cell compartment. Error terms used in tests of significance were based on the expectations of the mean squares for error. Data are presented as least squared means  $\pm$  standard errors (LSM  $\pm$  SEM).

## **2.4 Results**

#### *Establishment and validation of Multilabel Immunohistochemistry*

Effects of IHC labeling procedures on patterns of PR and ESR1 spatial labeling and expression are illustrated in Figure 5. Immunolabeling indicative of PR and ESR1 was similar between IHC procedures (Figure 5, A-B and D-E), PR and ESR1 signal was limited to the epithelium within the endometrium. Endometrial expression of PR and ESR1 (Figure 5; C and F) was greater in the epithelium as compared to stroma ( $P<0.01$ ), regardless of the IHC labeling procedure. Similar results were found when markers of

cell proliferation, BrdU and Ki67, labeling patterns were compared as illustrated in Figure 6 (A-B and D-E, respectively). Signal indicative of BrdU labeling, as previously determined at or above intensity threshold (LI) was greater ( $P < 0.001$ ) in the epithelium as compared to the stroma for both IHC labeling procedures (Figure 6; C). Overall, labeling patterns were equivalent between IHC procedures, meaning that all desired targets can be labeled simultaneously in a single tissue section without manipulation to target labeling patterns and signal intensity.

#### *Validation of Multispectral Imaging*

For validation of multispectral imaging, qualitative and quantitative image data for transcription factors ESR1, PR and cell proliferation markers Ki67, BrdU were extracted and analyzed using CP. Spectrally unmixed wavelength-specific images illustrating ESR1-, PR- and colocalized ESR1, PR-positive (ESR1+PR) immunolabeling and histograms summarizing target expression (MIU\*10) and LI (%) are presented in Figure 7. Cell compartment-specific ESR1 and PR (-A, -B forms) expression was measured and compared. Relative signal intensity indicative of cell nuclei determined ESR1- or PR-positive was higher ( $P < 0.001$ ) in the epithelium as compared to the stroma on PND 40 (Figure 7; B and E). Similar expression results were found for nuclei determined positive for ESR1+PR, where relative signal intensity was greater in the epithelium as compared to stroma (Figure 7; H). Labeling indices for ESR1- and PR-positive was greater ( $P < 0.001$ ) in the epithelium than stroma (Figure 7; C and F). As expected, labeling indices for ESR1+PR-positive nuclei were greater ( $P < 0.001$ ) in the epithelium than stroma (Figure 7; I). Spectrally unmixed wavelength specific images for nuclei determined positive for BrdU, Ki67 and BrdU+Ki67 and accompanied histograms

summarizing LI for targeted antigens are presented in Figure 8. Cell compartment-specific BrdU and Ki67 staining was measured and compared. Labeling indices for BrdU-positive and co-localized BrdU+Ki67 were greater ( $P<0.001$ ) in the epithelium than stroma (Figure 8; D and F). All quantitative data was reflected in qualitative spectrally unmixed images collected.

#### *Establishment and Validation of Digital Image Processing*

Wavelength-specific component images were processed using CP and CPA software as illustrated in Figure 4. Each wavelength channel was exported in monochromatic format and a low-level threshold was applied to determine signal area for each target (Figure 4A). Total cell nuclei were identified by nuclear POPO<sup>TM</sup>-1 iodide fluorescent staining. Epithelial and stromal cell compartments were delineated using CK8 labeling, an abundant cytoskeletal marker present in epithelial cells. With the epithelium (LE and GE) highlighted, the program was able to selectively analyze and measure only epithelial cells or selectively remove the highlighted area and measure only stromal cells for analysis (Figure 4B).

Identified cells within epithelial and stromal cell compartments were empirically determined ‘positive’ for a single target, co-localized for two targets or determined negative using CPA [201]. Cell classification was determined by target signal intensity measurements (relative intensity units; RIU), collected by CP, yet excluded trivial measurements of nuclei shape, size and location for a given image. Before classification parameters (or rules) were applied in automated batch quantitative image assessments, accuracy was assessed by comparing the ‘rules’ generated as a result of cell-sorting and random classifier function of CPA (see supplemental material, Figure 9-12). Accuracy of

selected ‘rules’ was determined based upon cell behavior as indicated by fluorescent labeling. Accuracy (y-axis) was plotted as a function of increasing number of ‘rules’ (x-axis) applied [210, 211]. All ‘rule’ sets were determined at or above 80% accuracy to proceed with analysis, as suggested by the program manual.

## 2.5 Discussion

Results presented here support the application of multilabel IHC, MSI and DIP technologies to studies of bovine endometrial development. Understanding the spatial relationship between two or more targets of interest in the same tissue section reveals information generally hidden with traditional methods of IHC involving single labeling procedures [168]. Methods developed here establish procedures for generation and collection of qualitative and quantitative image data from fluorescently labeled neonatal bovine tissue sections efficiently and effectively.

Validating methods of multilabel IHC required antibody cocktails based on host and immunoglobulin subtype to avoid cross-reactivity and ensure site-specific antigen detection [164, 165, 200, 207]. Limitations exist with the availability of antibodies directed against desired targets as well as compatibility between preferred primary antibodies. Validating the compatibility of antibody combinations is vital for downstream qualitative and quantitative analyses. For studies reported here, matched fluorescent secondary antibodies were selected from the AlexaFlour® series for strong, narrow emission peaks. This is important for successful spectral unmixing using the Nuance MSI camera and software [186]. Multispectral imaging is not confocal microscopy. This technology avoids layering images by collecting image data for the entire electromagnetic spectrum in a three-dimensional format [187, 199]. Collection

methods permitted digital removal of autofluorescence as well as extraction of wavelength-specific data for each target, as defined by a previously sampled spectral library. Together, these procedures enabled collection of qualitative and quantitative image data for multiple targets *in situ*.

CellProfiler<sup>TM</sup> (CP) and CellProfiler<sup>TM</sup> Analyst (CPA) software enabled automated collection of cell compartment-specific image data from bovine endometrial tissues. Using CP and CPA programs, automated and tailored DIP modules were developed to evaluate cell compartment-specific labeling [208]. Automated evaluation of compartment-specific cellular characteristics was made possible by the use of CK8 immunolabeling. Other structural targets were tested, including alpha smooth muscle actin and CD10 (cluster differentiation marker), markers of smooth muscle and stromal cell compartments, respectively [212]. However, since images were confined to the endometrium, use of CK8 to mark epithelium (LE and GE) was sufficient to enable computer learning as required to identify epithelial and stromal compartments automatically. Overall, results of this study established methods with which to: 1) target multiple antigens within single neonatal bovine tissue sections; 2) use MSI to collect qualitative and quantitative image data from fluorescently labeled IHC preparations; and 3) apply automated DIP algorithms to evaluate complex images. Establishment of these protocols set the stage for studies designed to evaluate aspects of neonatal uterine development.

## **2.6 Aknowledgements**

Authors declare there is no conflict of interest that could be perceived as prejudicing the impartiality of the research. Authors acknowledge collaborators at

Clemson University, notably Ms. N. Corn, Dr. S. Safayii and Dr. S. Ellis for laboratory and imaging methodology assistance. This work was supported by Auburn University College of Veterinary Medicine Animal Health and Disease Research grants (to Wilborn) and NSF-EPS 0814103/1158862 (to Bartol). Work involving vertebrate animals was approved by the Clemson University Institutional Animal Care and Use Committee.

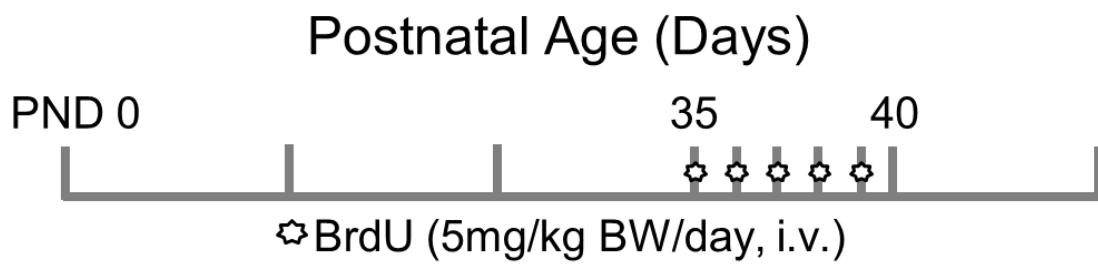


**Figure 1.** Experimental Design.

*Uterine tissue was collected from a single Holstein heifer treated with 5mg/kg BW 5'-bromo-2-deoxyuridine (BrdU) once daily for five days prior to euthanasia on PND 40.*

Primary Antibody	Host	Ig subtype	Manufacture	Clone	Concentration	Working Dilution
PR-A, -B forms	Mouse	IgG1	Thermoscientific	hPRa 2 + hPRa 3	200 µg/mL	1:100
ESR1	Mouse	IgG2a	Santa Cruz Biotechnology	C-311	200 µg/mL	1:100
CK	Rabbit	IgG	Abcam	polyclonal	N/D*	1:50
BrdU	Mouse	IgG1	Roche	BMC 9318	50 µg/500 µL	1:100
KI67	Rabbit	IgG	Abcam	SP6	N/D*	1:100
CK8	Mouse	IgG2a	Abcam	1E8	1 mg/mL	1:100

\*N/D: Not Determined

**Table 1.** Primary Antibodies.

Listed primary antibodies were combined based upon host and immunoglobulin (Ig) subtype.

Secondary Antibody	Host	IgG subtype	Manufacture	Catalog Number	Concentration	Working Dilution
Alexa Fluor 488	Goat	IgG1	Life Technologies Invitrogen™	A-21121	2 mg/mL	1:400
Alexa Fluor 546	Goat	Rabbit IgG	Life Technologies Invitrogen™	A-11010	2 mg/mL	1:400
Alexa Fluor 568	Goat	Guinea Pig	Life Technologies Invitrogen™	A-11075	2 mg/mL	1:400
Alexa Fluor 594	Goat	IgG2a	Life Technologies Invitrogen™	A-21135	2 mg/mL	1:400

**Table 2.** Secondary Antibodies.

*Listed secondary antibodies were selected based upon primary antibody combinations, paired specifically for individual primary antibodies.*

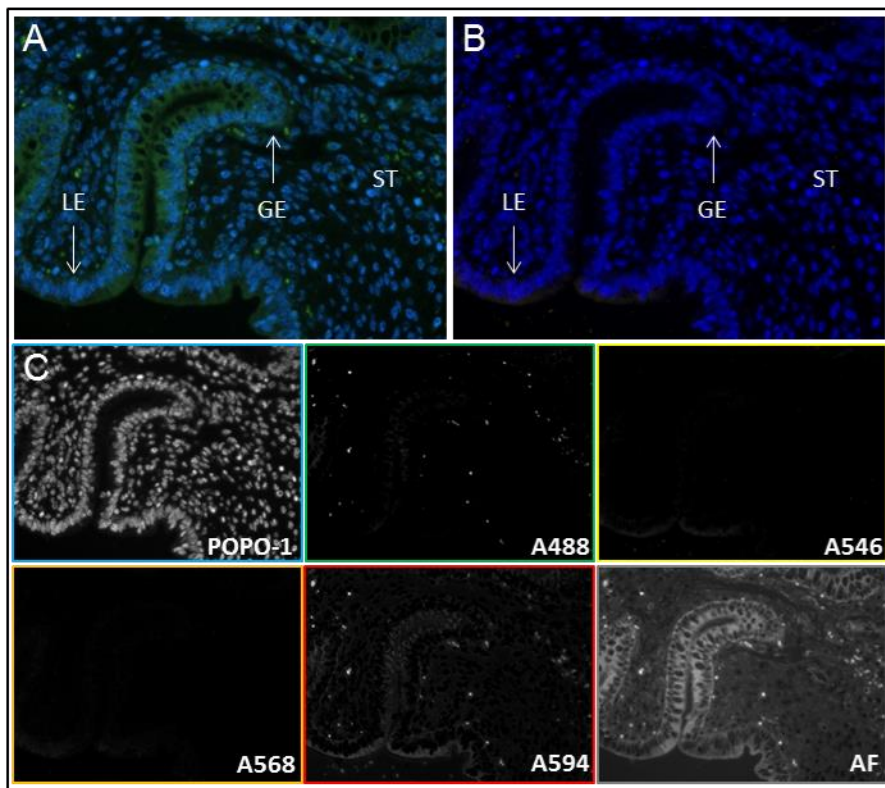


**Figure 2. Primary Antibody Validation.**

Primary antibodies were applied using an indirect, non-amplified, simultaneous immunohistochemical method. Antibodies were selected based upon host and immunoglobulin subtype, and applied to neonatal bovine uterine tissue. Primary antibodies were replaced by corresponding host isotypes and matched AlexaFluor®-labeled secondary antibodies were detected using a Nuance FX multispectral imaging camera. Raw images (A) were collected and spectrally unmixed to reveal composite images (B) and wavelength-specific component images (C) for cell nuclei (POPO-1), A488, A546, A568, A594 and tissue autofluorescence (AF).

Cube Description	Excitation Filter (nm)	Emission Filter (nm)
ET 405/20x, T425lpxr, ET460lp	395-415	460 LP
ET480/40x, T510lprxt, ET520lp	460-500	510 LP
ET545/25x, T565lpxr, ET575lp	520-570	565 LP
ET560/40x, T585lpxr, ET615lp	520-600	615 LP

**Table 3.** *Filter Cube Sets.*

*Unique excitation and emission filters were combined into filter cubes designed to selectively excite and permit emission of secondary antibodies.*

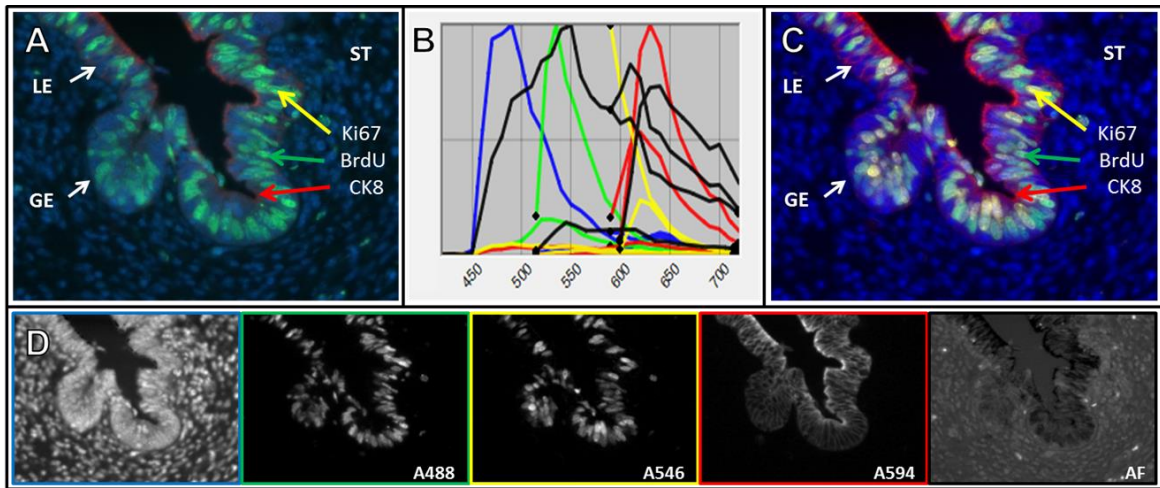


**Figure 3. MSI Process.**

Uterine tissue cross-sections were subjected to single- or multi-target IHC labeling procedures and imaged using a Nuance FX MSI system. Raw images (A) were spectrally unmixed using a spectral library (B) which removed total image autofluorescence (AF) and revealed the unmixed composite image (C). Wavelength-specific data (D) for POPO-1 (left), A488, A546, A594, and AF (right) were extracted from each captured image. Glandular epithelium = GE, luminal epithelium = LE, epithelium (EP) = GE + LE.

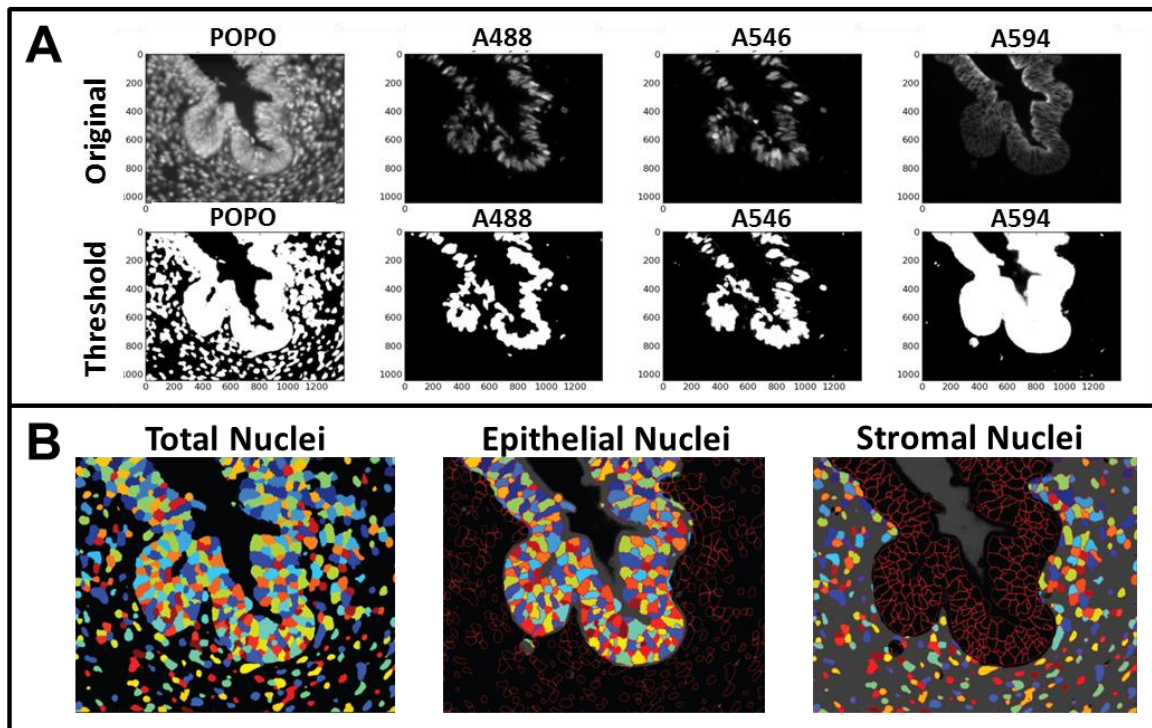


**Figure 4.** *CellProfiler<sup>TM</sup>* Image Analysis Process.

Each wavelength channel was loaded and a threshold was applied to remove excess background noise (A). The Cytokeratin 8 channel was used as a mask to enable delineation of epithelial versus stromal cell compartments (B). This mask was applied to each target channel in order to collect compartment-specific data.

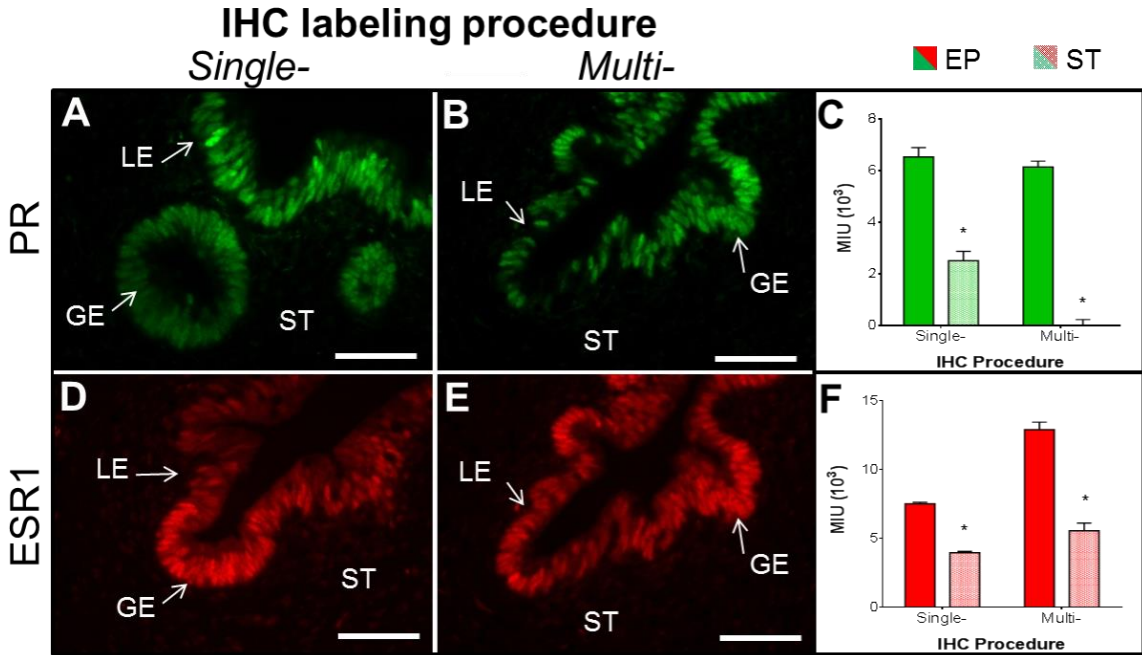


**Figure 5.** Comparison of PR (-A,-B forms) and ESR1 Immunostaining Procedures in Bovine Endometrium.

Spectrally unmixed, wavelength-specific images show PR- (A,B) and ESR1- (D,E) specific labeling patterns for single- (A,D) and multi-target (B,E) IHC procedures. PR intensity was greater in epithelium (EP) than stroma (ST) for both single- and multilabel IHC procedures ( $P < 0.01$ ). ESR1 intensity was greater in EP than ST for both single- and multilabel IHC procedures ( $P < 0.01$ ). Histograms (C, F): Asterisks denote differences (EP vs. ST). Glandular epithelium = GE, luminal epithelium = LE, EP = GE + LE. Original magnification 40X, scale bar = 50 $\mu$ m.

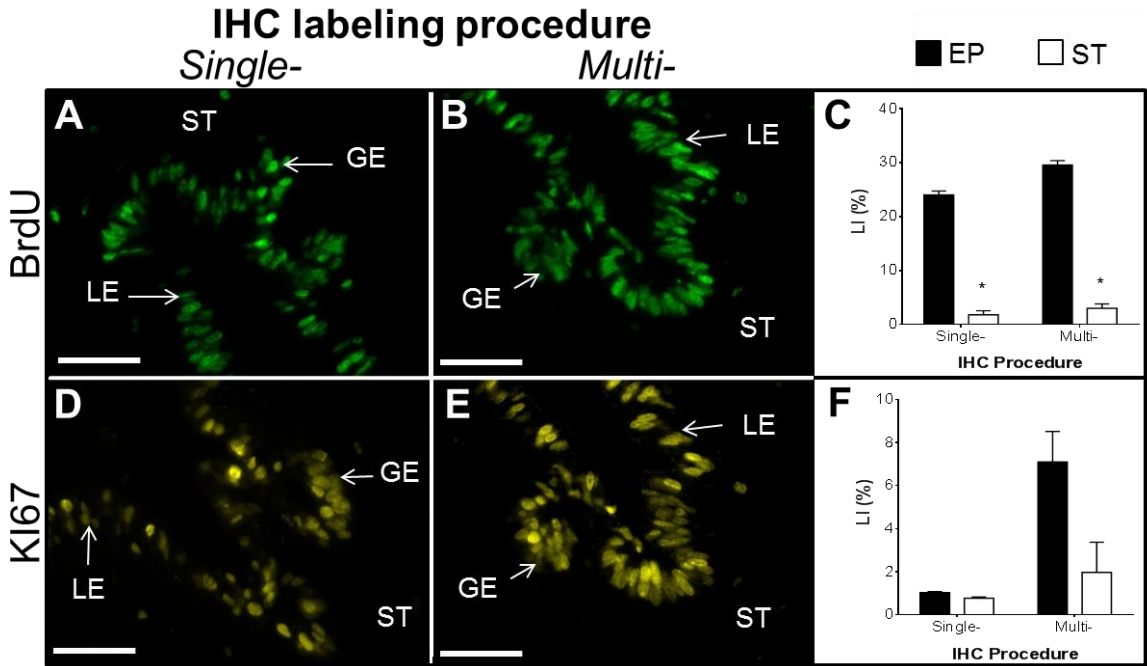


**Figure 5.** Comparison of BrdU and Ki67 Immunostaining Procedures in Bovine Endometrium.

Spectrally unmixed, wavelength-specific images show BrdU- (A,B) and Ki67- (D,E) specific labeling patterns for single- (A,D) and multi-target (B,E) IHC procedures. BrdU LI was greater in epithelium (EP) than stroma (ST) for both single- and multilabel IHC procedures ( $P < 0.001$ ). Histograms (C, F): Asterisks denote differences (EP vs. ST). Glandular epithelium = GE, luminal epithelium = LE, EP = GE + LE. Original magnification 40X, scale bar = 50 $\mu$ m.

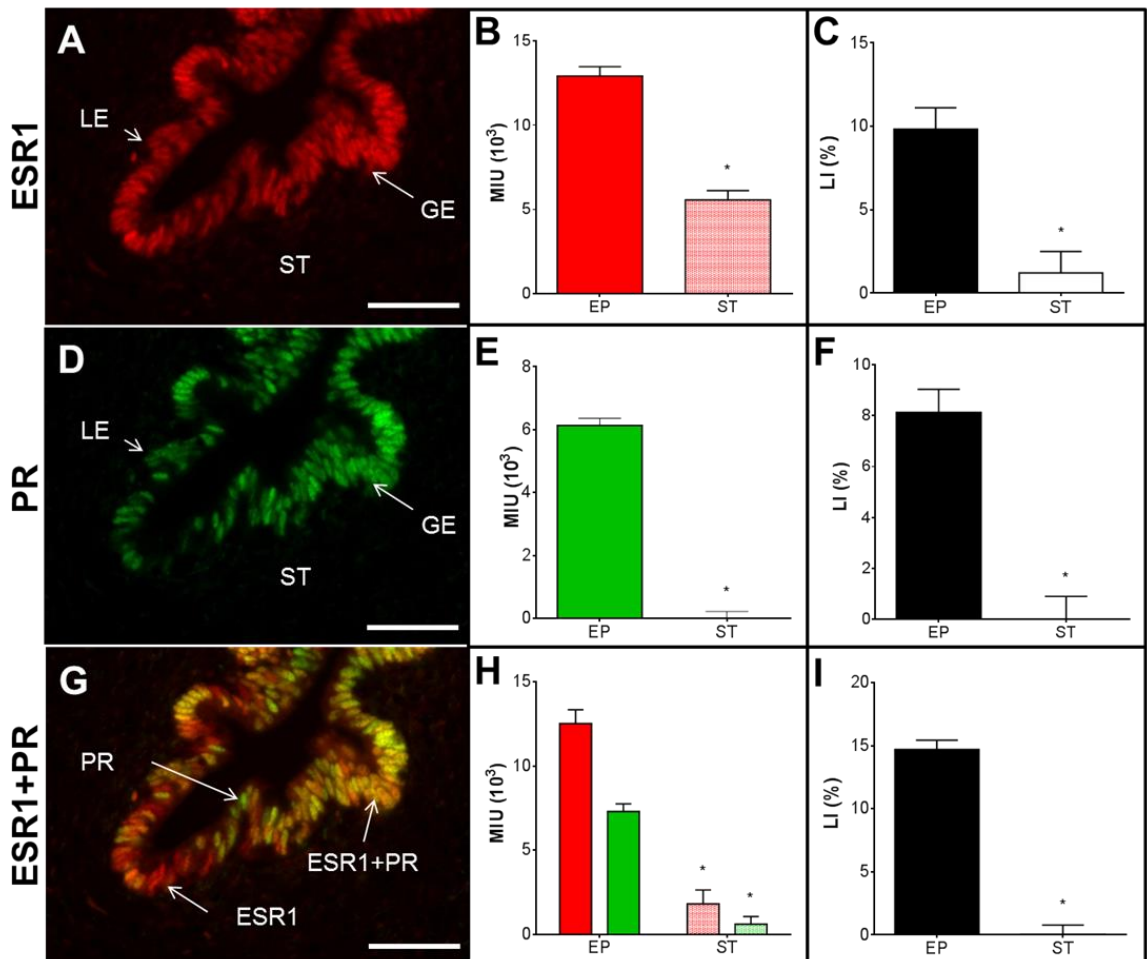


**Figure 6.** Compartment-specific Expression of ESR1, PR (-A, -B forms), and Co-localization of ESR1+PR.

Shown are unmixed wavelength-specific images for nuclear ESR1 in red (A), PR in green (D), and co-localized ESR1+PR (G). Relative signal intensities for ESR1 (B), PR (E), and ESR1+PR (H) were greater in EP as compared to ST ( $P<0.005$ ). A threshold was applied to determine the percent of positively labeled cells (labeling index = LI). Cells at or above threshold were considered positive. LI for ESR1 (C), PR (F), and ESR1+PR (I) were greater in EP than ST ( $P<0.05$ ). Glandular epithelium = GE, luminal epithelium = LE, EP = GE + LE. Original magnification 40X, scale bar = 50 $\mu$ m.

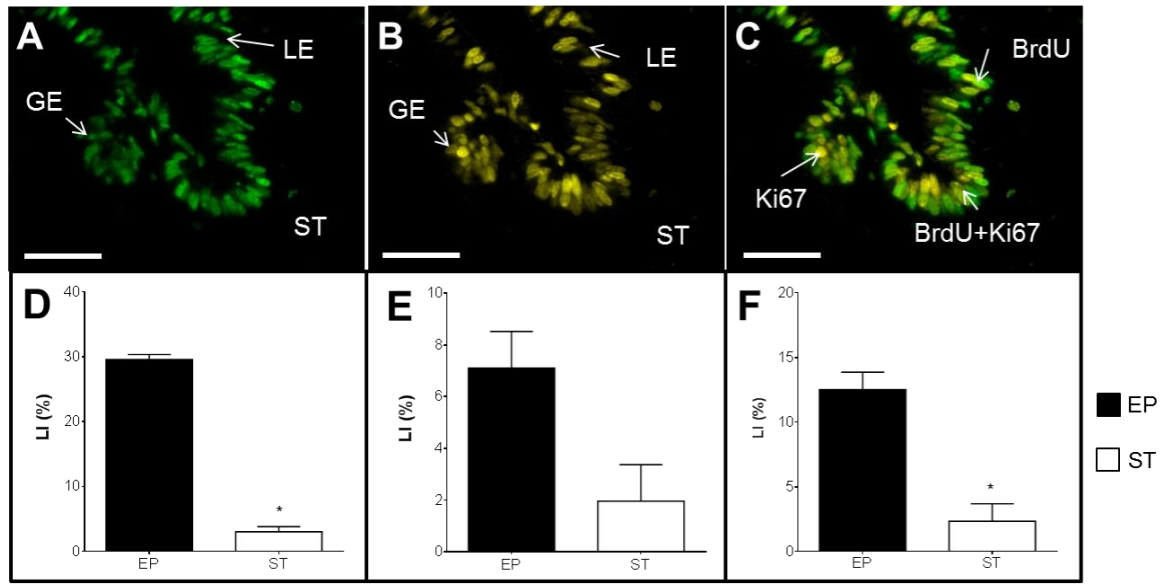


**Figure 7.** Compartment-specific Localization of BrdU, Ki67, and Co-localization of BrdU+Ki67.

Shown are spectrally unmixed wavelength-specific images for nuclear BrdU in green (A), Ki67 in yellow (B), and co-localized BrdU+Ki67 in yellow-green (C). Nuclear LI (%) for BrdU (D) and co-localized BrdU+Ki67 (F) were greater in EP than ST ( $P < 0.05$ ). Glandular epithelium = GE, luminal epithelium = LE, EP = GE + LE. Original magnification 40X, scale bar = 50 $\mu$ m.

## Supplemental Figures

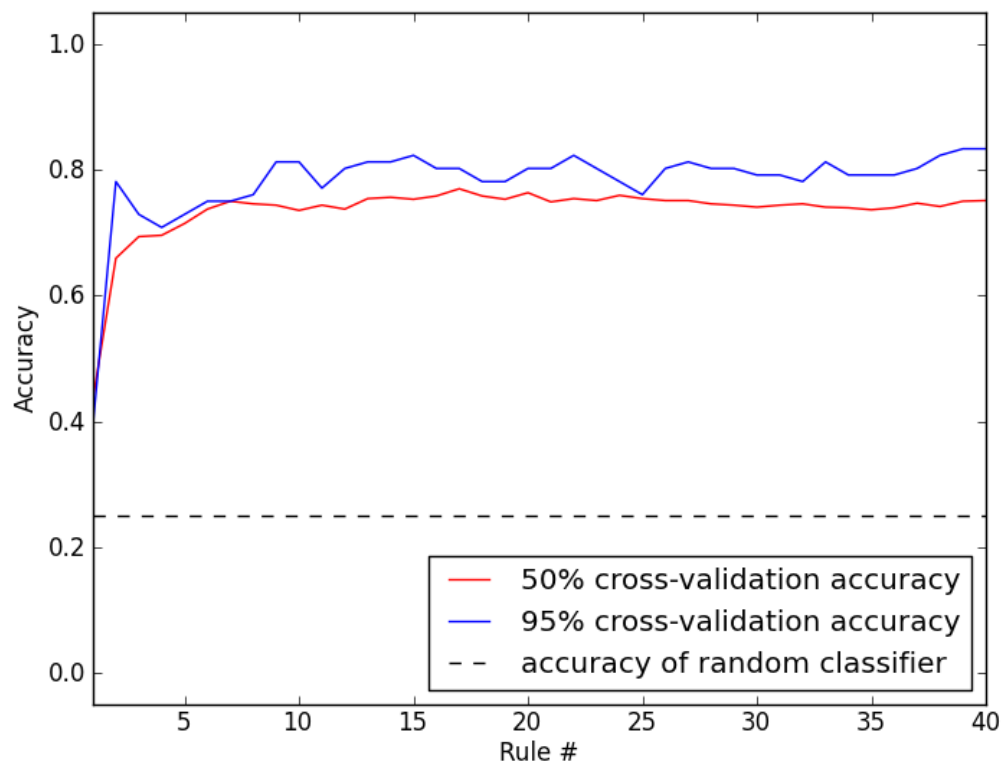


**Figure 8.** Cross-validation Accuracy Plot for ESR1-, PR- and ESR1+PR-positive cells.

Accuracy of rule parameters generated by CellProfiler<sup>TM</sup> Analyst cell-sorting function performed at or above 75% when 20 rules were employed. Software-based random classifier performed at 25% in comparison.

## IHC Labeling Procedure

*Single-*                    *Multi-*

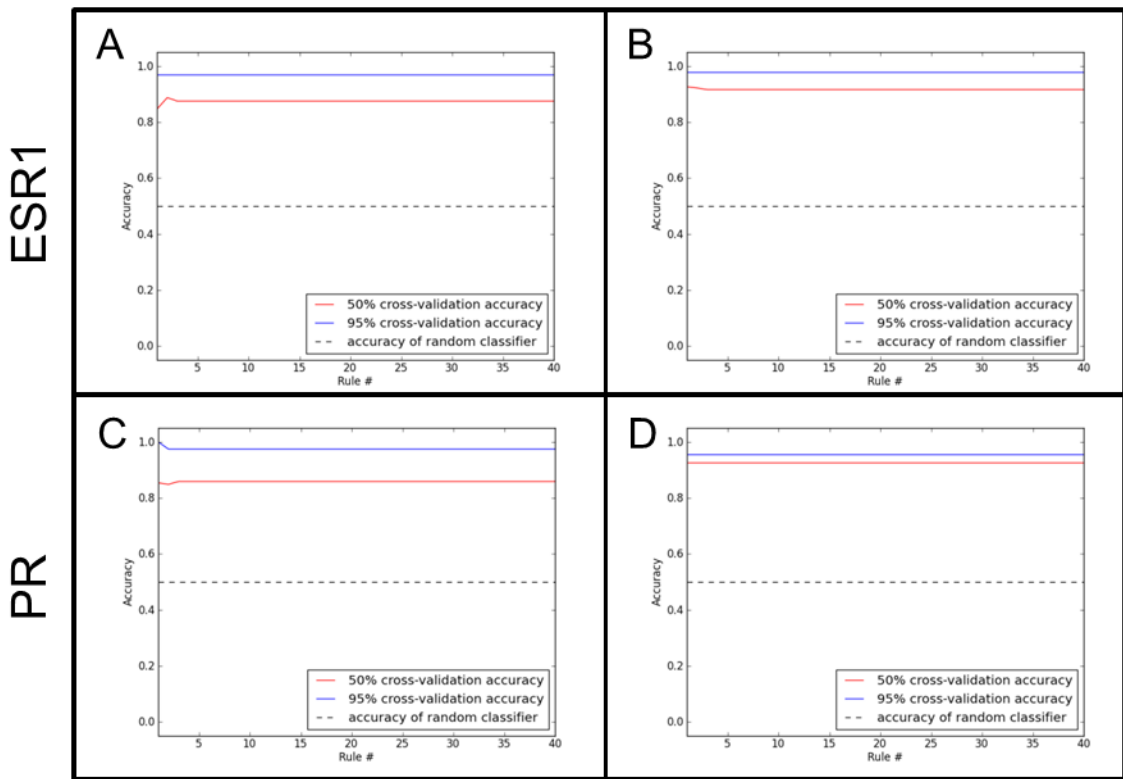


**Figure 9.** Effects of IHC-labeling Procedure on Cross-validation Accuracy Plot for ESR1- and PR-positive Cells.

Cross-validation plots illustrating the accuracy of empirically determined rule parameters for ESR1-positive (A, B) and PR-positive cell nuclei (C, D) are shown for single- (A, C) and multilabel (B, D) IHC procedures. Accuracy of rule parameters generated by CellProfiler<sup>TM</sup> Analyst cell-sorting function performed at or above 75% when 20 rules were employed. Software-based random classifier performed at 50% in comparison.

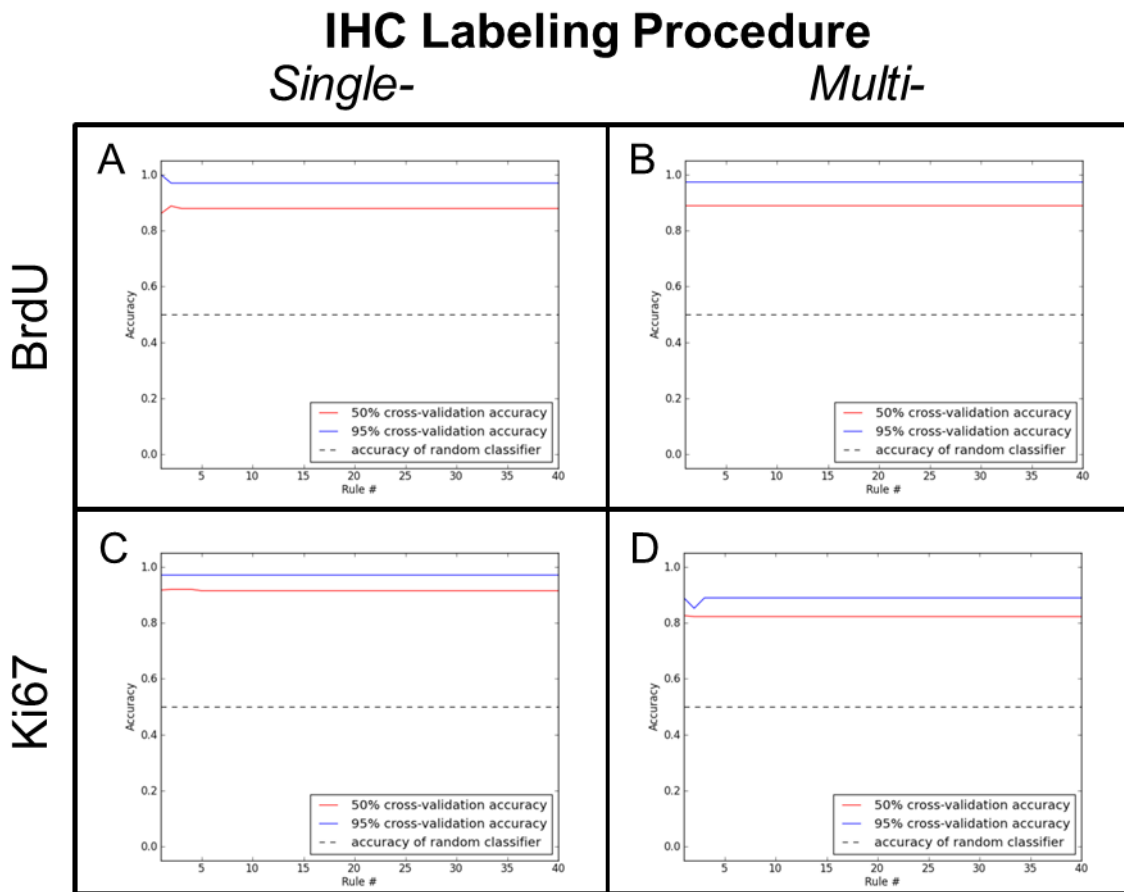


**Figure 10.** Effects of IHC-labeling Procedure on Cross-validation Accuracy Plot for BrdU- and Ki67-positive Cells.

Cross-validation plots illustrating the accuracy of empirically determined rule parameters for BrdU-positive (A, B) and Ki67-positive cell nuclei (C, D) are shown for single- (A, C) and multilabel (B, D) IHC procedures. Accuracy of rule parameters generated by CellProfiler<sup>TM</sup> Analyst cell-sorting function performed at or above 75% when 20 rules were employed. Software-based random classifier performed at 50% in comparison.

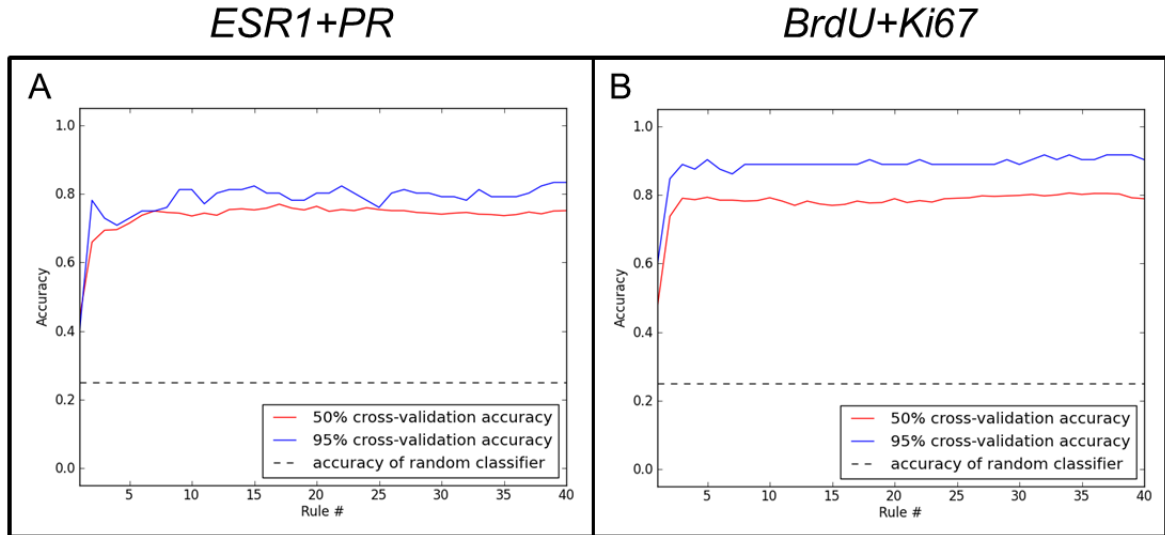


**Figure 11.** Cross-validation Accuracy Plot for *ESR1+PR*- and *BrdU+Ki67*-positive Cells.

*Cross-validation plots illustrating accuracy of empirically determined rule parameters for *ESR1+PR*- (A) and *BrdU+Ki67*-positive (B) cell nuclei. Accuracy of rule parameters generated by CellProfiler<sup>TM</sup> Analyst cell-sorting function performed at or above 80% when 20 rules were employed to determine *ESR1+PR*-positive cells (A) and *BrdU+Ki67*-positive cells (B). Software-based random classifier performed at 25% in comparison.*

## **Chapter 3:**

### Effects of Neonatal Age on Bovine Uterine Histoarchitecture Endometrial Cell Proliferation and Progesterone Receptor Expression

#### **3.1 Abstract**

Neonatal bovine uterine histogenesis is marked by the appearance and proliferation of endometrial glands. Disruption of this process by exposure of neonates to steroid compounds that act via progesterone receptor (PR)-mediated signaling can produce endometrial lesions that compromise uterine capacity to support pregnancy. Little is known about temporospatial patterns of cell proliferation or the relationship between such cell behaviors and patterns of PR expression in developing bovine endometrium. Here, objectives were to: (1) apply established methods for immunohistochemical (IHC) localization and semi-quantitative analysis of antigens, including PR, cytokeratin 8 (CK8), an epithelial marker, and 5-bromo-2-deoxyuridine (BrdU), a cell proliferation marker, in bovine uterine tissue sections using multispectral imaging (MSI) and digital image processing (DIP); (2) define normal patterns of bovine uterine histogenesis from birth (postnatal day = PND 0) to PND 42; and (3) determine effects of neonatal age from PND 0 on temporospatial patterns of endometrial cell proliferation and PR expression. Effects of neonatal age on endometrial cell compartment-specific cell proliferation and PR expression were determined in uterine tissues collected from Holstein heifers given BrdU systemically two hours prior to euthanasia on either PND 0, 7, 14, 21, 28, 35 or 42 ( $n = 4$  calves per age group). Within

the intercaruncular (IC) areas, nascent uterine gland buds were evident at birth as shallow epithelial invaginations that were elongated into tubules by PND 7. Coiled uterine glands were observed in underlying ST on PND 28. On PND 42, coiled, branched uterine glands had extended into deep layers of ST. Overall, BrdU LI (%) was greater ( $P < 0.0001$ ) in stroma than epithelial cell compartments. Epithelial PR LI (%) and signal intensity was consistently greater ( $P < 0.0001$ ) than that observed for ST across all age groups. Nuclear LI (%) for co-localized PR+BrDU, was greater in epithelium ( $P < 0.0001$ ) than stroma. Effects of postnatal age on epithelial and stromal PR expression were best described by 4<sup>th</sup> and 6<sup>th</sup> order polynomial equations. Histological results extend previous observations in the cow, and provide a more detailed timeline of events associated with neonatal bovine endometrial histogenesis. Results also illustrate age-dependent, cell-compartment specific changes in PR expression during phases of endometrial adenogenesis. This suggests a potential role for PR signaling in mediation of bovine endometrial development, as seen in other neonatal ruminants.

### **3.2 Introduction**

Relatively little is known about uterine endometrial histogenesis or mechanisms supporting endometrial development in the cow. More detailed studies of other species [65], and a few observations in the cow [1, 2] support the general observation that endometrial histogenesis begins prenatally and is completed postnatally as marked by development of endometrial glands or adenogenesis [2]. Bovine uterine glands develop in IC areas of the endometrium [1]. Rudimentary glands are first observed at about 250 days of gestation in the cow [1]. However, proliferation of nascent uterine glands is largely a postnatal process, occurring between birth and 3 months (90 days) of age [1, 2].

A simple, systematic description of neonatal bovine endometrial histogenesis and associated cell behaviors supporting this process is lacking.

Exposure of the developing endometrium to steroid hormones, including progestins and estrogens, can alter patterns of uterine development with long-term effects on the structure and/or function of adult uterine tissues, as seen in cows [2-4], sheep [5], and pigs [7]. Disruption of estrogen receptor-alpha (ESR1) and progesterone receptor (PR) –mediated uterine organizational events in ruminants can induce such effects [2]. In sheep, chronic progestin exposure from birth inhibited endometrial gland development, produced a glandless or ‘uterine gland knockout’ (UGKO) endometrial phenotype and, by consequence, suppressed uterine capacity to support pregnancy in UGKO adults [10, 11]. A similar UGKO Phenotype was induced in adult beef heifers exposed to a combination of progesterone and estradiol benzoate from birth [3]. Patterns of PR expression in developing neonatal bovine endometrium remain undescribed.

Here, objectives were to determine effects of neonatal age on bovine endometrial histogenesis and related patterns of cell proliferation and PR (-A, -B forms) expression using standard histotechniques and newly validated methods (See Chapter 2) of multilabel IHC, MSI, and DIP.

### **3.3 Materials and Methods**

#### *Animals and Tissues*

Animal and tissue handling procedures complied with the guide for Care and Use of Agricultural Animals and were approved by the Institutional Agricultural Animal Care and Use committee of the Clemson University System Agricultural Experiment Station (protocol #2009-062). Uterine tissues were collected from Holstein heifers (n=4 per age

group) at birth (postnatal day = PND 0), PND 7, 14, 21, 28, 35 and 42 treated with BrdU using a single dose of 5mg/kg BW/day, i.v. given two hours prior to euthanasia (Figure 13). Tissue was excised, immediately fixed in 4% paraformaldehyde and embedded in Paraplast-plus® (Fischer Scientific; Atlanta, GA). Paraffin blocks were transferred to laboratories at Auburn University, Auburn, AL to continue preparation and downstream analyses. Uterine tissues were sectioned at 4-6 µm thick and mounted on VWR Superfrost®Plus microscope slides (VWR International, LLC; Radner, PA).

#### *Immunofluorescent Staining*

Uterine cross-sections were deparaffinized in Hemo-De® (Scientific Safety Solvents; Keller, Texas) and rehydrated through a graded alcohol series into distilled water. Tissues were subjected to heat-induced antigen retrieval for 15 min in citrate buffer (pH 6) allowed to cool for 15 min and then a blocking solution of 10% non-immune goat serum in phosphate-buffered saline (PBS) was applied to all tissue sections at room temperature for 20 min. Primary antibodies were applied to tissue sections as a cocktail using an indirect, non-amplified, simultaneous immunohistochemical method and allowed 1 hour incubation at room temperature.

Primary and secondary antibodies used were selected based upon immunoglobulin (IgG)-specificity and paired accordingly. Primary antibodies were commercially produced and previously validated in house or by contributing collaborators [206]. IgG-specific labeling was validated by replacing the primary antibody with non-specific IgG from the appropriate host in the applied cocktail. Image results show a lack of fluorescent labeling specifically for the host IgG that was used.

Secondary fluorescent antibody labeling was specific to targeted antigens when paired alone and in combination, data not shown [207].

Uterine tissue collected from heifers (ages PND 0-42) were labeled with a cocktail of primary antibodies directed against PR, CK8 and rabbit anti-BrdU (polyclonal, 1:100, 100 $\mu$ g/100 $\mu$ L; Table 1). Slides were incubated at room temperature for 1 hour with corresponding cocktail of matched AlexaFluor®-labeled fluorescent secondary antibodies: goat anti-mouse 488, goat anti-rabbit 546, and goat anti-mouse 594 (Table 1). Slides were then incubated for 15 min at room temperature with POPO™-1 iodide (1:10, Invitrogen Corporation; Carlsbad, CA), a blue nuclear counterstain dye, coverslipped using VectaShield Mounting Medium for fluorescence (Vector Laboratories, INC.; Burliname, CA), and housed overnight at 4C in a humidified chamber void of light.

#### *Multispectral Imaging (MSI)*

Fluorescently labeled neonatal bovine endometrial cross-sections were imaged using a Nuance FX MSI system (Caliper Life Sciences, Hopkinton, MA) affixed to a Molecular Machines and Industries (MMI) CellCut Workstation using a Nikon TE-2000U inverted microscope (MMI, Haslett, MI). Images ( $n = 3/\text{section}$ , 5 sections/animal) were collected over 8 consecutive sessions. Raw, fluorescent images were captured at fixed exposure times every 10nm throughout the spectral range, 420-720nm (Figure 14). This system captured emission wavelength-specific images of fluorescent signals *in situ* using long-pass emission filter cubes optimized for the specific signals used; POPO™-1, A488, A546, and A594 (Chroma Technology Corp., Bellows Falls, VT). To distinguish each target signal, raw image data (Figure 14A) were

spectrally unmixed to produce composite (Figure 14C) and monochromatic component images (Figure 14D) based on a spectral library of emission wavelengths (Figure 14B) using Nuance FX software. Procedures enabled the collection of composite images devoid of autofluorescence, shown in Figure 14C. Development of the spectral library involved collection of wavelength-specific data from tissue sections treated with anti-PR, anti-CK8 or anti-ESR1 primary antibodies and matched secondary antibodies (A488 or A546 or A594), or stained with POPO-1<sup>TM</sup> alone. Negative controls included the omission of primary antibodies, resulting in a total lack of corresponding immunoreactivity. Procedures permitted removal of autofluorescence and collection of wavelength-specific data from all captured images [208].

*Digital Image Processing (DIP) and identification of endometrial cell compartments*

Exported wavelength-specific data were analyzed using CellProfiler<sup>TM</sup> and CellProfiler<sup>TM</sup> Analyst (CP and CPA; [www.cellprofiler.com](http://www.cellprofiler.com)) (Figure 15). Using this DIP software, a series of steps were defined for automated identification of epithelium and stromal cell compartments. Each wavelength-specific channel corresponded to a specific targeted antigen. CK8, an epithelial-specific structural marker, was used as a mask to highlight epithelium (intensity threshold range 0.00-1.0 relative intensity units; RIU). Images were captured such that only epithelial and stromal compartments appeared in the field of view. Therefore, all cells not masked by CK8-specific signal were defined as stroma by default and masked accordingly, revealing only cells of the epithelium. All objects in a field were identified using a nuclear counterstain (POPO-1<sup>TM</sup>) based upon measurement ranges of object size (20-150 pixels in diameter) and relative intensity (0.0-1.0 RIU). Merged objects were distinguished using relative intensity calculations.

With the DIP protocol established, data collected for epithelial and stromal cell compartments included: (1) mean signal intensity indicative of applied primary antibody targets, expressed in MIU (MIU x 103); and (2) target labeling index (LI), defined as the percentage of cells in a given compartment determined to express target at or above a signal threshold (A488, A546 and A594). The signal threshold used in LI calculations was determined empirically for epithelium and stroma by means of machine-learning algorithms developed using CPA [201]. Factors considered included measures of secondary antibody (A488, A546, and A594) intensity and objectively excluded other factors such as object shape, size, and texture. Procedures enabled the identification and scoring of 56, 882 epithelial and 97,299 stromal cells as being positive for single targets PR and BrdU, the co-localization of PR and BrdU (PR+BrdU) or negative.

#### *Statistical Analyses*

All quantitative image data were subjected to analysis of variance using General Linear Models (GLM) procedures in Statistical Analysis Software system (2009-10; SAS) to evaluate technical sources of variation [209]. Analyses considered main effects of cell compartment and neonatal age as appropriate. Error terms used in tests of significance were based on the expectations of the mean squares for error. Data are presented as least squared means  $\pm$  standard errors (LSM  $\pm$  SEM).

### **3.4 Results**

Effects of neonatal age on endometrial histoarchitectural development are illustrated in Figure 16. Hematoxylin stained images of developing bovine endometrium depict the progression of uterine adenogenesis and growth into the underlying stroma from birth (PND 0) to PND 42. Nascent glandular epithelium was present on PND 0 in

the intercaruncular areas of bovine endometrium. From PND 7-14 glandular buds elongated into glandular tubes into the underlying stratum compactum. Shallow tight coils of uterine glands were present on PND 21, as evident by circular uterine gland cross-sections seen histologically. Coiling of uterine glands continued to PND 42, extending through the stratum compactum with few reaching into stratum spongiosum layers. Uterine glands were regularly distributed within the intercaruncular areas whereas the caruncular areas were devoid of uterine glands entirely.

*Temporospatial labeling patterns of PR protein and BrdU*

Spectrally unmixed composite images of developing bovine endometrium depict the progression of uterine adenogenesis from PND 0-PND 42 (column 1, Figure 17). Wavelength specific composite images depict the effect of neonatal age on patterns of PR protein expression in column 2, cell proliferation (BrdU labeling; column 3), PR+BrdU labeled cells (column 4) and cell compartment comparisons of PR+BrdU labeled cells in column 5. Endometrial expression of PR protein was abundant on PND 0 in the epithelium and remained present regardless of neonatal age. Cell proliferation, indicated by BrdU labeling, was present in both epithelial and stromal cell compartments. DIP automated procedures identified and characterized a total of 56,882 epithelial and 97,299 stromal cell nuclei as PR-positive, BrdU-positive, PR+BrdU-positive or negative.

Effects of postnatal age on endometrial immunolabeling of PR protein and BrdU are illustrated in figure 18. Nuclear LI (%) of PR-positive cells were greater in the epithelium ( $P<0.0001$ ) than stroma across all age groups (Figure 18 A). Epithelial PR was highest at birth and decreased afterwards. Proliferating cells, indicated by BrdU immunolabeling, were more predominant (%) in stroma ( $P<0.0001$ ) overall than

epithelium (Figure 18 B). Epithelial BrdU immunolabeling increased from birth to PND 14 and decreased thereafter until PND 42. Populations of endometrial cell nuclei colocalized for PR and BrdU (PR+BrdU) were greater in epithelial ( $P < 0.0001$ ) than stromal cell compartments overall (Figure 18C). Epithelial and stromal PR+BrdU nuclei LI (%) were similar at birth. Epithelial PR+BrdU LI(%) steadily increased after PND 7 whereas colocalized PR+BrdU stromal LI (%) decreased afterbirth and stayed decreased until PND 35.

Endometrial expression (relative intensity units, RIU x 10<sup>3</sup>) of PR protein was determined for epithelial and stromal cell compartments from birth to PND 42. Expression of PR protein was greater in epithelium ( $P < 0.0001$ ) than stroma consistently across all age groups (Figure 19A). Epithelial and stromal PR expression was greatest at birth, declined thereafter and increased to PND42. Relationships of epithelial and stromal PR expression, as an effect of postnatal age, were best described by 4th and 6th order polynomial equations, respectively, illustrated in 7 A. Raw data for PR-positive cells in epithelium (LE+GE; green) and stroma (white) compartments are illustrated in Figure 19 B. Speckled color (green and white) data depicts cell nuclei-specific PR expression data for over 150,000 epithelial and stromal cells.

### 3.5 Discussion

Results reported here support the utility of digital imaging, multilabel IHC, MSI, and DIP technologies in studies of bovine endometrial development. Beyond new information presented here pertaining to neonatal bovine endometrial histogenesis, results advance understanding of cellular and molecular events associated with this important process. Procedures employed here enabled not only qualitative, but quantitative data to

be captured from digital images, providing more precise information related to endometrial development in the cow.

Endometrial glands are common to all eutherian mammals and are required for reproductive success [32]. In the present study, nascent endometrial glandular epithelium was observed at birth in IC areas of the bovine endometrium. Findings complement and extend an earlier study in the cow indicating presence of glandular buds as early as gestational day 250, and well developed glands in intercaruncular endometrium by PND 90 [1]. Also consistent with observations reported here, uterine glands are absent or rudimentary at birth in other ungulates, including the sheep [11] and pig [56], and develop extensively in the postnatal period. Patterns of endometrial histogenesis reported here for the cow were similar to those described for sheep [13, 56], with tubulogenesis evident by PND 14 and extensively coiled and even branched endometrial glands approaching the myometrium by PND 42.

Administration of BrdU to calves prior to collection of uterine tissues enabled *in vivo* labeling of all cells in the S-phase (DNA synthesis) of the cell cycle [213]. Similar protocols were employed to evaluate patterns of cell proliferation in developing uterine tissues obtained from pigs [25]. Patterns of endometrial cell proliferation reported here for Holstein heifer calves were similar, though not identical to those seen in neonatal sheep [10, 19], pigs [8, 24, 28] and rodents [37, 100, 111, 162], in which proliferating cells were identified *in situ* using techniques including localization of radioactive thymidine-labeled cells, and immunohistochemical localization of Ki67 and proliferating cell nuclear antigen (PCNA). Similar to observations for the sheep and pig [19, 28], epithelial proliferation increased from PND 0 to PND 14 in the bovine endometrium, and

declined after PND 21. Stromal cell proliferation was high at birth in both neonatal ovine and porcine endometrium as observed in the cow [19, 28]. However, unlike the pig and sheep, stromal cell proliferation spiked at PND 14 and PND 42 approximately 3-4 fold higher than epithelial (LE and GE) cell compartments. Consistent with data on neonatal endometrial cell proliferation associated with adenogenesis in other ungulate species, present data support that idea that mechanisms regulating gland genesis in the neonate involve events that can be affected by cell-cell and cell-matrix interactions [65, 101].

Not surprisingly, the endometrium is undergoing significant histoarchitectural changes that require epithelium to proliferate and differentiate as glands penetrate underlying stroma [1]. Transcription factors ESR1 and PR can affect cell behaviors including differentiation and proliferation. Neonatal exposure to P4 inhibited uterine epithelial proliferation and blocked development of endometrial glands in mice [38, 108]. Similarly, adult ewes treated with a synthetic progestin from birth displayed a glandless, UGKO phenotype [10, 11, 71]. Consistently, an adult UGKO phenotype was induced in beef heifers exposed to a combination of P4 and estradiol benzoate from birth [3]. Collectively, these studies support the idea that the success of progestin-sensitive events supporting uterine wall development shortly after birth may determine endometrial phenotype and, ultimately, functionality. Results of the present study confirm that the neonatal bovine endometrium, as reflected here by data obtained from Holstein heifers, is PR-positive at birth, and that patterns of endometrial PR expression change in association with age between birth and PND 42.

Actions of progestins are mediated through the PR, the product of a single gene [110]. A member of the steroid/nuclear receptor superfamily, signal transduction through

PR requires ligand-binding for receptor dimerization and transcriptional effects to occur. PR is present at birth in murine [65], canine [111] and ovine [19] endometrium. In sheep, PR expression was identified in neonatal uteri on PND 7 associated with proliferating and differentiating GE [19]. In the cow, the presence and percentage of cells labeled positively for both PR and BrdU within IC areas were greater in epithelium (LE + GE) than stroma across all age groups. Using the mouse as a model, inhibitory effects of progestins on E2-induced epithelial DNA synthesis were shown to act through stromal and epithelial PR [109, 214]. Recent studies [114] implicated *Hand2*, a unique PR-induced transcription factor, as a regulator of progestin-mediated communication between epithelial and stromal cell compartments in the uterus. Through PR signaling, *Hand2* inhibits production of fibroblast growth factors (FGFs) that act as mitogens in response to ESR1 activation [114]. Here, temporospatial patterns of PR protein expression and cell proliferation, as reflected by BrdU immunostaining, suggest similar mechanistic relationships in the developing bovine endometrium.

Collectively, observations parallel previous reports in the cow [1], confirming the presence of nascent endometrial glandular epithelium in the bovine endometrium at birth. Like the sheep, PR is present at birth in the bovine endometrium and is primarily located in epithelium. Changes in PR expression coincide with changes in epithelial proliferation suggesting a role for PR-mediated signaling in postnatal development of the bovine endometrium.

### **3.6 Acknowledgements:**

Authors acknowledge collaborators at Clemson University, notably Ms. N. Corn, Dr. S. Safayii and Dr. S. Ellis for laboratory and imaging methodology assistance. This

work was supported by Auburn University College of Veterinary Medicine Animal Health and Disease Research grants (to Wilborn) and NSF-EPS 0814103/1158862 (to Bartol). Work involving vertebrate animals was approved by the Clemson University Institutional Animal Care and Use Committee.

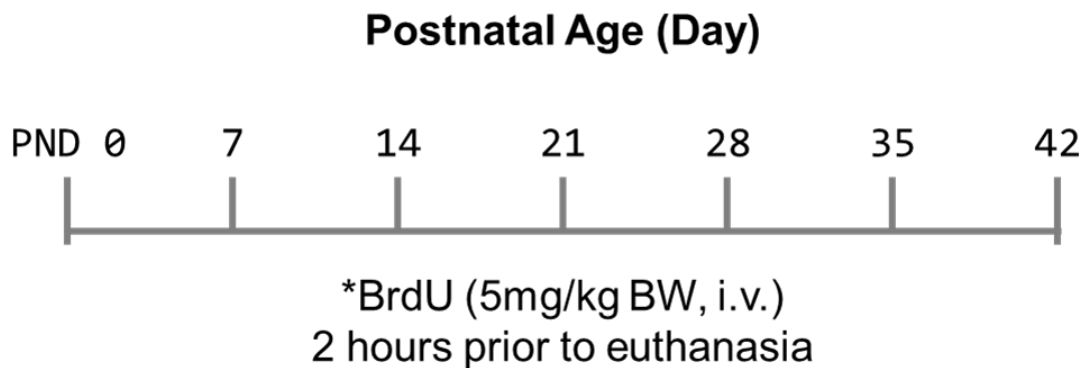


**Figure 12. Experimental Design**

*Heifers (n = 4/group) were injected with 5' bromo-2-deoxyuridine (5 mg/kg BW, i.v.) two hours prior to euthanasia. Uteri were collected at PND 0, 7, 14, 21, 28, 35, or 42.*

Primary Antibody	Host	Ig subtype	Manufacture	Clone/Catalog identification	Concentration	Working Dilution
PR-A, -B	Mouse	IgG1	Thermo Fisher Scientific	hPRa 2 + hPRa 3	200 µg/mL	1:100
BrdU	Rabbit	polyclonal	Bioss Inc.	bs-0917R	1 mg/mL	1:100
CK8	Mouse	IgG2a	Abcam	1E8	1 mg/mL	1:100

**Table 4. Primary Antibodies**

*Listed primary antibodies were combined based upon host and immunoglobulin (Ig) subtype.*

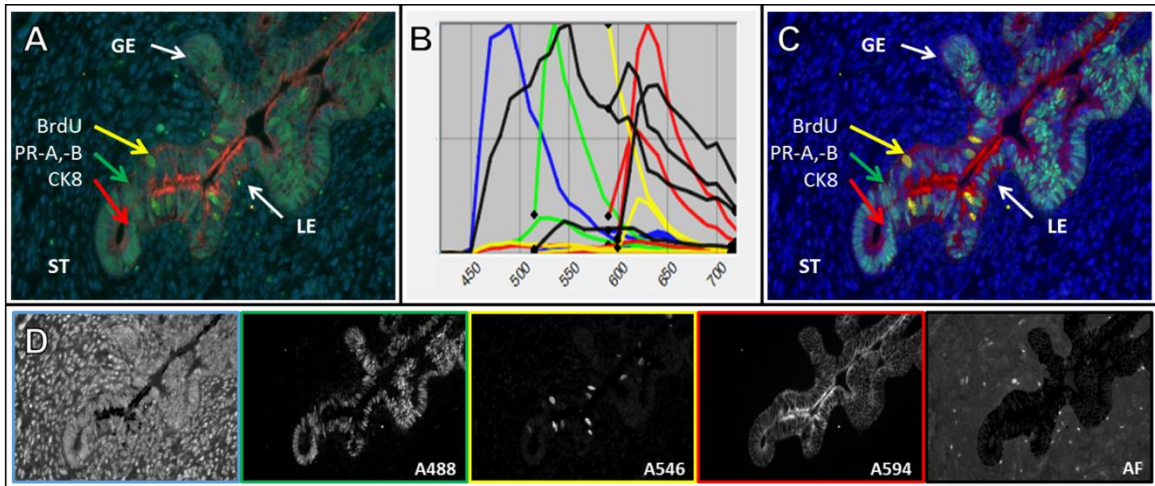


**Figure 13. MSI Process**

Uterine tissue cross-sections were subjected to single- or multi-target IHC labeling procedures and imaged using a Nuance FX MSI system. Raw images (A) were spectrally unmixed using a spectral library (B) which removed total image autofluorescence (AF) and revealed the unmixed composite image (C). Wavelength-specific data (D) for POPO-1 (left), A488, A546, A594, and AF (right) were extracted from each captured image. Glandular epithelium = GE, luminal epithelium = LE, EP = GE + LE.

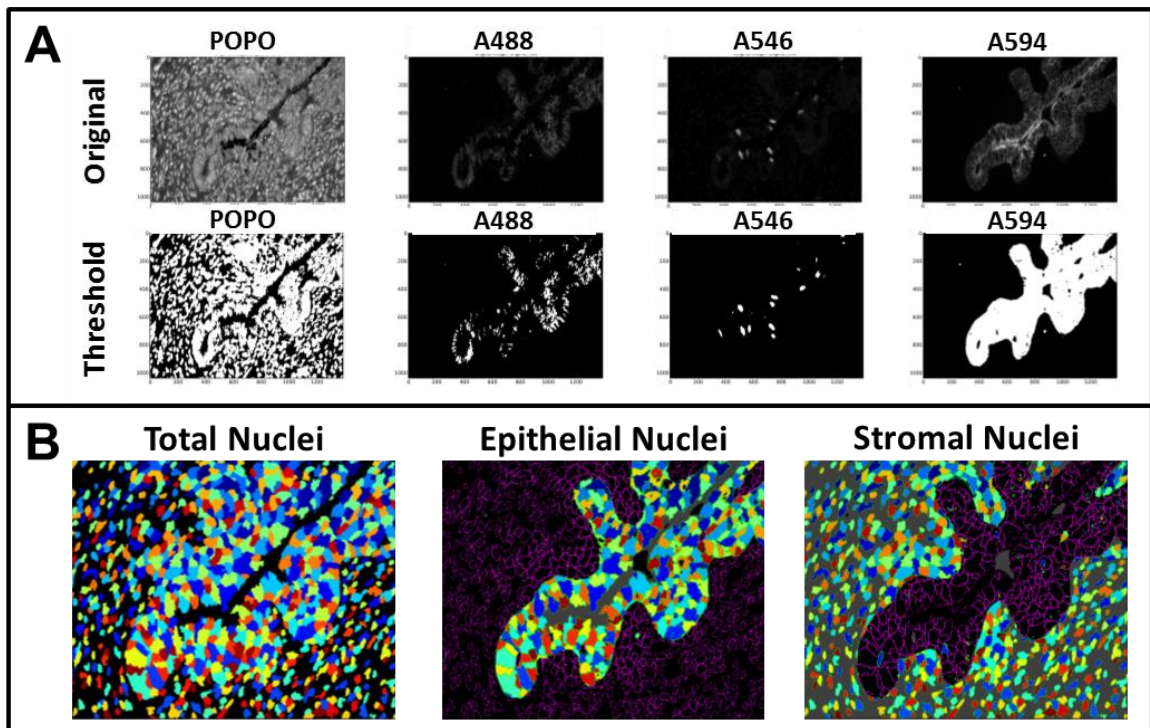


**Figure 14.** *CellProfiler<sup>TM</sup> Image Analysis Process*

*Each wavelength channel was loaded and a threshold was applied to remove excess background noise (A). The Cytokeratin 8 channel was used as a mask to enable delineation of epithelial versus stromal cell compartments (B). This mask was applied to each target channel in order to collect compartment-specific data.*

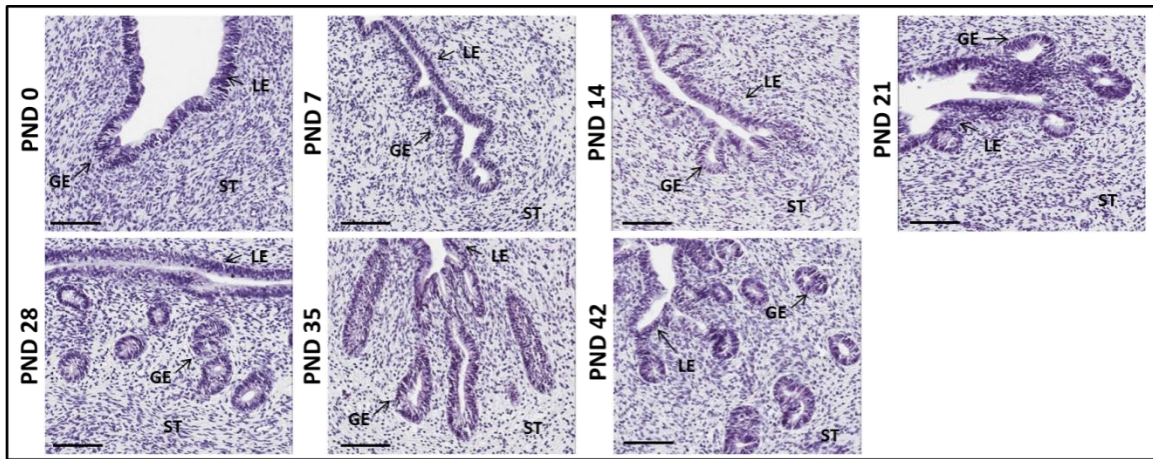


**Figure 15. Effects of Postnatal Age on Endometrial Histoarchitecture**

Images of hematoxylin stained bovine endometrium, PND0-42. Original magnification: 40X, scale bar = 50 $\mu$ m. Glandular epithelium = GE, luminal epithelium = LE, EP = GE + LE.

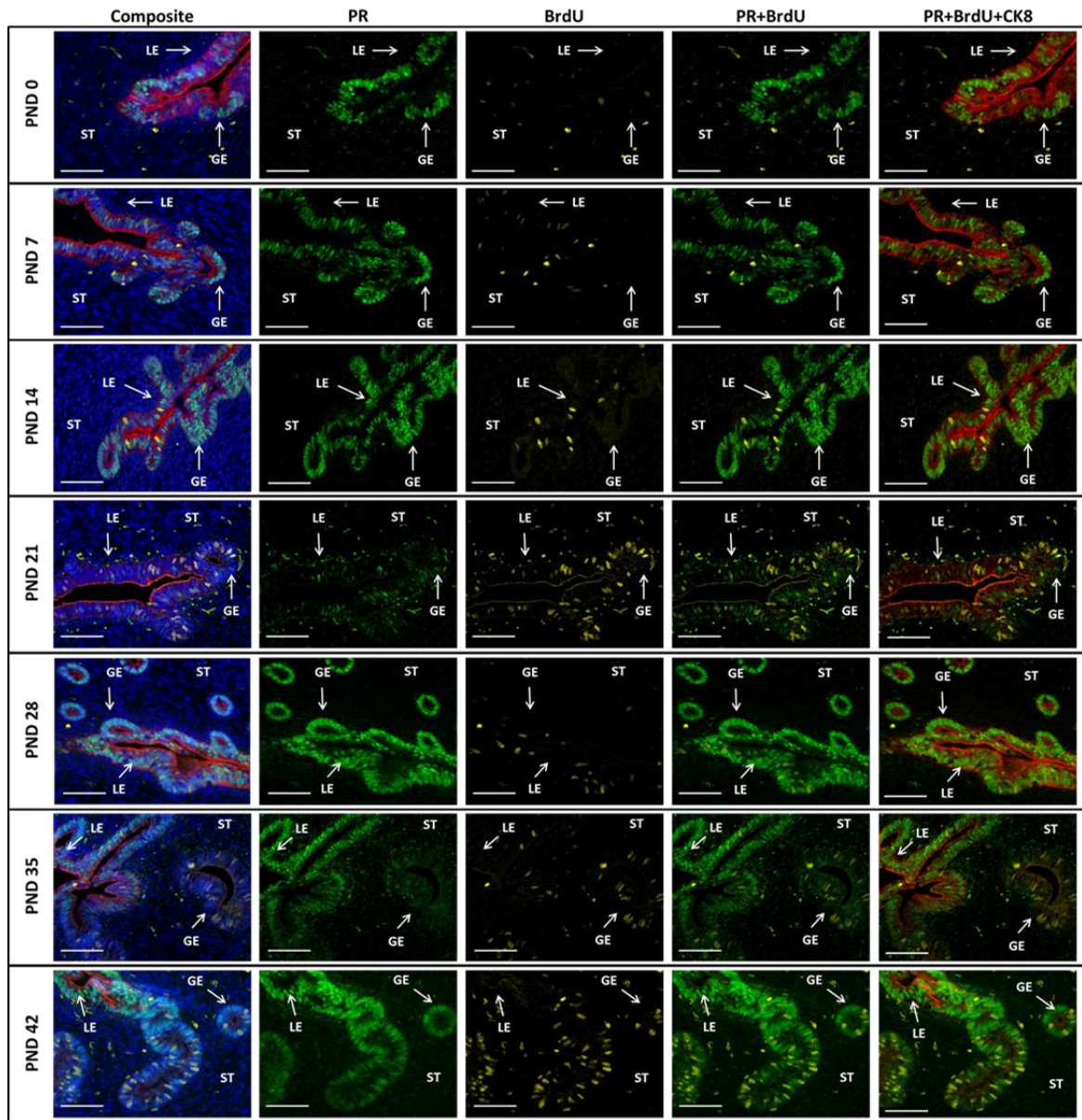


**Figure 16.** Effects of Postnatal Age on Endometrial Labeling Patterns of PR (-A, -B forms) and BrdU

Spectrally unmixed composite images of bovine endometrium, PND0-42. Corresponding wavelength-specific images depicting PR-A, -B in green (A488), BrdU in yellow (A546), PR+BrdU, and PR+BrdU with epithelial-specific marker CK8 in red (A594). Original

*magnification: 40X, scale bar = 50 $\mu$ m. Glandular epithelium = GE, luminal epithelium = LE, EP = GE + LE.*

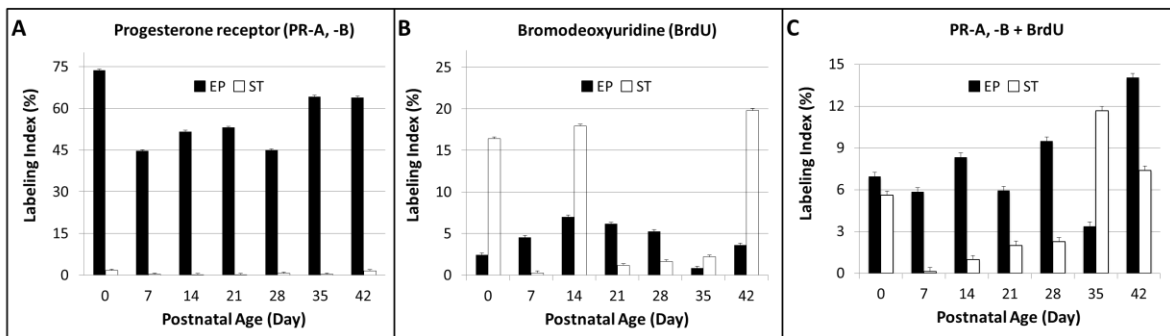


**Figure 17.** Effects of Postnatal Age on Endometrial Labeling Indices of PR protein and BrdU

Epithelial PR labeling index (LI, %) was consistently greater ( $P<0.0001$ ) than stroma cell compartments across all age groups (A). Overall, BrdU LI (%) was greater ( $P<0.0001$ ) in stroma than epithelial cell compartments (B). Colocalized epithelial PR+Brdu LI (%) was greater ( $P<0.0001$ ) than stromal cell compartments across all age groups (C). No treatment interactions were detected.

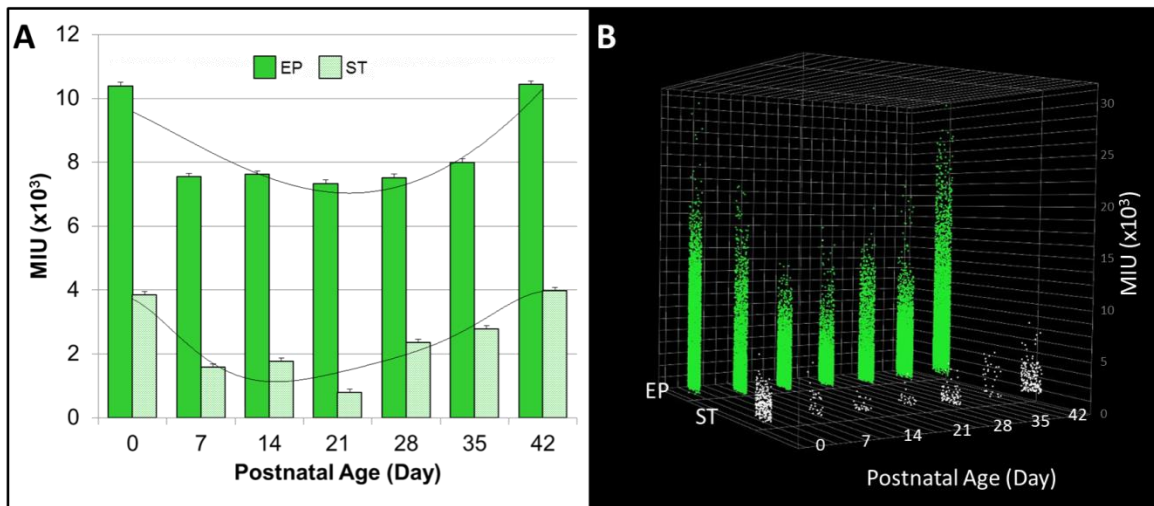


**Figure 18.** Effects of Postnatal Age on Endometrial Expression of PR protein

PR-specific labeling intensity was greater in EP than ST (A,  $P<0.0001$ ). Cell compartment-specific differences were consistent across all age groups ( $P<0.0001$ ). Effects of postnatal age on epithelial and stromal PR expression were best described by 4th ( $y = 0.00002023x^4 - 0.00172475x^3 + 0.05276261x^2 - 0.67034314x + 10.35540326$ ;  $P<.0001$ ,  $R^2 = 0.288686$ ) and 6th ( $y = 0.00002023x^4 - 0.00172475x^3 + 0.05276261x^2 - 0.67034314x + 10.35540326$ ;  $P<.0001$ ,  $R^2 = 0.288686$ ) order polynomial equations (illustrated in panel A). Raw PR expression data for individual EP (green) and ST (white) nuclei are illustrated in panel B. Overall 56,882 EP and 97,299 ST nuclei were identified and measured for PR-A, -B protein (B).

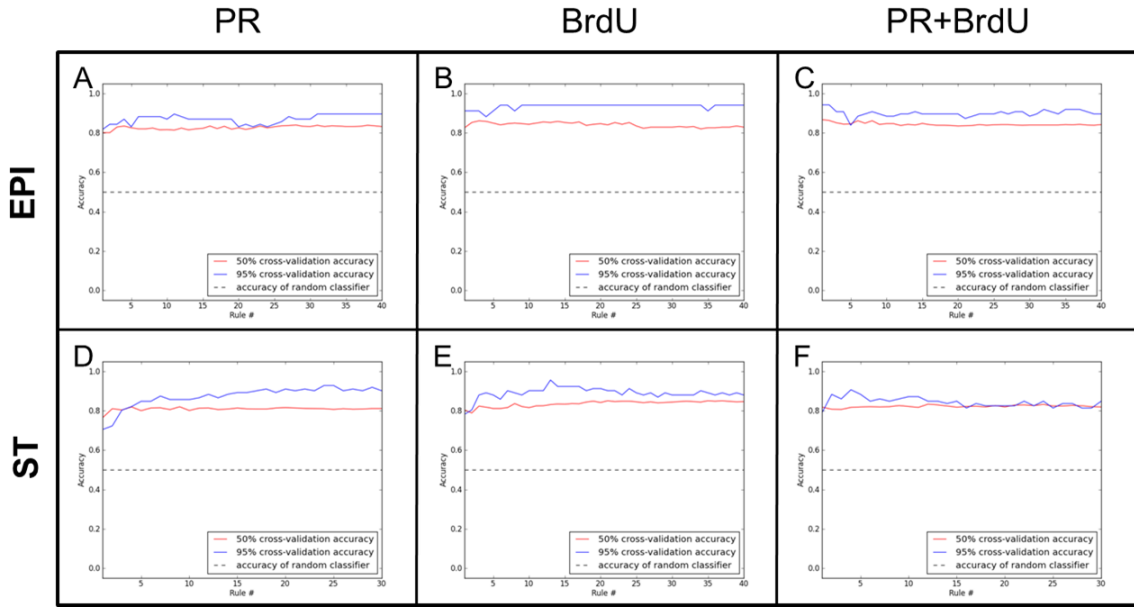


**Figure 19.** Cross-validation Accuracy Plots for PR-, BrdU- and PR+BrdU-positive Cells

Cross-validation plots illustrating accuracy of empirically determined rule parameters for PR- (A,D), BrdU- (B,E) and PR+BrdU-positive (C,F) cell nuclei in epithelial (EPI, A-C) and stroma (ST, D-F) cell compartments. Accuracy of rule parameters generated by CellProfiler<sup>TM</sup> Analyst cell-sorting function performed at or above 80% when 20 rules were employed to determine PR-, BrdU- and PR+BrdU-positive cells. Software-based random classifier performed at 50% in comparison.

## **Chapter 4:** Tamoxifen Affects Prepubertal Bovine Endometrial Development

### **4.1 Abstract**

Bovine uterine development, which is completed postnatally and marked by formation of endometrial glands, is a steroid hormone-sensitive process. Disruption of this process by exposure of neonatal calves to progestins and estrogens can alter patterns of endometrial development and compromise uterine function in adults. The extent to which estrogen receptor (ER) -mediated events contribute to bovine endometrial development is unclear. Here, tamoxifen (TAM), a selective ER modulator (SERM), was used to determine effects of disruption of ER-mediated events on endometrial morphogenesis. Proliferation of endometrial epithelial, stromal and myometrial cells was evaluated *in situ* after fluorescence immunohistochemical (IHC) staining for Ki67, proliferating cell nuclear antigen (PCNA), and 5-bromo-2'-deoxyuridine (BrdU). Data were captured using multispectral imaging (MSI) and subjected to digital image processing (DIP). Heifers (n=7-8 per treatment; 15 animals total) were treated daily with vehicle or TAM (300 $\mu$ g/kg BW/day, s.q.) from postnatal day (PND) 28-120, a period when bovine uterine tissues are known to be sensitive to steroid hormones. All animals were given BrdU (5mg/kg BW/day; i.v.) for five days beginning on PND 90 to enable localization of BrdU-retaining cells in uterine tissues obtained on PND 120. Tissues collected on PND 120 were fixed in 4% (w/v) paraformaldehyde, embedded in Paraplast-plus®, sectioned (4 $\mu$ m) and subjected to antigen retrieval in citrate buffer (pH 6). An

indirect, non-amplified, multilabel IHC protocol was employed using primary antibodies chosen based upon target specificity, host species and immunoglobulin subtype. Matched AlexaFluor<sup>®</sup>-labeled secondary antibodies (Invitrogen Corporation; Carlsbad, CA) were used to obtain target-specific signals. All tissue sections were counterstained with POPO-1 to reveal nuclear DNA. Fluorescent signal for cytokeratin 8+18 (CK8) was used to mark epithelium and to facilitate automated identification of epithelial and stromal cell compartments using DIP. Images (30/animal) were captured using a Nuance FX MSI system (Caliper Life Sciences; Hopkinton, MA). Fluorescent signals were extracted and data were generated using CellProfiler<sup>TM</sup> and CellProfiler<sup>TM</sup> Analyst software ([www.cellprofiler.com](http://www.cellprofiler.com)). Cross-sections of uterine tissues were evaluated histomorphometrically to determine endometrial thickness and endometrial gland penetration depth using Aperio<sup>®</sup> image analysis software (Vista, CA). Data were subjected to analyses of variance. Compared to vehicle-treated controls in which endometrial glands were regularly coiled and distributed densely throughout the stroma, TAM treatment induced irregularly large, cystic endometrial glands. Treatment with TAM reduced endometrial gland penetration ( $P<0.05$ ) without affecting endometrial thickness. Cell proliferation, reflected by Ki67 and PCNA staining, was not affected by TAM. However, overall, BrdU labeling was markedly reduced ( $P=0.05$ ) in TAM-treated animals. Further, BrdU LI was greater ( $P<0.001$ ) in stroma than in epithelium or myometrium, and in deep stroma and glandular epithelium as compared to shallow, adluminal endometrial zones. Thus, mechanisms regulating cell proliferation and radial patterning of the prepubertal bovine endometrium, including gland genesis, are TAM-

sensitive. Results indicate that normal, radial patterning of the bovine endometrium requires temporospatially appropriate, ER-mediated signaling.

#### **4.2 Introduction**

The uterus is incompletely developed at birth. Development of the uterine wall is principally a postnatal event, involving organization of the endometrium, myometrium and perimetrium [2]. Postnatal uterine histogenesis requires the organization and stratification of stroma, growth and differentiation of myometrial smooth muscle layers, and development of uterine glands (See Chapter 3). In the cow, as is other mammalian species [65], uterine glands begin as invaginations of the luminal epithelium. First observed at about 250 days of gestation in the bovine fetus [1], significant proliferation and development of nascent uterine glands occurs between birth and three months of age [1, 2]. Uterine adenogenesis in the bovine neonate occurs rapidly after birth such that coiled, branched glands can be found throughout intercaruncular (IC) endometrium by PND 42 (See Chapter 3). In the adult, uterine glands are functionally important for conceptus survival and development [65].

Exposure of the developing endometrium to steroids, including progestins and estrogens, can alter patterns of uterine development with long-term effects on the structure and/or function of adult uterine tissues, as seen in cows [2, 3, 29], sheep [5, 11], and pigs [26, 131, 215]. Previous studies in the cow suggested a critical window of sensitivity to steroids and other endocrine disrupting compounds between birth and PND 45 [2, 3]. Neonatal exposure of beef heifers to a combination of progesterone and estradiol benzoate over a period of approximately 200 days from birth resulted in adult uterine hypoplasia and endometrial aglandularity. Results indicated that disruption of

PR- and/or ER-mediated uterine organizational events in the neonate could affect tissue programming and adult uterine function [3, 65].

Tamoxifen (TAM), a selective estrogen receptor modulator (SERM), can activate or repress ER-mediated gene transcription [149]. Relative agonistic and antagonistic effects of TAM are species- and tissue-specific [149]. Nevertheless, measured responses to TAM exposure indicate ER-mediated events. The extent to which such events affect bovine endometrial development is unclear.

Objectives of this study were to determine the effects of TAM administration from PND 28–120 on endometrial development in Holstein heifers as reflected by: 1) endometrial histology; 2) patterns of endometrial epithelial, stromal and myometrial cell proliferation as reflected by immunostaining for Ki67, PCNA, and BrdU; and 3) temporospatial nuclear immunostaining patterns for estrogen receptor alpha (ESR1) and PR (-A, -B forms) on PND 120.

#### **4.3 Materials and Methods**

##### *Animals and Tissues*

Animal and tissue handling procedures complied with the guide for Care and Use of Agricultural Animals and were approved by the Institutional Agricultural Animal Care and Use committee of Virginia Tech (Animal Use Protocol: 11-208-DASC). Holstein heifer calves ( $n = 8$  per treatment group; 16 heifers total) were treated with placebo or selective estrogen receptor modulator TAM (300 $\mu$ g/kg BW; i.v.) between PND 28 – 120 (see Figure 21). Beginning on PND 90, animals were treated with BrdU (5mg/kg BW, i.v.) for five consecutive days. On PND 120, calves were sacrificed, uterine tissue was excised, fixed immediately in 4% paraformaldehyde and embedded in Paraplast-plus®

(Fisher Scientific; Atlanta, GA). Tissues were sectioned at 4 $\mu$ m and mounted on VWR Superfrost®Plus micro slides (VWR International, LLC; Radner, PA). Animal handling and experimental procedures were done in consent with the Virginia Tech Institutional Animal Care and Use Committee.

#### *Immunofluorescent Staining*

Whole uterine cross-sections were processed as described in Davolt et al. 2012 [216] (see Chapter 2). Tissue sections were labeled with one of two primary antibody combinations (see Table 5): (1) mouse anti-human PR-A and –B forms (hPRA 2+hPRA 3, 1:100 200ug/mL), mouse anti-bovine ESR1 (C-311, 1:100 200ug/mL) and guinea pig anti-bovine CK8 (polyclonal, 1:500); or (2), rabbit anti-human KI67 (SP6, 1:100), mouse anti-human PCNA (F-2, 1:100 200ug/mL), mouse anti-BrdU (BMC 9318, 1:100 50ug/500ul) and guinea pig anti-bovine CK8 (polyclonal, 1:500). Matched AlexaFluor®-labeled secondary antibodies included goat anti-mouse 488, goat anti-rabbit 546 or goat anti-guinea pig 546, goat anti-guinea pig 568 and goat anti-mouse 594 (1:400, 2mg/mL) were used to fluorescently label targets.

#### *Multispectral Imaging (MSI)*

Images (n = 2-3/zone, 2 zones/section) were captured using a Nuance FX MSI system (PerkinElmer, Santa Clara, CA) affixed to a Nikon TE-2000U inverted microscope. Image data were collected at 10nm increments along the electromagnetic spectrum (420-720nm) for as many as five unique fluorescent signals simultaneously. Quantifiable image data were spectrally unmixed (Figure 22) into component data files and exported for further analyses.

### *Histomorphometry*

Following multispectral imaging, tissue sections were rinsed using phosphate buffered saline (PBS), counterstained with Hematoxylin QS (Vector Laboratories, Inc.; Burlingame, CA), and scanned using the Aperio® ePathology Solutions system (Vista, CA). Digital brightfield images acquired using the Aperio® slide scanning system (at 20X magnification) were analyzed using VisioPharm digital pathology software (Broomfield, CO). Here, paired 250 $\mu\text{m}^2$  sampling regions (4-5 regions/zone, 2 zones/section, 3 sections/animal) were digitally applied to uterine cross-sections illustrated in Figure 23. Regions of interest were placed such that superficial zones were no more than 250 $\mu\text{m}$  from the lumen and deep zones were no more than 250 $\mu\text{m}$  from the stroma-muscle interface. Morphometric characteristics of endometrial gland cross-sections were identified and measurements were collected to evaluate density, area as a percentage of the whole, mean area, and mean perimeter.

### *Digital Image Processing analysis*

Exported, wavelength-specific data were analyzed using CellProfiler™ and CellProfiler™ Analyst software ([www.cellprofiler.com](http://www.cellprofiler.com)). Data were processed using a ‘pipeline’ constructed of modules to eliminate noise, delineate cell compartments and sub-compartments, identify primary objects (cell nuclei), and collect quantitative measurements. CellProfiler™ Analyst was used to identify defining measurements of single labels and colocalized labels to be used as ‘rules’ to filter identified cells into corresponding populations. Procedures enabled capture of spectrally unmixed, cell compartment-specific target signal intensity data.

### *Statistical Analyses*

All quantitative image data were subjected to analyses of variance using General Linear Models (GLM) procedures in the Statistical Analysis System [209]. Analyses considered main effects of treatment, cell compartment (luminal epithelium, LE; glandular epithelium, GE; stroma, ST; and myometrium, MYO), and zone (superficial, deep) as appropriate. Data are presented as LSM  $\pm$  SEM.

#### 4.4 Results

Representative photomicrographs of bovine endometrial tissues from superficial and deep zones of vehicle- and TAM-treated heifers on PND 120 are illustrated in Figure 24, together with histograms depicting treatment effects on uterine gland penetration and endometrial thickness. Endometrium from PND 120 (column 1, Figure 24) depicts tightly coiled uterine glands extending from the lumen and penetrating to stromal-myometrial junction in the IC areas. Treatment with TAM resulted in a range of endometrial phenotypes shown in columns 2-4, Figure 24. In contrast to PND 120 endometrium, IC areas contained varying sizes of cyst-like glandular structures that presented irregular distribution and penetration into the underlying ST. Histologic analyses illustrate three distinct uterine gland phenotypes in the endometrium of TAM-treated heifers: 1) short glandular invaginations into underlying stroma (column 2, Figure 24), 2) frequent large cystic glandular structures with moderate glandular invasion into stroma (column 3), and 3) small cystic coiled uterine glands extending to the stromal-myometrial junction in column 4. Overall, uterine gland penetration was reduced ( $P < 0.05$ ) in TAM-treated heifers while endometrial thickness was unaffected shown in histograms in column 5, Figure 24.

Endometrial gland morphology was described based on cross-sectional values and distribution within superficial and deep zones of vehicle- and TAM-treated uterine samples (see Figure 25). Representative photomicrographs of endometrial tissues from vehicle- (Figure 25 A, E) and TAM-treated (Figure 25 B, F) groups are shown, along with histograms depicting TAM-treatment effect on uterine gland morphology illustrated in Figure 25 panels C-D and G-H, respectively. On average, individual uterine gland cross-section area was larger ( $P < 0.05$ ) in TAM-treated animals in comparison to vehicle-treated animals on PND 120. Regardless of treatment, average individual gland cross-section area and perimeter was larger ( $P < 0.01$ ) in superficial zones, near the lumen, compared to deep zones. Overall, total uterine gland cross-section area was greater ( $P < 0.1$ ) in TAM-treated animals on PND 120, whereas uterine gland density was markedly decreased ( $P < 0.05$ ). There was a treatment x endometrial zone interaction detected ( $P < 0.05$ ) for total uterine gland cross-section area and density data.

Effects of TAM-treatment was seen with immunofluorescence and evaluated with DIP technology to expose quantitative levels of expression and qualitative patterns of spatial labeling for steroid hormone receptors and markers of cell proliferation. Spectrally unmixed composite images show labeling patterns for cell proliferation markers BrdU (green), Ki67 (yellow) and PCNA (red), cell nuclei (POPO-1; blue) and CK8 (orange) in superficial and deep zones of vehicle- and TAM-treated animals on PND 120 in Figure 26 (A,F and B,G respectively) along with wavelength specific images depicting BrdU and CK8 (orange) alone in figure panels C, H for vehicle- and D, I for TAM-treated groups. Histograms in panels E and J, describe labeling indices of BrdU within epithelial and stromal cell compartments. Endometrial BrdU LI was greater ( $P <$

0.05) in deep GE as compared to superficial GE and LE, though treatment with TAM did not affect BrdU staining in superficial and deep epithelial cell compartments (Figure 26 E). Stromal BrdU LI was greater ( $P < 0.05$ ) in deep endometrial ST than superficial and yet, was reduced ( $P < 0.1$ ) in TAM-treated heifers (Figure 26 J). Neither Ki67 nor PCNA LI were affected by TAM for superficial or deep endometrial zones (data not shown). Differences in staining patterns between markers of cell proliferation might be attributed to the timing of BrdU treatment on PND 90 and label retention in comparison to endogenous markers of cell proliferation, Ki67 and PCNA evaluated on PND 120.

Immunolabeling of steroid hormone receptors PR (green) and ESR1 (red) are illustrated via spectrally unmixed composite images for superficial and deep endometrial zones of vehicle- and TAM-treated tissues in Figure 27 (panels A, G and B, H; respectively). Wavelength-specific composite images for PR are shown in Figure 27 panels C, I for vehicle- and D, J for TAM-treated comparisons, together with histograms describing PR LI (%) in panels E, K and expression levels in panels F, L as affected by TAM treatment. Treatment with TAM increased ( $P < 0.0001$ ) nuclear LI for PR in epithelium without causing marked changes in signal intensity, indicative of PR expression and activity as shown in panels E, F respectively. Endometrial PR LI was greater ( $P < 0.0001$ ) in LE as compared to superficial and deep GE (panel E) whereas PR signal intensity was highest ( $P < 0.0005$ ) in deep GE as compared to LE and superficial GE (panel F); a treatment x cell interaction was also detected ( $P < 0.05$ ). Treatment with TAM did not affect stromal PR LI and signal intensity in superficial and deep endometrial areas (panels K, L). While stromal PR LI was higher ( $P < 0.05$ ) in deep as

compared to superficial bovine endometrial areas (panel K), PR signal intensity was higher ( $P < 0.0001$ ) for superficial ST (panel L).

Figure 28 illustrates effects of TAM exposure on prepubertal endometrial ESR1 immunolabeling and expression. Wavelength specific composite images for ESR1 (red) depict superficial and deep endometrial areas for vehicle- (panels A, E) and TAM-treated (panels B, F) animals, along with histograms describing effects on ESR1 LI and signal intensity in panels C, G and D, H respectively. Compared to vehicle-treated controls, neonatal exposure to TAM reduced ( $P < 0.0001$ ) epithelial ESR1 LI and signal intensity, indicative of ESR1 expression in LE, superficial and deep GE (panels C, D). Nuclear ESR1 LI was highest ( $P < 0.001$ ) in deep GE as compared to LE and superficial GE, and a treatment x cell interaction was detected ( $P < 0.001$ ; panel C). Treatment with TAM did not affect stromal ESR1 LI (panel G), yet, reduced ( $P < 0.05$ ) stromal ESR1 signal intensity (panel H). Regardless of treatment, ESR1 signal intensity was greater ( $P < 0.0001$ ) in deep endometrial areas, and a treatment x cell compartment interaction was detected ( $P < 0.05$ ). Low levels of ESR1 immunolabeling were detected in superficial and deep stromal cells; however, nuclear LI for ESR1 was greater ( $P < 0.05$ ) in deep compared to shallow endometrial areas. These results are illustrated in the wavelength specific composite images in Figure 28, panel B, F.

#### **4.5 Discussion**

In the current study, ER-mediated events in postnatal bovine endometrial development were evaluated in heifer calves as reflected by responses to chronic TAM exposure from PND 28 to PND 120. Histological analyses showed clearly that bovine uterine gland development is TAM-sensitive. Effects of TAM were generally

antiadenogenic, and associated with altered, cystic uterine gland morphology and reduced endometrial development and glandularity on PND 120 in Holstein heifers.

Endometrial adenogenesis is primarily a postnatal event in ungulate [40, 100, 110] and rodent [10, 38] species such that the uterine wall undergoes marked structural remodeling shortly after birth. Epithelial cells lining the lumen within developing IC areas invaginate into the stroma as nascent uterine glands on approximately gestation day 250 in the bovine fetus [65]. After birth, nascent uterine glands proliferate rapidly, developing through stages of bud formation, tubulogenesis, coiling, and branching until glandular epithelium reaches the inner circular layer of the myometrium [38]. In the cow, a critical developmental window for steroid sensitivity was identified between birth and PND 45, when the endometrium is vulnerable to insult developmentally [2]. By PND 90 uterine glands are present on the lateral boarders of the caruncular stroma and extend through IC stroma to the myometrium. While uterine glands continue to branch and coil through the first year of life, adult uterine histoarchitecture is evident by six months of age [1, 110].

Prepubertal exposure to TAM altered bovine endometrial development on PND 120. Disruptive effects of TAM on bovine endometrial development, particularly glandular morphogenesis described here, were similar to earlier studies of other ungulate species in response to various steroid hormones and steroidal compounds [2, 3, 5, 10, 26]. TAM treatment resulted in a variety of endometrial phenotypes that were distinct from vehicle-treated controls. Specifically, TAM dysregulated endometrial development as reflected by generally reduced glandularity, and aberrant glandulation resulting in cyst-like glandular structures at PND 120. Similar antiadenogenic effects were observed in

sheep given norgestomet (NOR), a potent synthetic progestin, from birth through 8, 16, or 32 weeks of age [11]. Likewise, treatment of beef heifers with a combination of progesterone (P) and estradiol benzoate (E), delivered chronically over approximately 200 days, reduced adult endometrial gland density in a manner that was related to age at first PE exposure. Effects were most pronounced when PE exposure began at birth [3]. In this light, depending upon the extent to which ER-mediated organizational events govern early postnatal programming of endometrial development, effects of TAM reported here could differ and even be more severe and lasting if exposure was initiated earlier after birth.

It is well established that disrupting communication between stromal and epithelial compartments can have deleterious effects on uterine wall development [36, 68, 100, 109]. Consequently, to understand if and how disruption of ER-mediated signaling by TAM contributes to prepubertal bovine endometrial development, effects were evaluated on a cell-compartment basis. ER-mediated events associated with neonatal uterine wall development vary between species. Estrogen-induced effects on epithelial proliferation, differentiation and gland development are mediated through ligand binding with ERs, where ESR1 predominates in the uterus [96]. In the murine ESR1-knockout model, normal mitotic stimulation of epithelial, stromal and myometrial cells was disrupted due to the absence of ESR1 expression, resulting in infertility [40]. Based on data for the mouse, uterine epithelial proliferation is regulated by stromal ESR1 [40, 100]. Administration of ER-antagonists during the normal period of gland development inhibited uterine growth and development [103].

As in other ruminants [6, 19], results of this study show that disruption of ER-mediated signaling using TAM reduced endometrial gland penetration without remarkable effects on epithelial proliferation on PND 120, as reflected by immunostaining for endogenous Ki67 and PCNA. Interestingly, stromal cell proliferation, reflected by BrdU LI data, was reduced in TAM exposed heifers. However, it is important to note that effects of TAM on BrdU label retention reflects cell proliferation activity beginning on PND 90 (when BrdU labeling began), whereas proliferation markers Ki67 and PCNA indicate the state of cell proliferation at the time of tissue excision. Thus, dysregulation of ER-mediated signaling induced by TAM reflects time- and cell-compartment specific effects in prepubertal bovine endometrium.

Effects of chronic exposure to TAM on the developing bovine endometrium described here represent new observations. Because TAM is a mixed-function SERM, observed effects cannot be attributed directly to agonistic or antagonistic mechanisms. However, results do support the idea that disruption of the normal state of ER activation in neonatal bovine uterine tissues will alter the normal program of endometrial development.

Estrogen and progesterone are important effectors of growth, development and reproduction in domestic animals [65, 110]. Thus, alterations in patterns of PR and/or ER expression would likely alter developmental programming of affected tissues and organs. In the bovine endometrium on PND 120, TAM treatment reduced endometrial ESR1 expression patterns without marked effects on PR expression. To the extent that TAM is working either agonistically or antagonistically via ER-mediated signaling mechanisms, present results suggest that endometrial ESR1, but not PR expression is

supported by ER-mediated signaling events. Classically, estrogen upregulates expression of its own receptor and downregulates PR, as shown in studies of ovine endometrium [217]. By contrast, progestins inhibit many estrogen actions in the uterus, including stimulation of epithelial proliferation [65]. ESR1 signaling is important for support of cell proliferation and differentiation during endometrial adenogenesis in ruminants, pigs, rodents and humans [42, 65]. In this light it is not surprising that TAM effects on endometrial development were documented in the postnatal uterus as described here.

Present data suggest that bovine endometrial development during the prepubertal period involves temporospatially regulated, ER-mediated signaling. Heifers began TAM treatment on PND 28. By this time nascent uterine glands are developing rapidly throughout IC endometrium (See Chapter 3). It is likely that both PR- and ER-mediated events are involved in initiation and/or support of endometrial adenogenesis in the cow, as suggested by previous studies [2, 3]. Results of the present study emphasize the requirement of proper temporospatial regulation of ER-mediated signaling during this pre-pubertal period of bovine endometrial development for normal uterine gland development

#### **4.6 Acknowledgements**

Authors acknowledge collaborators Dr. M. Akers and Hannah Tucker at Virginia Tech University for their assistance and Dr. S. Ellis for his mentorship along the way.

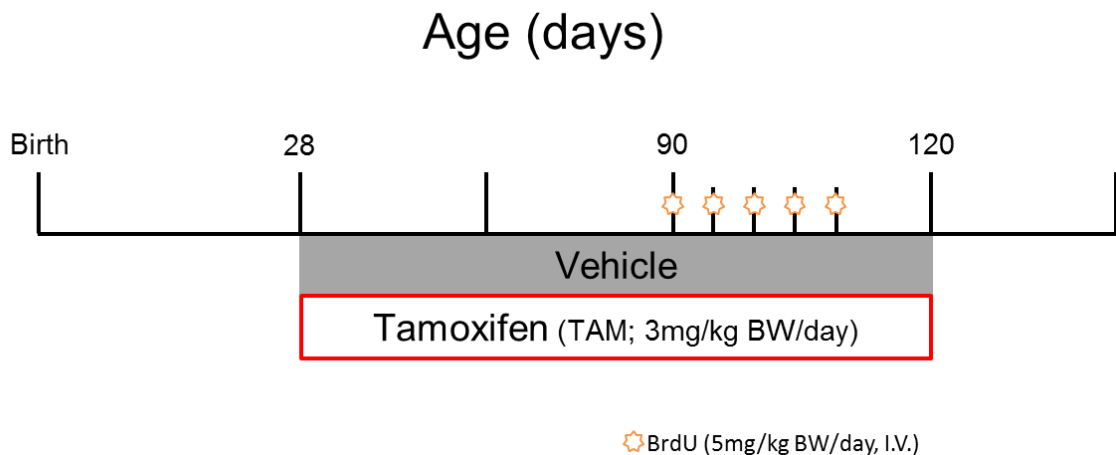


**Figure 20. Experimental Design**

*Heifers (n=7-8 per treatment; 15 animals total) were treated daily with vehicle or TAM (300 $\mu$ g/kg BW/day; s.q.) from postnatal day (PND) 28-120. All animals were injected with BrdU (5mg/kg BW/day; i.v.) for 5 days beginning on PND 90 in order to localize BrdU-retaining cells at PND 120. Uteri were collected on PND 120.*

Primary Antibody	Host	Ig subtype	Manufacture	Clone	Concentration	Working Dilution
PR-A, -B forms	Mouse	IgG1	Thermoscientific	hPRA 2 + hPRA 3	200 µg/mL	1:100
ESR1	Mouse	IgG2a	Santa Cruz Biotechnology	C-311	200 µg/mL	1:100
CK8+18	Guinea Pig		Fitzgerald Industries International	polyclonal	100 µL	1:250
BrdU	Mouse	IgG1	Roche	BMC 9318	50 µg/500 µL	1:100
KI67	Rabbit	IgG	Abcam	SP6	N/D*	1:100
PCNA	Mouse	IgG2a	Santa Cruz Biotechnology	F-2	200 µg/mL	1:100

\*N/D: Not Determined

**Table 5.** Primary Antibodies

*Listed primary antibodies were combined based upon host and immunoglobulin (Ig) subtype.*

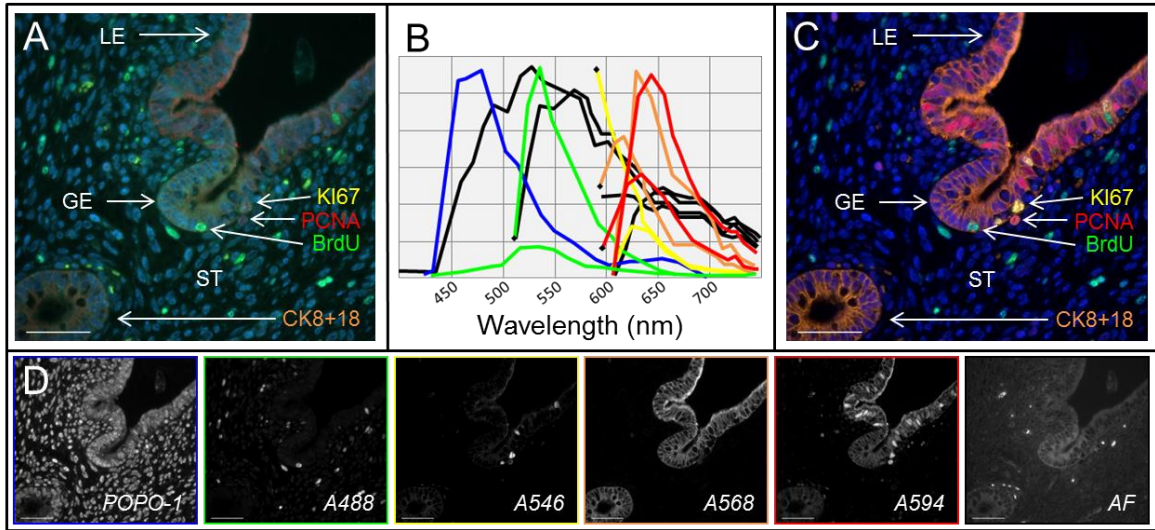


**Figure 21.** *MSI Process.*

*Uterine tissue cross-sections were subjected to multi-target IHC labeling procedures and imaged using a Nuance FX MSI system. Raw images (A) were spectrally unmixed using a spectral library (B) which removed total image autofluorescence (AF) and revealed the unmixed composite image (C). Wavelength-specific data (D) for POPO-1 (left), A488, A546, A568, A594, and AF (right) were extracted from each captured image. Original magnification, 40X. Scale bar = 50 $\mu$ m.*

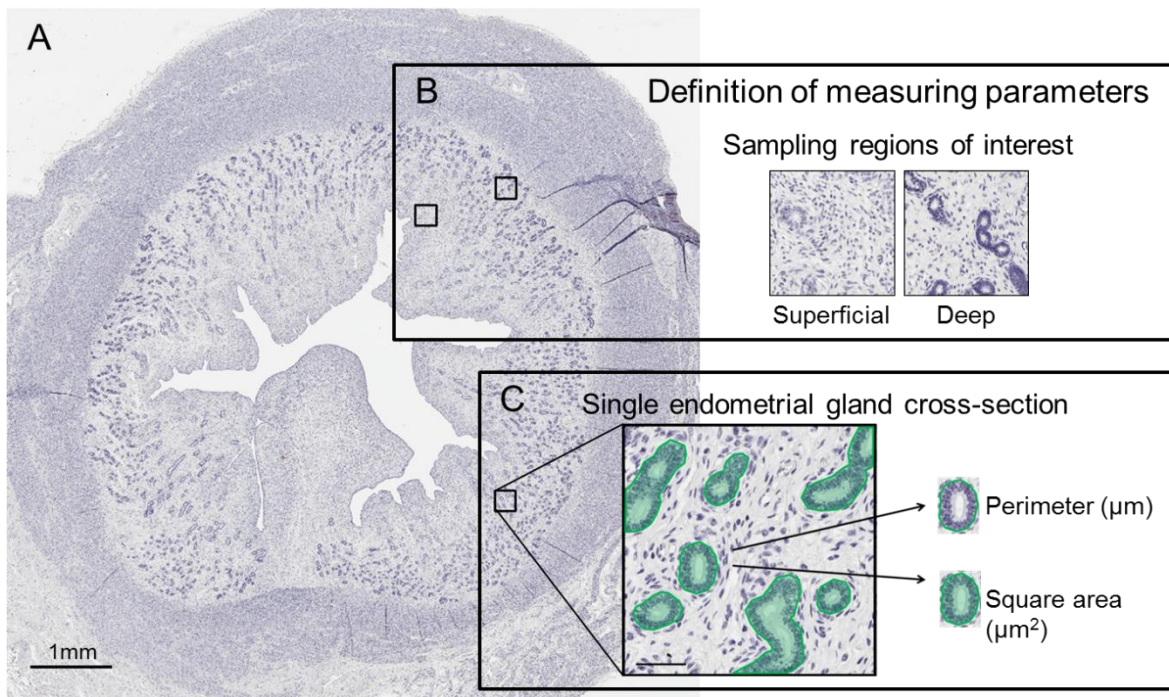


**Figure 22.** Use of VisioPharm Software to Quantify Endometrial Glandularity in Bovine Endometrium

Images of uterine cross-sections (A) were loaded and regions of interest in the endometrium (superficial and deep) were identified (B). Within each region of interest endometrial gland cross-sections were defined through manual instruction and automated classification (C). Measurements were collected for endometrial gland cross-sections including mean perimeter, square area and gland density. Scale bar = 50 $\mu\text{m}$ .

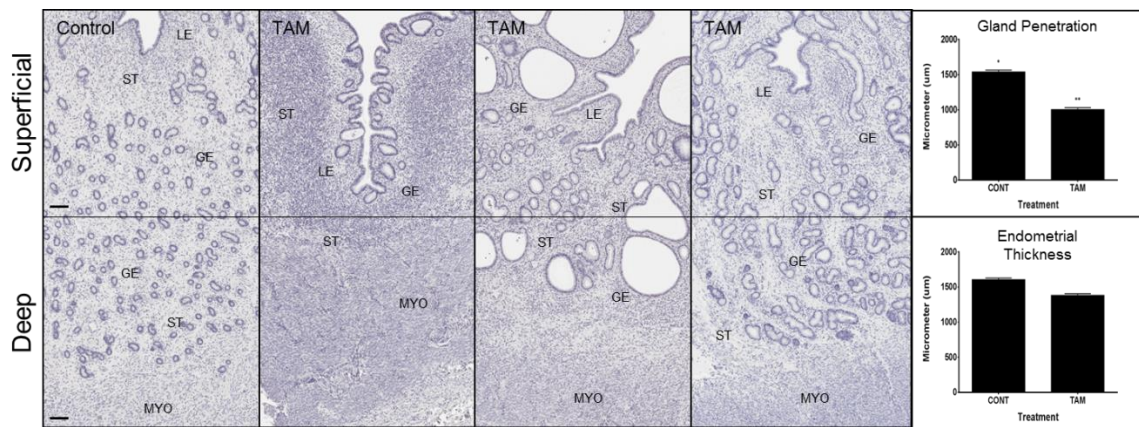


**Figure 23.** *Endometrial Histoarchitecture affected by TAM*

Photomicrographs of hematoxylin stained tissue sections depict superficial (A-D) and deep (F-I) zones of bovine uterine endometrium on PND 120 for vehicle- (A, F) or TAM-treated animals (B-D, G-I). On PND 120 endometrial gland penetration depth (E) was reduced ( $P<0.05$ ) in TAM-treated animals. However, endometrial thickness was not affected by treatment with TAM (J). Original magnification 20X, scale bar = 50 $\mu$ m.

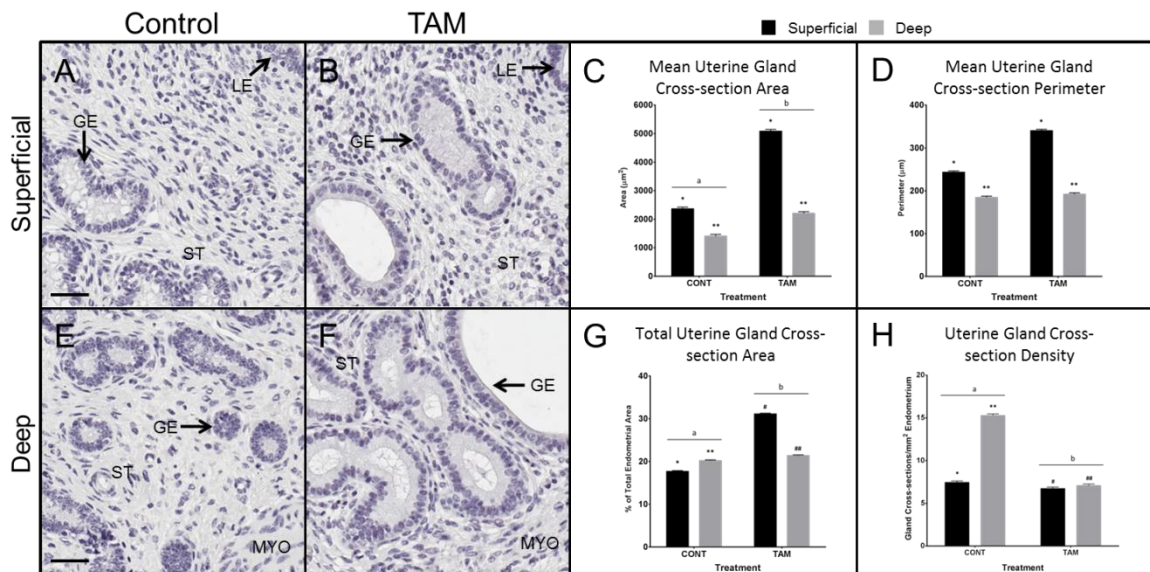


**Figure 24. TAM affects Gland Morphogenesis**

Photomicrographs of hematoxylin stained bovine endometrium depict superficial (A, B) and deep (E, F) zones of vehicle- (A, E) and TAM-treated (B, F) animals. Average (C) endometrial gland cross-section area was larger ( $P<0.05$ ) in TAM-treated animals on PND 120. Average area (C) and perimeter (D) for individual endometrial gland cross-sections were larger ( $P<0.01$ ) in superficial zones in both groups. Treatment with TAM did not affect average endometrial gland cross-section perimeter (D). Total endometrial gland cross-section area (G) was greater ( $P<0.1$ ) in TAM-treated animals. However, endometrial gland cross-section density was reduced ( $P<0.05$ ) by TAM treatment. There was a treatment x zone interaction for total endometrial gland cross-section area and density values ( $P<0.05$ ). Scale bar = 50  $\mu\text{m}$ .

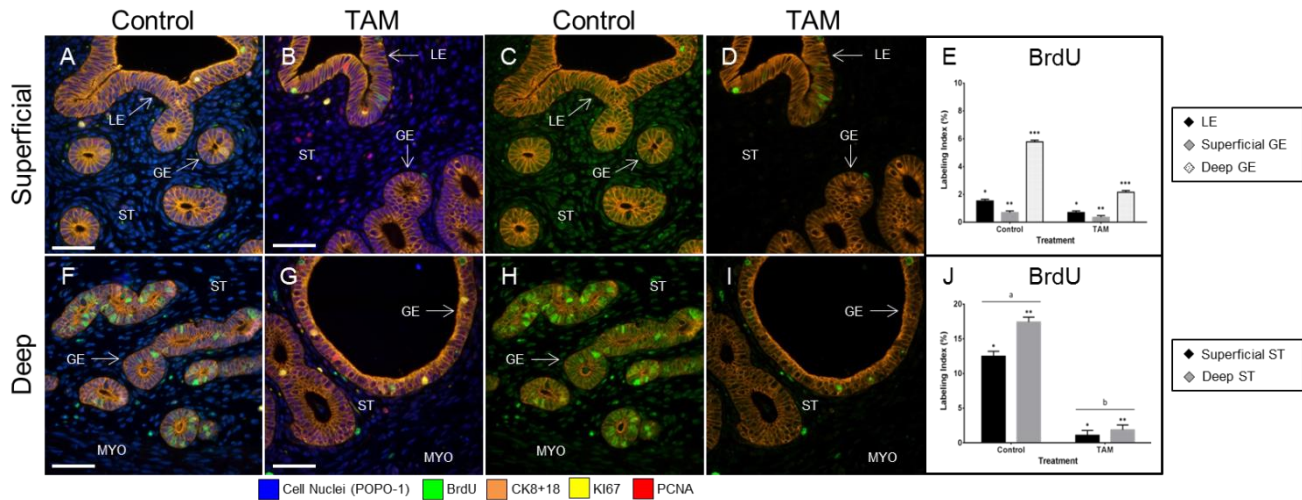


**Figure 25. Compartment-specific Localization of BrdU**

Spectrally unmixed composite images depict superficial (A,B) and deep (F,G) zones of bovine endometrium in vehicle- (A,F) and TAM-treated animals (B,G) labeled for cell nuclei (POPO-1) in blue, BrdU in green, CK8 in orange, KI67 in yellow and PCNA in red. Wavelength-specific images for nuclear BrdU and structural CK8 are shown for superficial (C, D) and deep (H, I) zones of vehicle-(C, H) and TAM-treated animals (D, I). Nuclear LI (%) for BrdU (E) was greater in deep GE as compared to superficial GE and LE ( $P<0.05$ ). Treatment with TAM did not affect BrdU staining in LE, superficial or deep GE. Neither KI67 nor PCNA LI were affected by TAM (data not shown). Stromal BrdU LI (J) was reduced in TAM-treated animals ( $P<0.1$ ). Overall, BrdU LI was greater in deep than in superficial ST ( $P<0.05$ ). Original magnification 40X, scale bar = 50 $\mu$ m.

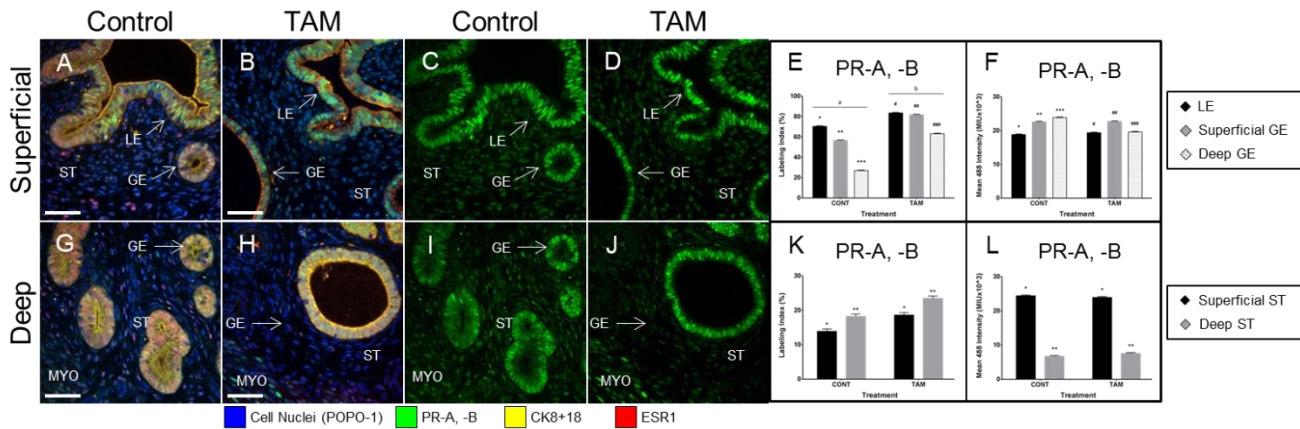


**Figure 26. TAM affects Compartment-specific Expression of PR protein (-A, -B forms)**

Spectrally unmixed composite images depict superficial (A,B) and deep (G,H) zones of bovine endometrium for vehicle- (A,G) and TAM-treated animals (B,H) labeled for cell nuclei (POPO-1) in blue, PR in green, CK8 in yellow and ESR1 in red. Wavelength-specific images for nuclear PR in green for superficial (C, D) and deep (I, J) areas of vehicle-(C, I) and TAM-treated (D, J) animals. Treatment with TAM increased PR LI (E;  $P<0.0001$ ) for LE, and both superficial and deep GE without affecting signal intensity indicative of PR expression (F). Nuclear LI (E) for PR was greatest in LE as compared to superficial and deep GE ( $P<0.0001$ ), while PR signal (F) was highest in deep GE in comparison to superficial GE and LE ( $P<0.0005$ ). A treatment x cell interaction was detected for both PR LI (E) and signal intensity (F) in superficial zones of bovine endometrium ( $P<0.05$ ). TAM did not affect PR LI (K) or signal (L) in deep endometrial areas. PR LI (K) was greater in deep ST ( $P<0.05$ ), while PR signal was greater in superficial ST ( $P<0.0001$ ). Original magnification 40X, scale bar = 50 $\mu$ m.

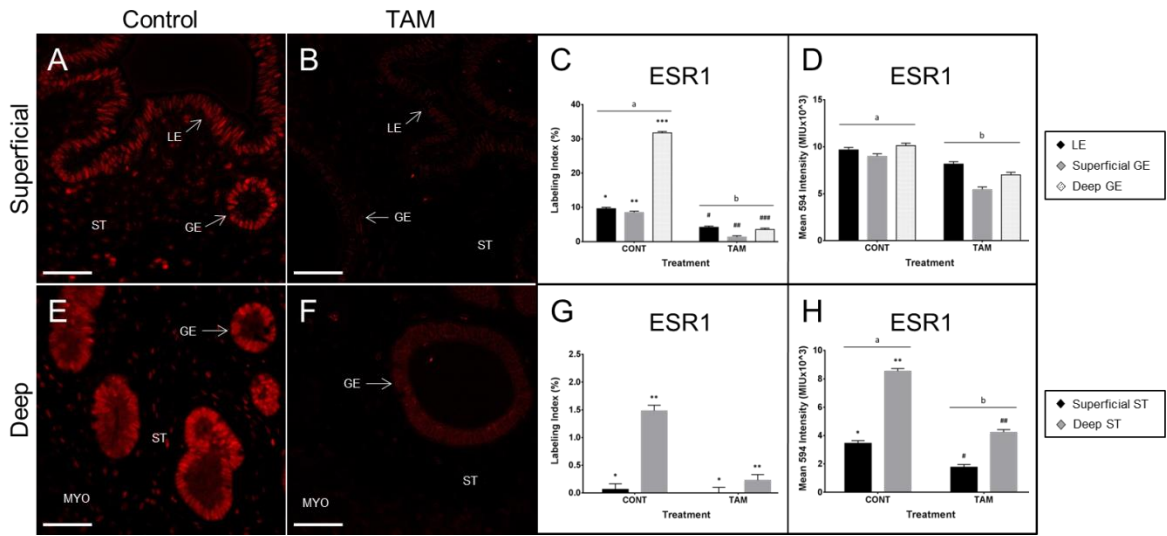


**Figure 27.** *TAM affects Compartment-specific Expression of ESR1*

Spectrally unmixed wavelength-specific images for nuclear ESR1 are shown for superficial (A, B) and deep (E, F) zones of vehicle-(A, E) and TAM-treated animals (B, F). Treatment with TAM reduced ESR1 LI (C) and signal intensity indicative of ESR1 expression (D) for LE, superficial and deep GE ( $P<0.0001$ ). ESR1 LI (C) was highest in deep GE ( $P<0.001$ ), and a treatment x cell compartment interaction was identified ( $P<0.001$ ). Nuclear LI (G) for ESR1 was greater in deep ST ( $P<0.05$ ) than in shallow ST. Treatment with TAM reduced ( $P<0.05$ ) stromal ESR1-specific signal intensity (H). However, ESR1 signal (H) was greater in deep ST ( $P<0.0001$ ), and a treatment x cell compartment interaction was identified ( $P<0.05$ ). Original magnification 40X, scale bar = 50 $\mu$ m.

## **Appendix A.**

### **Immunohistochemistry**

#### ***Materials:***

1. ESR1: Santa Cruz Biotechnology mouse monoclonal C-311; 1:100
2. PR (-A, -B): Thermo Scientific mouse monoclonal hPR<sub>A</sub> 2 + hPR<sub>A</sub> 3; 1:100
3. CK8: Abcam rabbit polyclonal; 1:50
4. CK8: Abcam mouse monoclonal 1E8; 1:100
5. CK8+18: Fitzgerald Industries International guinea pig polyclonal; 1:250
6. BrdU: Roche mouse monoclonal BMC 9318; 1:100
7. KI67: Abcam rabbit monoclonal SP6; 1:100
8. Alexa Fluor 488: Invitrogen Corporation goat anti-mouse IgG<sub>1</sub>; 1:400
9. Alexa Fluor 546: Invitrogen Corporation goat anti-rabbit; 1:400
10. Alexa Fluor 594: Invitrogen Corporation goat anti-mouse IgG<sub>2a</sub>; 1:400
11. POPO<sup>TM</sup>-1 iodide: Invitrogen Corporation; 1:10
12. DMSO
13. VectaShield Mounting Medium for Fluorescence: Vector Laboratories
14. Mouse IgG: Vector Laboratories
15. Goat Serum: Vector Laboratories
16. 1X PBS
17. Hemo-De

18. 100% ETOH, 95% ETOH, 70% ETOH
19. Citric Acid-mono hydrate
20. Sodium citrate dehydrate

**Procedure:** (as adapted from Clemson University Immunohistochemical procedures and protocols)

1. Section tissues at 4-6 um thick.
2. Mount 2-5 non-sequential sections on VWR Superfrost®Plus glass slides.
3. Allow slides to dry overnight.
4. To deparaffinize slides:
  - a. Prepare 2 containers Hemo-De, 2 containers 100% ETOH, 2 containers 95% ETOH, 1 container 75% ETOH, and 1 container distilled H<sub>2</sub>O.
  - b. Submerge slides for 3 minutes in each container sequentially.
5. Boil in 600 ml of 10mM Citrate buffer pH 6.0 for 15 minutes.
  - a. Preparation of Citric Acid buffer (pH 6.0)
    - i. Combine 10.8 ml of stock 1M citric acid monohydrate (FW 210.14) with 49.2 ml of stock 0.1M sodium citrate dehydrate (FW 294.1)
    - ii. Add dH<sub>2</sub>O to approximately 450ml in a graduated cylinder
    - iii. pH to 6.0 with sodium hydroxide (~5M)
    - iv. Bring volume to 600ml (This volume is the needed amount to cover standing slides in a 1L beaker)
6. Cool in Citrate buffer for 15 minutes.
7. Wash in 1X PBS 2 times for 3 minutes each.
  - a. Prepare 2 containers of 1X PBS.
8. Circle individual sections with immuopen.
9. Block with 10% non-immune goat serum for 20 minutes.

10. Apply primary antibody
11. Wash slides in 1X PBS 2 times for 3 minutes each.

\*Remaining steps must be done with limited light\*
12. Apply secondary antibody
13. Wash in 1X PBS 2 times for 3 minutes each.
14. Apply POPO<sup>TM</sup>-1 (Invitrogen Corporation; 1:10 in DMSO) counterstain for 15 minutes.
15. Wash in 1X PBS 2 times for 3 minutes each.

## **Appendix B.**

### **Multispectral Imaging of Uterine Tissues**

#### ***Protocol:* Set Up**

1. Settings of Acquire/Fluorescence tab
  - a. Binning And Region Of Interest box
    - i. Set Binning to 1X1
    - ii. Set ROI to Full
  - b. Filter/Wavelength Selection
    - i. Check the Narrow box
2. Determine filter cube set
  - a. Under the Acquire/Fluorescence tab/Multi Filter Support box add desired filter cubes in order of acquisition preference
3. Pull lever (located on ocular head) out
4. Focus on sample using the FITC equivalent filter cube using digital computer monitor screen
5. Click *Autoexpose Cube* in the Wavelength and Exposure panel box
6. Click *Acquire Cube* (Software will prompt the filter cube turret position, adjust as directed)
7. Record exposure times for each filter cube
  - a. Right click captured image
  - b. Scroll down to cube info
8. Save protocol

- a. Click File
- b. Scroll down to Save protocol

## Spectral Library Set Up

### ***Materials:***

1. Single-labeled tissue sections for desired targets
  - a. For example: with a goal of capturing 4 fluorescent signals for A, B, C, and blue cell nuclei counterstain targets one should prepare a single slide labeled for:
    - i. A + secondary antibody
    - ii. B + secondary antibody
    - iii. C + secondary antibody
    - iv. Blue nuclei counterstain
    - v. Autofluorescence, AF (only secondary antibodies applied)

### ***Procedure: Creating a spectral library***

1. Load protocol (using the protocol set up for acquisition of multiple labels) under the File drop down menu located at the top of the window
2. Capture sample image for each preparation
  - a. Pull lever (located on ocular head) out
  - b. Focus on sample using the FITC equivalent filter cube using digital computer monitor screen
  - c. Click *Acquire Cube* (Software will prompt the filter cube turret position, adjust as directed)
  - d. Save Cube (Click Save Cube icon on top tool bar and name accordingly)
3. Sampling fluorescent signals from captured cube images
  - a. Select Spectra tab
  - b. Load Cube of desired single labeled signal

- c. Click the pencil icon located next to the first listing
  - d. Sample signal
    - i. Using the pencil, hold down the left mouse button and drag the cursor over the labeled target specific to that preparation
    - ii. Name the sampled signal as signal\_mix in the space provided
      1. The signal sampled here is a mix of the target signal and AF
    - iii. Repeat until all single labeled preparations are sampled (including AF)
4. Removing AF from sampled signals
  - a. Click Manual Compute Spectra
  - b. In the top window scroll down and select AF profile
  - c. In the next window select your desired target signal profile
    - i. The result will appear in the bottom window
    - ii. Rename to signal\_pure
    - iii. Click transfer to library
    - iv. Repeat for all signals
5. Save Spectral Library
  - a. Click File
  - b. Scroll down to Save Spectral Library

## Spectral Unmixing IM3 Files to Component Data Files

### ***Materials***

1. Cube IM3 files
2. Saved Spectral Library

### ***Procedure: Setting up spectral unmixing Batch Processing***

1. Set up and Save Colocalization settings
  - a. Click Co-localization icon in top tool bar

- b. Settings
    - i. Select the “Display” tab
    - ii. Click Raw scale
  - c. Save settings: do not include spaces or underscore markings in title
    - i. Click File
    - ii. Scroll down to Save Colocalization settings
2. Click Tools
- a. Scroll down to Batch
  - b. Settings
    - i. Choose Spectra box
      - 1. Click Load and select the spectral library previously set up
    - ii. Measurement Options box
      - 1. Check No Measurements (Unmix only)
    - iii. Co-localization Options box
      - 1. Check Measure Co-localization
      - 2. Click Load and select the Colocalization settings previously saved
    - iv. Save Options box
      - 1. Uncheck Unmixed results sets
      - 2. Check Component Images
      - 3. Check Co-localization Images
    - v. Choose Cubes box
      - 1. Click Find Candidate Cubes and select file of desired IM3 files
      - 2. Once all candidate cubes are listed in the left-hand panel click Add

- a. All candidate cubes should have moved over to the right-hand panel
- b. Click Clear Candidate Cubes
- c. Click Run Batch
  - i. *Go to lunch/home...this will take a while*

## **Appendix C.**

### **Digital Image Analysis: CellProfiler™ Analyses of Fluorescent Signals**

All pipeline files can be found at [http://www.cellprofiler.org/published\\_pipelines.shtml](http://www.cellprofiler.org/published_pipelines.shtml)

#### ***Materials***

1. CellProfiler™ Image Analysis software (downloaded [www.cellprofiler.com](http://www.cellprofiler.com))
2. CellProfiler™ Analyst software (downloaded [www.cellprofiler.com](http://www.cellprofiler.com))
3. Spectrally unmixed component data files
4. Identified input folder
5. Identified output folder

#### ***Procedure:* CellProfiler™ pipeline modules**

#### **Technology Establishment and Validation:** no rule filter

**Aim:** Using CellProfiler™ wavelength-specific image data sets were uploaded, epithelial (LE+GE) and stromal cell compartments were identified using CK8 mask (direct and inverted, respectively), cell nuclei were identified within each cell compartment, measurements of signal intensity were collected and data sets were exported for SAS analysis.

#### ***Pipeline name: EPI vs ST***

1. Load Images
  - a. Loads and extracts metadata from first component image in image set
2. Load Single Image

- a. Loads a single image for use in all image cycles
- 3. Apply Threshold
  - a. Sets pixel intensities below or above a certain threshold to zero producing a binary image for component image corresponding to AlexaFluor 488
- 4. Apply Threshold
  - a. Repeated for component image corresponding to AlexaFluor 546
- 5. Apply Threshold
  - a. Repeated for component image corresponding to POPO-1
- 6. Apply Threshold
  - a. Repeated for component image corresponding to AlexaFluor 594
- 7. Image Math
  - a. Performs basic mathematical operations on image intensities
  - b. Binary images produced from ‘Apply Threshold’ modules for component images corresponding to AlexaFluor 488, 546, 594 and POPO-1 were added and renamed ‘total’
- 8. Mask Image
  - a. Hides certain portions of an image (based on previously identified objects or a binary image) so they are ignored by subsequent mask-respecting modules in the pipeline
  - b. The ‘total’ binary image produced from Image Math was applied to the component image corresponding to AlexaFluor 488 to remove excess background noise
- 9. Mask Image
  - a. Repeated for component image corresponding to AlexaFluor 546
- 10. Mask Image
  - a. Repeated for component image corresponding to AlexaFluor 594

11. Identify Primary Objects

- a. Identifies objects in an image
- b. The component image corresponding to AlexaFluor 594 was used to identify the epithelium
- c. The component image corresponding to AlexaFluor 594 targets Cytokeratin 8, unique structural protein of epithelial cells

12. Expand or Shrink Objects

- a. Expands or shrinks objects by a defined distance

13. Convert Objects to Image

- a. Converts objects you have identified into an image

14. Mask Image

- a. Resulting image from ‘Convert Objects to Image’ was applied as a mask to the component image corresponding to cell nuclei (POPO-1) to hide all stromal nuclei

15. Measure Object Intensity

- a. Measures several intensity features for identified objects

16. Measure Object Size Shape

- a. Measures several area and shape features of identified objects

17. Measure Correlation

- a. Measures the correlation between intensities in different images (e.g., different color channels) on a pixel-by-pixel basis, within identified objects or across an entire image

18. Measure Granularity

- a. Outputs spectra of size measurements of the textures in the image

19. Measure Texture

- a. Measures the degree and nature of textures within objects (versus smoothness)

20. Overlay Outlines

- a. Places outlines produced by an Identify module over a desired image

21. Save Images

- a. Saves images or movie files

22. Export to Database

- a. Exports data directly to a database, or in database readable format, including an imported file with column names and a CellProfiler™ Analyst properties file
- b. Select One Table per Object Type

23. Export to Spreadsheet

- a. Exports measurements into one or more files that can be opened in Excel or other spreadsheet programs
- b. This is especially helpful when metadata is used

**Bovine Endometrial Development:** rule filter included

**Aim:** Using CellProfiler™ wavelength-specific image data sets were uploaded, cell nuclei were identified, measurements of signal intensity for all signals (PR (-A, -B forms), BrdU and CK8) were collected and data sets were exported for CellProfiler™ Analyst.

***Pipeline name: Total nuclei***

1. Load Images

- a. Loads and extracts metadata from first component image in image set

2. Load Single Image

- a. Loads a single image for use in all image cycles
- 3. Apply Threshold
  - a. Sets pixel intensities below or above a certain threshold to zero producing a binary image for component image corresponding to AlexaFluor 488
- 4. Apply Threshold
  - a. Repeated for component image corresponding to AlexaFluor 546
- 5. Apply Threshold
  - a. Repeated for component image corresponding to POPO-1
- 6. Apply Threshold
  - a. Repeated for component image corresponding to AlexaFluor 594
- 7. Image Math
  - a. Performs basic mathematical operations on image intensities
  - b. Binary images produced from ‘Apply Threshold’ modules for component images corresponding to AlexaFluor 488, 546, 594 and POPO-1 were added and renamed ‘total’
- 8. Mask Image
  - a. Hides certain portions of an image (based on previously identified objects or a binary image) so they are ignored by subsequent mask-respecting modules in the pipeline
  - b. The ‘total’ binary image produced from Image Math was applied to the component image corresponding to AlexaFluor 488 to remove excess background noise
- 9. Mask Image
  - a. Repeated for component image corresponding to AlexaFluor 546
- 10. Mask Image
  - a. Repeated for component image corresponding to AlexaFluor 594

11. Identify Primary Objects

- a. Identifies objects in an image
- b. The image corresponding to step 14 was used to identify all nuclei

12. Measure Object Intensity

- a. Measures several intensity features for identified objects

13. Measure Object Size Shape

- a. Measures several area and shape features of identified objects

14. Measure Correlation

- a. Measures the correlation between intensities in different images (e.g., different color channels) on a pixel-by-pixel basis, within identified objects or across an entire image

15. Measure Granularity

- a. Outputs spectra of size measurements of the textures in the image

16. Measure Texture

- a. Measures the degree and nature of textures within objects (versus smoothness)

17. Overlay Outlines

- a. Places outlines produced by an Identify module over a desired image

18. Save Images

- a. Saves images or movie files

19. Export to Database

- a. Exports data directly to a database, or in database readable format, including an imported file with column names and a CellProfiler™ Analyst properties file

- b. Select One Table per Object Type

20. Export to Spreadsheet

- a. Exports measurements into one or more files that can be opened in Excel or other spreadsheet programs

## Digital Image Analysis: CellProfiler™ Analyst

**Aim:** Using CellProfiler™ Analyst exported measurement files and thumbnail images from CellProfiler™ were used to identify cell behavior and phenotype.

Before running CellProfiler™ Analyst:

1. Open the ‘properties’ file (for ‘Total’ or both ‘Epithelial’ and ‘Stromal’ CellProfiler™ pipeline runs; depending on method used)
  - a. Input folder will not change
  - b. Output folder will change
2. CellProfiler™ Analyst must be run on the same computer the CellProfiler™ pipelines were executed on to support the path/file information of cubes/thumb nail data
3. Type ‘cellcalls’ into the space provided in the ‘classes’ paragraph

*Procedure: CellProfiler™ Analyst rule definitions*

1. Open CellProfiler™ Analyst from your desktop, when prompted open the (modified) ‘Total nuclei’ properties file saved from previous CellProfiler™ run.
2. Select the Classifier icon on the tool bar
3. Edit color assignment of wavelength-specific channels (i.e. select original\_488, using drop down menu select green)
4. Select View from tool bar to adjust size of thumbnails
5. Assign bins located at the bottom of the window
  - a. Start with all desired categories: PR-positive, BrdU-positive, PR+BrdU-positive, and negative

6. Select the number of thumbnails to view in the window next to ‘Fetch’ (100 is suggested)
7. Click ‘Fetch!’
8. 100 thumbnails from your experiment will appear in the ‘unclassified cells’ window
  - a. Click and drag thumbnails to desired bins
9. Once you’ve identified some cells in each category click ‘Train Classifier’
  - a. This will build an algorithm based on your selections
  - b. The ‘rules’ or definitions created by manual cell sorting will appear in the window above the thumbnails
    - i. Be sure to exclude any ‘rules’ that include size, shape, location etc. (the focus of the algorithm must be on signal intensity measurements only to allow downstream application in CellProfiler™)
10. Once you’ve identified 10-15 cells in each category test your algorithm by selecting ‘Check Progress’
  - a. A window displaying a line graph named ‘cross validation accuracy’ will appear
  - b. As per the CellProfiler™ manual: a cross validation accuracy of 80% or more should be aimed for if 2 bins are used, if 3 or more bins are used a cross validation accuracy of 90% or more should be aimed for.
11. Return to the Classifier window and save your workspace by File>Save Workspace
12. Open saved workspace and for each category select the thumbnails in the other bins and move them to the ‘negative bin’ so there is only a positive bin and a negative bin. This method insures that a cell positive for two colocalized signals is not included in the analysis of cells positive for just one of the labeled signals.
  - a. For this experiment the following bin pairs were made:
    - i. PR-positive, PR-negative

- ii. BrdU-positive, BrdU-negative
  - iii. PR+BrDU-positive, PR+BrDU-negative
13. For each positive and negative pair, rerun ‘Check Progress’ and save the cross validation accuracy plot for supplemental material
14. Select and copy ‘rules’ for each positive-negative pair in plain text format
15. Exit CellProfiler™ Analyst

**Pipeline name: Epi with rules (for PR+, BrdU+, PR+Brdu and negative nuclei)**

1. Load Images
  - a. Loads and extracts metadata from first component image in image set
2. Load Single Image
  - a. Loads a single image for use in all image cycles
3. Apply Threshold
  - a. Sets pixel intensities below or above a certain threshold to zero producing a binary image for component image corresponding to AlexaFluor 488
4. Apply Threshold
  - a. Repeated for component image corresponding to AlexaFluor 546
5. Apply Threshold
  - a. Repeated for component image corresponding to POPO-1
6. Apply Threshold
  - a. Repeated for component image corresponding to AlexaFluor 594
7. Image Math
  - a. Performs basic mathematical operations on image intensities
  - b. Binary images produced from ‘Apply Threshold’ modules for component images corresponding to AlexaFluor 488, 546, 594 and POPO-1 were added and renamed ‘total’

8. Mask Image

- a. Hides certain portions of an image (based on previously identified objects or a binary image) so they are ignored by subsequent mask-respecting modules in the pipeline
- b. The ‘total’ binary image produced from Image Math was applied to the component image corresponding to AlexaFluor 488 to remove excess background noise

9. Mask Image

- a. Repeated for component image corresponding to AlexaFluor 546

10. Mask Image

- a. Repeated for component image corresponding to AlexaFluor 594

11. Identify Primary Objects

- a. The component image corresponding to AlexaFluor 546 was used to identify the epithelium
- b. The component image corresponding to AlexaFluor 546 targets Cytokeratin 8, unique structural protein of epithelial cells

12. Expand or Shrink Objects

- a. Expands or shrinks objects by a defined distance

13. Convert Objects to Image

- a. Converts objects you have identified into an image

14. Mask Image

- b. Resulting image from ‘Convert Objects to Image’ was applied as a mask to the component image corresponding to cell nuclei (POPO-1) to hide stromal cell nuclei

15. Identify Primary Objects

- a. The component image corresponding to POPO was used to identify all epithelial (LE and GE) nuclei

16. Measure Object Intensity

- a. Measures several intensity features for identified epithelial objects

17. Measure Object Size Shape

- a. Measures several area and shape features of identified epithelial objects

18. Measure Granularity

- a. Outputs spectra of size measurements of the textures in the image

19. Measure Texture

- a. Measures the degree and nature of textures within epithelial objects (versus smoothness)

20. Measure Correlation

- a. Measures the correlation between intensities in different images (e.g., different color channels) on a pixel-by-pixel basis, within identified epithelial objects or across an entire image

21. Filter Objects

- a. Eliminates objects based on their measurements (e.g., area, shape, texture, intensity)
- b. Select Nuclei, from Identify Primary Objects, to be filtered
- c. Select Rules as the filtering mode
- d. Upload rule file for desired target, each target requires a ‘FilterObjects’ module
- e. Select Class 1 (denoted ‘positive’ class)
- f. Name according to cell compartment and target: Epi\_PR

22. Filter Objects

- a. Same as described above

- b. Name according to cell compartment and target: Epi\_BrdU

23. Filter Objects

- a. Same as described above
- b. Name according to cell compartment and target: Epi\_PRBrdU

24. Filter Objects

- a. Same as described above
- b. Name according to cell compartment and target: Epi\_neg

25. Measure Object Intensity

- b. Measures several intensity features for filtered epithelial objects

26. Measure Object Size Shape

- a. Measures several intensity features for filtered epithelial objects

27. Measure Granularity

- b. Outputs spectra of size measurements of the textures in the image

28. Measure Texture

- b. Measures the degree and nature of textures within filtered epithelial objects  
(versus smoothness)

29. Measure Correlation

- b. Measures the correlation between intensities in different images (e.g.,  
different color channels) on a pixel-by-pixel basis, within filtered epithelial  
objects or across an entire image

30. Overlay Outlines

- a. Places outlines produced by an Identify module over a desired image

31. Save Images

- a. Saves images or movie files
- b. Repeat step 30/31 for each of your desired targets

32. Export to Database

- a. Exports data directly to a database, or in database readable format, including an imported file with column names and a CellProfiler™ Analyst properties file
  - b. No CellProfiler™ Analyst properties file is needed
  - c. Select One Table per Object Type
33. Export to Spreadsheet
- a. Exports measurements into one or more files that can be opened in Excel or other spreadsheet programs

***Pipeline name: St with rules (for PR+, BrdU+, PR+BrdU and negative nuclei)***

\*similar pipeline as above with 14 Mask Image select invert mask to hide epithelial nuclei\*

1. Load Images
  - a. Loads and extracts metadata from first component image in image set
2. Load Single Image
  - a. Loads a single image for use in all image cycles
3. Apply Threshold
  - a. Sets pixel intensities below or above a certain threshold to zero producing a binary image for component image corresponding to AlexaFluor 488
4. Apply Threshold
  - a. Repeated for component image corresponding to AlexaFluor 546
5. Apply Threshold
  - a. Repeated for component image corresponding to POPO-1
6. Apply Threshold
  - a. Repeated for component image corresponding to AlexaFluor 594
7. Image Math
  - a. Performs basic mathematical operations on image intensities

- b. Binary images produced from ‘Apply Threshold’ modules for component images corresponding to AlexaFluor 488, 546, 594 and POPO-1 were added and renamed ‘total’

8. Mask Image

- a. Hides certain portions of an image (based on previously identified objects or a binary image) so they are ignored by subsequent mask-respecting modules in the pipeline
- b. The ‘total’ binary image produced from Image Math was applied to the component image corresponding to AlexaFluor 488 to remove excess background noise

9. Mask Image

- a. Repeated for component image corresponding to AlexaFluor 546

10. Mask Image

- a. Repeated for component image corresponding to AlexaFluor 594

11. Identify Primary Objects

- a. The component image corresponding to AlexaFluor 546 was used to identify the epithelium
- b. The component image corresponding to AlexaFluor 546 targets Cytokeratin 8, unique structural protein of epithelial cells

12. Expand or Shrink Objects

- a. Expands or shrinks objects by a defined distance

13. Convert Objects to Image

- a. Converts objects you have identified into an image

14. Mask Image

- a. Resulting image from ‘Convert Objects to Image’ was applied as an *inverted* mask to the component image corresponding to cell nuclei (POPO-1) to hide epithelial cell nuclei

15. Identify Primary Objects

- a. The component image corresponding to POPO was used to identify all stromal (LE and GE) nuclei

16. Measure Object Intensity

- a. Measures several intensity features for identified stromal objects

17. Measure Object Size Shape

- a. Measures several area and shape features of identified stromal objects

18. Measure Granularity

- a. Outputs spectra of size measurements of the textures in the image

19. Measure Texture

- a. Measures the degree and nature of textures within stromal objects (versus smoothness)

20. Measure Correlation

- a. Measures the correlation between intensities in different images (e.g., different color channels) on a pixel-by-pixel basis, within identified stromal objects or across an entire image

21. Filter Objects

- a. Eliminates objects based on their measurements (e.g., area, shape, texture, intensity)
- b. Select Nuclei, from Identify Primary Objects, to be filtered
- c. Select Rules as the filtering mode
- d. Upload rule file for desired target, each target requires a ‘FilterObjects’ module

- e. Select Class 1 (denoted ‘positive’ class)
- f. Name according to cell compartment and target: St\_PR

22. Filter Objects

- a. Same as described above
- b. Name according to cell compartment and target: St\_BrdU

23. Filter Objects

- a. Same as described above
- b. Name according to cell compartment and target: St\_PRBrdU

24. Filter Objects

- a. Same as described above
- b. Name according to cell compartment and target: St\_neg

25. Measure Object Intensity

- a. Measures several intensity features for filtered stromal objects

26. Measure Object Size Shape

- a. Measures several intensity features for filtered stromal objects

27. Measure Granularity

- a. Outputs spectra of size measurements of the textures in the image

28. Measure Texture

- a. Measures the degree and nature of textures within filtered stromal objects  
(versus smoothness)

29. Measure Correlation

- a. Measures the correlation between intensities in different images (e.g.,  
different color channels) on a pixel-by-pixel basis, within filtered stromal  
objects or across an entire image

30. Overlay Outlines

- a. Places outlines produced by an Identify module over a desired image

31. Save Images

- a. Saves images or movie files
- b. Repeat step 30/31 for each of your desired targets

32. Export to Database

- a. Exports data directly to a database, or in database readable format, including an imported file with column names and a CellProfiler™ Analyst properties file
- b. No CellProfiler™ Analyst properties file is needed
- c. Select One Table per Object Type

33. Export to Spreadsheet

- a. Exports measurements into one or more files that can be opened in Excel or other spreadsheet programs

**TAM: rule filter included with additional cell compartments identified manually**

**Aim:** Previously build pipelines were modified in order to identify, analyze and compare LE and GE as well as compare shallow and deep endometrial areas. Upgraded CellProfiler™ software was used (CellProfiler™ 2.1.1). The below pipelines/processes were run for antibody combination PR (A488), ESR1 (A594) and CK8 (A568) as well as antibody combination BrdU (A488), KI67 (A546), CK8 (A568) and PCNA (A594).

***Pipeline name: Epi nuclei***

- 1. Images
  - a. Select and drag folder containing component images
- 2. Metadata
  - a. Select Yes to extract metadata
  - b. Select ‘extract from file/folder names’
  - c. Using regular expressions enter field names that correspond to image sets

- i. Example: Animal, Age, Date, Section, Target etc.
  - d. Click the ‘Update’ button to double check work
3. Names and Types
- a. Select Images matching rules in name assignment
  - b. Describe the rule
    - i. Example: File Does Contain 488\_Data
  - c. Identify all wavelength channels of interest (POPO-1, 488, 546, 568, 594) where applicable
4. Groups: this option was not applicable for this data set
5. Apply Threshold
- a. Sets pixel intensities below or above a certain threshold to zero producing a binary image for component image corresponding to AlexaFluor 488, and repeated for additional wavelength channels, where appropriate
6. Apply Threshold
- a. Repeated for component image corresponding to AlexaFluor 546
7. Apply Threshold
- a. Repeated for component image corresponding to AlexaFluor 568
8. Apply Threshold
- a. Repeated for component image corresponding to AlexaFluor 594
9. Apply Threshold
- a. Repeated for component image corresponding to POPO-1
10. Image Math
- a. Performs basic mathematical operations on image intensities
  - b. Binary images produced from ‘Apply Threshold’ modules for component images (corresponding to AlexaFluor 488, 546, 568, 594 and POPO-1) were added and renamed ‘total’

11. Mask Image

- a. Hides certain portions of an image (based on previously identified objects or a binary image) so they are ignored by subsequent mask-respecting modules in the pipeline
- b. The ‘total’ binary image produced from Image Math was applied to the component image corresponding to AlexaFluor 488, and other wavelength channels, where appropriate to remove excess background noise,

12. Mask Image

- a. Repeated for component image corresponding to AlexaFluor 546

13. Mask Image

- a. Repeated for component image corresponding to AlexaFluor 568

14. Mask Image

- a. Repeated for component image corresponding to AlexaFluor 594

15. Mask Image

- a. Repeated for component image corresponding to POPO-1

16. Identify Primary Objects

- a. The component image corresponding to AlexaFluor 568 was used to identify the epithelium
- b. The component image corresponding to AlexaFluor 568 targets Cytokeratin 8, unique structural protein of epithelial cells

17. Expand or Shrink Objects

- a. Expands or shrinks objects by a defined distance

18. Convert Objects to Image

- a. Converts objects you have identified into an image

19. Mask Image

- a. Resulting image from ‘Convert Objects to Image’ was applied as a mask to the component image corresponding to cell nuclei (POPO-1) to hide stromal cell nuclei

20. Identify Primary Objects

- a. Identifies objects in an image
- b. The image corresponding to step 14 was used to identify all epithelial nuclei

21. Measure Object Intensity

- a. Measures several intensity features for identified objects

22. Measure Object Size Shape

- a. Measures several area and shape features of identified objects

23. Measure Correlation

- a. Measures the correlation between intensities in different images (e.g., different color channels) on a pixel-by-pixel basis, within identified objects or across an entire image

24. Measure Granularity

- a. Outputs spectra of size measurements of the textures in the image

25. Measure Texture

- a. Measures the degree and nature of textures within objects (versus smoothness)

26. Overlay Outlines

- a. Places outlines produced by an Identify module over a desired image

27. Save Images

- a. Saves images or movie files

28. Export to Database

- a. Exports data directly to a database, or in database readable format, including an imported file with column names and a CellProfiler™ Analyst properties file
- b. Select One Table per Object Type

29. Export to Spreadsheet

- a. Exports measurements into one or more files that can be opened in Excel or other spreadsheet programs

**Pipeline name: St nuclei**

- a. Using the pipeline Epi nuclei, on step 14: Mask Image, select invert mask
- b. Rename, where appropriate
- c. Run as before

Exported properties files, as a result of pipeline *Epi nuclei* and *St nuclei*, should be loaded into CellProfiler™ Analyst and steps 1-14 should be followed to identify rules associated with identified targets. Please see section *CellProfiler™ Analyst rule definitions*.

**Pipeline name: Manual Tracing for LE, GE and St**

1. Images
  - a. Select and drag folder containing component images
2. Metadata
  - a. Select Yes to extract metadata
  - b. Select ‘extract from file/folder names’
  - c. Using regular expressions enter field names that correspond to image sets
    - i. Example: Animal, Age, Date, Section, Target etc.
  - d. Click the ‘Update’ button to double check work
3. Names and Types
  - a. Select Images matching rules in name assignment
  - b. Describe the rule
    - i. Example: File Does Contain 488\_Data
  - c. Identify all wavelength channels of interest (POPO-1, 488, 546, 568, 594) where applicable

4. Groups: this option was not applicable for this data set
5. Apply Threshold
  - a. Sets pixel intensities below or above a certain threshold to zero producing a binary image for component image corresponding to AlexaFluor 488, and repeated for additional wavelength channels, where appropriate
6. Apply Threshold
  - a. Repeated for component image corresponding to AlexaFluor 546
7. Apply Threshold
  - a. Repeated for component image corresponding to AlexaFluor 568
8. Apply Threshold
  - a. Repeated for component image corresponding to AlexaFluor 594
9. Apply Threshold
  - a. Repeated for component image corresponding to POPO-1
10. Image Math
  - a. Performs basic mathematical operations on image intensities
  - b. Binary images produced from ‘Apply Threshold’ modules for component images (corresponding to AlexaFluor 488, 546, 568, 594 and POPO-1) were added and renamed ‘total’
11. Mask Image
  - a. Hides certain portions of an image (based on previously identified objects or a binary image) so they are ignored by subsequent mask-respecting modules in the pipeline
  - b. The ‘total’ binary image produced from Image Math was applied to the component image corresponding to AlexaFluor 488, and other wavelength channels, where appropriate to remove excess background noise
12. Mask Image

- a. Repeated for component image corresponding to additional wavelength channels, where appropriate

13. Identify Primary Objects

- a. The component image corresponding to AlexaFluor 568 was used to identify the epithelium
- b. The component image corresponding to AlexaFluor 568 targets Cytokeratin 8, unique structural protein of epithelial cells

14. Expand or Shrink Objects

- a. Expands or shrinks objects by a defined distance

15. Convert Objects to Image

- a. Converts objects you have identified into an image

16. Identify Objects Manually

- a. Allows you to identify objects in an image by hand rather than automatically
- b. In order to continue to use the automatic processing software and compare LE from GE, this module was used to physically trace the LE and make a separate mask to discern LE from GE

17. Convert Objects to Image

- a. Converts objects you have identified into an image

18. Mask Image

- a. Resulting image from 17 ‘Convert Objects to Image’ was applied as a mask to the component image corresponding to cell nuclei (POPO-1) to hide everything but LE cell nuclei

19. Identify Primary Objects

- a. Identifies objects in an image
- b. The image corresponding to step 18 was used to identify LE nuclei

20. Measure Object Intensity

- a. Measures several intensity features for identified objects

21. Measure Object Size Shape

- a. Measures several area and shape features of identified objects

22. Measure Granularity

- a. Outputs spectra of size measurements of the textures in the image

23. Measure Texture

- a. Measures the degree and nature of textures within objects (versus smoothness)

24. Measure Correlation

- a. Measures the correlation between intensities in different images (e.g., different color channels) on a pixel-by-pixel basis, within identified objects or across an entire image

25. Filter Objects

- a. Eliminates objects based on their measurements (e.g., area, shape, texture, intensity)
- b. Select Nuclei, from Identify Primary Objects, to be filtered
- c. Select Rules as the filtering mode
- d. Upload rule file for desired target, each target requires a ‘Filter Objects’ module
- e. Select Class 1 (denoted ‘positive’ class)
- f. Name according to cell compartment and target: LE\_Target

26. Filter Objects

- a. Same as described above, repeat for each additional target or target combination

27. Filter Objects

- a. Select Class 2 for negative cells

28. Measure Object Intensity

- a. Measures several intensity features for filtered objects

29. Measure Object Size Shape

- a. Measures several area and shape features of filtered objects

30. Measure Granularity

- a. Outputs spectra of size measurements of the textures in the image

31. Measure Texture

- a. Measures the degree and nature of textures within filtered objects (versus smoothness)

32. Measure Correlation

- a. Measures the correlation between intensities in different images (e.g., different color channels) on a pixel-by-pixel basis, within identified objects or across an entire image

33. Overlay Outlines

- a. Places outlines produced by an Identify module over a desired image

34. Save Images

- a. Saves images or movie files
- b. Repeat 36/37 for each target filtered

35. Mask Image

- a. Load Image of cell nuclei (POPO) from 12 Mask Image module
- b. Select resulting image from Mask Image module that corresponds to cell nuclei counter stain (i.e. POPO)

36. Mask Image

- a. Load image from previous (35) Mask Image
- b. Using the LE mask from 17 Convert Objects to Image select invert mask to hide all cell nuclei but GE

37. Identify Primary Objects

- a. Identifies objects in an image
- b. The image corresponding to step 36 was used to identify GE nuclei

38. Measure Object Intensity

- a. Measures several intensity features for identified objects

39. Measure Object Size Shape

- a. Measures several area and shape features of identified objects

40. Measure Granularity

- a. Outputs spectra of size measurements of the textures in the image

41. Measure Texture

- a. Measures the degree and nature of textures within objects (versus smoothness)

42. Measure Correlation

- a. Measures the correlation between intensities in different images (e.g., different color channels) on a pixel-by-pixel basis, within identified objects or across an entire image

43. Filter Objects

- a. Eliminates objects based on their measurements (e.g., area, shape, texture, intensity)
- b. Select Nuclei, from Identify Primary Objects, to be filtered
- c. Select Rules as the filtering mode
- d. Upload rule file for desired target, each target requires a ‘Filter Objects’ module
- e. Select Class 1 (denoted ‘positive’ class)
- f. Name according to cell compartment and target: GE\_Target

44. Filter Objects

- a. Same as described above, repeat for each additional target or target combination

45. Filter Objects

- a. Select Class 2 for negative cells

46. Measure Object Intensity

- a. Measures several intensity features for filtered objects

47. Measure Object Size Shape
  - a. Measures several area and shape features of filtered objects
48. Measure Granularity
  - a. Outputs spectra of size measurements of the textures in the image
49. Measure Texture
  - a. Measures the degree and nature of textures within filtered objects (versus smoothness)
50. Measure Correlation
  - a. Measures the correlation between intensities in different images (e.g., different color channels) on a pixel-by-pixel basis, within identified objects or across an entire image
51. Overlay Outlines
  - a. Places outlines produced by an Identify module over a desired image
52. Save Images
  - a. Saves images or movie files
  - b. Repeat 51/52 for each target filtered
53. Mask Image
  - a. Resulting image from 15 ‘Convert Objects to Image’ was applied as a mask to the component image corresponding to cell nuclei (POPO-1) to hide everything but St
54. Identify Primary Objects
  - a. Identifies objects in an image
  - b. The image corresponding to step 17 was used to identify St nuclei
55. Measure Object Intensity
  - a. Measures several intensity features for identified objects
56. Measure Object Size Shape

- a. Measures several area and shape features of identified objects

57. Measure Granularity

- a. Outputs spectra of size measurements of the textures in the image

58. Measure Texture

- a. Measures the degree and nature of textures within objects (versus smoothness)

59. Measure Correlation

- a. Measures the correlation between intensities in different images (e.g., different color channels) on a pixel-by-pixel basis, within identified objects or across an entire image

60. Filter Objects

- a. Eliminates objects based on their measurements (e.g., area, shape, texture, intensity)
- b. Select Nuclei, from Identify Primary Objects, to be filtered
- c. Select Rules as the filtering mode
- d. Upload rule file for desired target, each target requires a ‘Filter Objects’ module
- e. Select Class 1 (denoted ‘positive’ class)
- f. Name according to cell compartment and target: St\_Target

61. Filter Objects

- a. Same as described above, repeat for each additional target or target combination

62. Filter Objects

- a. Select Class 2 for negative cells

63. Measure Object Intensity

- a. Measures several intensity features for filtered objects

64. Measure Object Size Shape

- a. Measures several area and shape features of filtered objects

65. Measure Granularity

- a. Outputs spectra of size measurements of the textures in the image

66. Measure Texture

- a. Measures the degree and nature of textures within filtered objects (versus smoothness)

67. Measure Correlation

- a. Measures the correlation between intensities in different images (e.g., different color channels) on a pixel-by-pixel basis, within identified objects or across an entire image

68. Overlay Outlines

- a. Places outlines produced by an Identify module over a desired image

69. Save Images

- a. Saves images or movie files
- b. Repeat 68/69 for each target filtered

70. Export to Database

- a. Exports data directly to a database, or in database readable format, it is not necessary to include an imported file with column names and a CellProfiler<sup>TM</sup> Analyst properties file
- b. Select One Table per Object Type

71. Export to Spreadsheet

- a. Exports measurements into one or more files that can be opened in Excel or other spreadsheet programs

***Pipeline name: Manual Tracing for GE, St and Myo***

1. Images

- a. Select and drag folder containing component images

2. Metadata

- a. Select Yes to extract metadata
  - b. Select ‘extract from file/folder names’
  - c. Using regular expressions enter field names that correspond to image sets
    - i. Example: Animal, Age, Date, Section, Target etc.
  - d. Click the ‘Update’ button to double check work
3. Names and Types
  - a. Select Images matching rules in name assignment
  - b. Describe the rule
    - i. Example: File Does Contain 488\_Data
  - c. Identify all wavelength channels of interest (POPO-1, 488, 546, 568, 594) where applicable
4. Groups: this option was not applicable for this data set
5. Apply Threshold
  - a. Sets pixel intensities below or above a certain threshold to zero producing a binary image for component image corresponding to AlexaFluor 488, and repeated for additional wavelength channels, where appropriate
6. Apply Threshold
  - a. Repeated for component image corresponding to AlexaFluor 546
7. Apply Threshold
  - a. Repeated for component image corresponding to AlexaFluor 568
8. Apply Threshold
  - a. Repeated for component image corresponding to AlexaFluor 594
9. Apply Threshold
  - a. Repeated for component image corresponding to POPO-1
10. Image Math
  - a. Performs basic mathematical operations on image intensities

- b. Binary images produced from ‘Apply Threshold’ modules for component images (corresponding to AlexaFluor 488, 546, 568, 594 and POPO-1) were added and renamed ‘total’

#### 11. Mask Image

- a. Hides certain portions of an image (based on previously identified objects or a binary image) so they are ignored by subsequent mask-respecting modules in the pipeline
- b. The ‘total’ binary image produced from Image Math was applied to the component image corresponding to AlexaFluor 488, and other wavelength channels, where appropriate to remove excess background noise

#### 12. Mask Image

- a. Repeated for component image corresponding to additional wavelength channels, where appropriate

#### 13. Identify Primary Objects

- a. The component image corresponding to AlexaFluor 568 was used to identify the epithelium
- b. The component image corresponding to AlexaFluor 568 targets Cytokeratin 8, unique structural protein of epithelial cells

#### 14. Expand or Shrink Objects

- a. Expands or shrinks objects by a defined distance

#### 15. Convert Objects to Image

- a. Converts objects you have identified into an image

#### 16. Identify Objects Manually

- a. Allows you to identify objects in an image by hand rather than automatically
- b. In order to continue to use the automatic processing software and compare deep GE from St and Myo, this module was used to physically trace the Myo

17. Convert Objects to Image

- a. Converts objects you have identified into an image

18. Mask Image

- a. Resulting image from 17 ‘Convert Objects to Image’ was applied as a mask to the component image corresponding to cell nuclei (POPO-1) to hide everything but stromal cell nuclei

19. Identify Primary Objects

- a. Identifies objects in an image
- b. The image corresponding to step 18 was used to identify stromal nuclei

20. Measure Object Intensity

- a. Measures several intensity features for identified objects

21. Measure Object Size Shape

- a. Measures several area and shape features of identified objects

22. Measure Granularity

- a. Outputs spectra of size measurements of the textures in the image

23. Measure Texture

- a. Measures the degree and nature of textures within objects (versus smoothness)

24. Measure Correlation

- a. Measures the correlation between intensities in different images (e.g., different color channels) on a pixel-by-pixel basis, within identified objects or across an entire image

25. Filter Objects

- a. Eliminates objects based on their measurements (e.g., area, shape, texture, intensity)
- b. Select Nuclei, from Identify Primary Objects, to be filtered
- c. Select Rules as the filtering mode

- d. Upload rule file for desired target, each target requires a ‘Filter Objects’ module
- e. Select Class 1 (denoted ‘positive’ class)
- f. Name according to cell compartment and target: St\_Target

26. Filter Objects

- a. Same as described above, repeat for each additional target or target combination

27. Filter Objects

- a. Select Class 2 for negative cells

28. Measure Object Intensity

- a. Measures several intensity features for filtered objects

29. Measure Object Size Shape

- a. Measures several area and shape features of filtered objects

30. Measure Granularity

- a. Outputs spectra of size measurements of the textures in the image

31. Measure Texture

- a. Measures the degree and nature of textures within filtered objects (versus smoothness)

32. Measure Correlation

- a. Measures the correlation between intensities in different images (e.g., different color channels) on a pixel-by-pixel basis, within identified objects or across an entire image

33. Overlay Outlines

- a. Places outlines produced by an Identify module over a desired image

34. Save Images

- a. Saves images or movie files
- b. Repeat 33/34 for each target filtered

35. Mask Image

- a. Load Image of cell nuclei (POPO) from 12 Mask Image module
- b. Using the LE mask from 17 Convert Objects to Image select invert mask to hide all cell nuclei but GE

36. Identify Primary Objects

- a. Identifies objects in an image
- b. The image corresponding to step 35 was used to identify Myo nuclei

37. Measure Object Intensity

- a. Measures several intensity features for identified objects

38. Measure Object Size Shape

- a. Measures several area and shape features of identified objects

39. Measure Granularity

- a. Outputs spectra of size measurements of the textures in the image

40. Measure Texture

- a. Measures the degree and nature of textures within objects (versus smoothness)

41. Measure Correlation

- a. Measures the correlation between intensities in different images (e.g., different color channels) on a pixel-by-pixel basis, within identified objects or across an entire image

42. Filter Objects

- a. Eliminates objects based on their measurements (e.g., area, shape, texture, intensity)
- b. Select Nuclei, from Identify Primary Objects, to be filtered
- c. Select Rules as the filtering mode
- d. Upload rule file for desired target, each target requires a ‘Filter Objects’ module
- e. Select Class 1 (denoted ‘positive’ class)
- f. Name according to cell compartment and target: Myo\_Target

43. Filter Objects

- a. Same as described above, repeat for each additional target or target combination

44. Filter Objects

- a. Select Class 2 for negative cells

45. Measure Object Intensity

- a. Measures several intensity features for filtered objects

46. Measure Object Size Shape

- a. Measures several area and shape features of filtered objects

47. Measure Granularity

- a. Outputs spectra of size measurements of the textures in the image

48. Measure Texture

- a. Measures the degree and nature of textures within filtered objects (versus smoothness)

49. Measure Correlation

- a. Measures the correlation between intensities in different images (e.g., different color channels) on a pixel-by-pixel basis, within identified objects or across an entire image

50. Overlay Outlines

- a. Places outlines produced by an Identify module over a desired image

51. Save Images

- a. Saves images or movie files
- b. Repeat 50/51 for each target filtered

52. Mask Image

- a. Resulting image from 15 ‘Convert Objects to Image’ was applied as a mask to the component image corresponding to cell nuclei (POPO-1) to hide everything but GE

53. Identify Primary Objects

- a. Identifies objects in an image
- b. The image corresponding to step 18 was used to identify GE nuclei

54. Measure Object Intensity

- a. Measures several intensity features for identified objects

55. Measure Object Size Shape

- a. Measures several area and shape features of identified objects

56. Measure Granularity

- a. Outputs spectra of size measurements of the textures in the image

57. Measure Texture

- a. Measures the degree and nature of textures within objects (versus smoothness)

58. Measure Correlation

- a. Measures the correlation between intensities in different images (e.g., different color channels) on a pixel-by-pixel basis, within identified objects or across an entire image

59. Filter Objects

- a. Eliminates objects based on their measurements (e.g., area, shape, texture, intensity)
- b. Select Nuclei, from Identify Primary Objects, to be filtered
- c. Select Rules as the filtering mode
- d. Upload rule file for desired target, each target requires a ‘Filter Objects’ module
- e. Select Class 1 (denoted ‘positive’ class)
- f. Name according to cell compartment and target: GE\_Target

60. Filter Objects

- a. Same as described above, repeat for each additional target or target combination

61. Filter Objects

a. Select Class 2 for negative cells

62. Measure Object Intensity

a. Measures several intensity features for filtered objects

63. Measure Object Size Shape

a. Measures several area and shape features of filtered objects

64. Measure Granularity

a. Outputs spectra of size measurements of the textures in the image

65. Measure Texture

a. Measures the degree and nature of textures within filtered objects (versus smoothness)

66. Measure Correlation

a. Measures the correlation between intensities in different images (e.g., different color channels) on a pixel-by-pixel basis, within identified objects or across an entire image

67. Overlay Outlines

a. Places outlines produced by an Identify module over a desired image

68. Save Images

a. Saves images or movie files

b. Repeat 67/68 for each target filtered

69. Export to Database

a. Exports data directly to a database, or in database readable format, it is not necessary to include an imported file with column names and a CellProfiler<sup>TM</sup> Analyst properties file

b. Select One Table per Object Type

70. Export to Spreadsheet

- a. Exports measurements into one or more files that can be opened in Excel or other spreadsheet programs

## **Appendix D.**

### **Aperio® ePathology Solutions**

Leica Biosystems: The Pathology Company

#### ***Materials***

1. Slides stained with hematoxylin and coverslipped

**Aim:** Histomorphology; Gland Penetration and Endometrial Thickness measurements

Use Aperio slide scanner and software to measure gland penetration and endometrial thickness in bovine endometrium.

#### ***Procedure: Collecting images***

1. Load slides in 5 slide holder
  - a. Adjust magnification to reflect 40X with Doubler
2. Open Scan Scope Console software
  - a. Enter localhost (one word) into Controller Name box
  - b. Enter username and password
3. Under ‘Start’ tab
  - a. Select first slide
  - b. Click Manual load, and proceed to ‘Scan Area’ tab
4. Under ‘Scan Area’ tab
  - a. Adjust green box to fit tissue section (tip: one cross section at a time)
  - b. Proceed to ‘Focus Points’ tab

5. Under 'Focus Points' tab
  - a. Select Autofocus (optional)
  - b. Click Auto Select
    - i. Always have at least 4-5 focus points per section
    - ii. To add focus points right click tissue over desired area to add and select 'add focus point' from drop down menu
    - iii. Tip: Adjust focus points on edges of tissue slightly inward towards center of tissue
  - c. Proceed to 'Calibrate' tab
6. Under 'Calibrate' tab
  - a. Click Calibrate
    - i. Always have a clear image, no debris, stain or other interfering material
    - ii. Adjust calibration point by returning to 'Scan Area' tab and moving calibration point (blue diamond)
    - iii. When calibration image is appropriate proceed to 'Scan' tab
7. Under 'Scan' tab
  - a. Click Start Scan
  8. Repeat for additional sections on slide at step d
  9. Repeat for additional slides at step c
  10. Avoid 'One Touch' option

*Procedure:* Collecting morphometric data

11. To view digital slides: Open Spectrum login or go to <http://spectrum.vetmed.auburn.edu>
  - a. Click Digital Slides
  - b. Click Continue
12. Select the images to view by: selecting boxes or clicking Image ID

13. Save Image views under File>Save Image views
14. Select Ruler Tool (F4) from tool bar
  - a. Click and drag to create measurement
  - b. Repeat as appropriate
15. Select Annotations from tool bar
  - a. Rename 'layer' as desired measurement (i.e. endometrial thickness or gland penetration)
  - b. Repeat as needed
16. To save click icon for Export grid to Excel spreadsheet
17. As a result the below measurements were collected and/or calculated
  - a. Gland Penetration (um)
  - b. Endometrial Thickness (um)
  - c. Ratio of gland penetration to endometrial thickness (%)

## **Appendix E.**

### **VisioPharm® image analysis and stereology software**

Turning Images into Knowledge

#### ***Materials***

1. Previously scanned slides using Aperio®

**Aim:** Histomorphology; Gland Duct Frequency, Area, Perimeter, Total Gland Duct Area, Total Endometrial Area, and Ratio measurements and calculations

Use VisioPharm® image analysis software to identify glandular epithelium, determine regions of interest and quantify endometrial gland histomorphology using customized automated program directives (much like CellProfiler™ software). Note: For each new user you must set the default program to open .sis file extension to vishook (in program files under visiopharm), see vetmed campus IIT department if necessary.

**Procedure:** Synching Aperio® and VisioPharm® software

1. Log onto VisioPharm® computer
2. Select VIS
  - a. Enter username and password – you will be prompted twice
3. Open Spectrum via Internet Explorer (do not use Google Chrome)
  - a. Select digital images
  - b. Open images by selecting View Images
    - i. Images will automatically open using Aperio® ImageScope, close this program and click over to opened VisioPharm® window

- c. Dialogue box ‘Automated Save’ will open
4. Rename image slides in the bottom explorer page to reflect animal, treatment etc.

*Procedure:* Use of VisioPharm® software to identify and classify endometrial gland ducts in bovine endometrium.

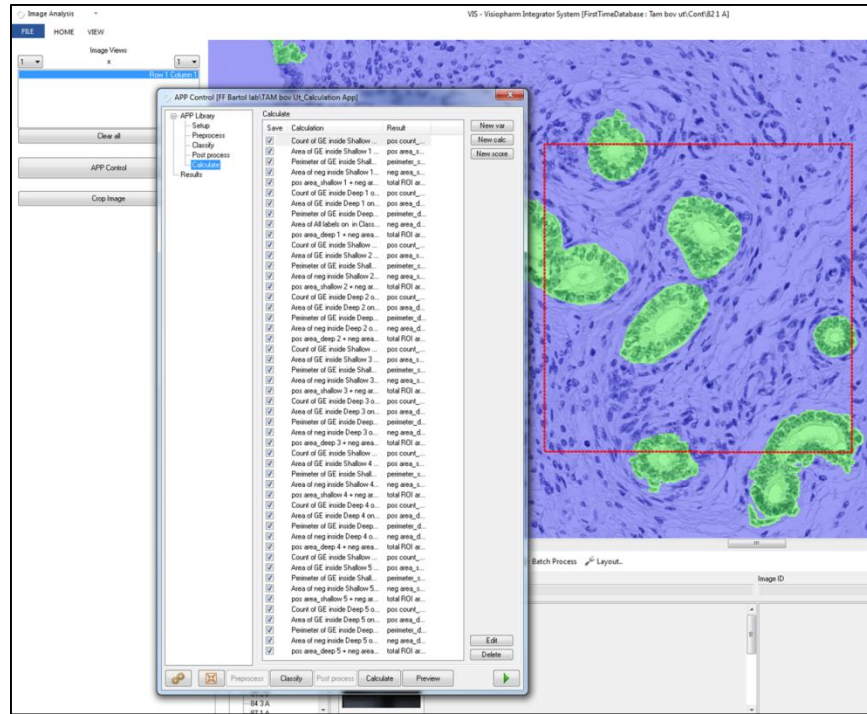
1. Load TAM bov Ut\_Classify App
  - a. Setup: Adjust magnification to 20X
  - b. Preprocess: Identify regions of interest (ROI)
    - i. Under ‘View’ click show tool bar
    - ii. Select the ROI tab on the tool bar
      1. Select the draw option and choose the shape desired (square)
      2. Click to start drawing and outline area of interest
      3. Double click to set the ROI
        - a. To delete select the red ‘X’ in the draw portion of the ROI tab and click the ROI to be deleted
      4. To draw a new ROI you will have to re-select the shape tool
      5. To name, double click on the ROI listed
      6. Change ROI to have different fields
    - c. Classify: Use Bayesian methods and Stored parameters to base classifications on
    - d. Post process: Adjust identified areas in Preprocess
      - i. Modules can be selected to modify identified areas for batch processing
        1. Modules used include:
          - a. Dilate; increased identified GE by 4.00 pixels
          - b. Change Small; Identified GE smaller than 100um2 replace with negative (or designate as endometrium)

- c. Fill Holes; any space found surrounded by identified GE should be filled and designated GE
  - e. Calculate: no calculations were made at this time
2. Batch Run TAM bov Ut\_Classify App
    - a. Result: 5 shallow and deep (total of 10) ROI were defined for each bovine endometrial cross section, endometrium was classified as positive (GE) or negative (background stroma)
  3. Review all slides
    - a. Manual adjustments were made within ROI for identified/classified GE

*Procedure:* Use of VisioPharm software to quantify endometrial gland ducts in bovine endometrium.

1. Load TAM bov Ut\_Calculation App
  - a. Steps for Setup, Preprocess, Classify, Post process were left blank
  - b. Previously processed images as a result of TAM bov Ut\_Classify App were loaded for analysis
  - c. Calculate: Modules were customized to collect measurements of individual GE ducts and total GE ducts within each ROI
    - i. Single GE duct measurements
      1. Perimeter
      2. Square area
    - ii. Total GE ducts within each ROI
      1. Total number of gland ducts per zone
      2. Mean number of gland ducts per zone
      3. Mean gland duct perimeter
      4. Mean gland duct area

5. Total endometrial area (void; zones are fixed at 250umX250um)
6. Gland duct density (ducts/unit endometrium)
7. Gland duct area (% of total endometrial area)
8. See Image below:



2. Batch Run TAM bov Ut\_Calculation App
  - a. Result: Above measurements collected and calculated for 5 shallow and deep (total of 10) ROI in each bovine endometrial cross section
3. Select Excel view at bottom of workspace
  - a. Select icon to Export data to Microsoft Office Excel

## **References**

1. Atkinson BA, King GJ, Amoroso EC. Development of the caruncular and intercaruncular regions in the bovine endometrium. *Biology of Reproduction* 1984; 30:763-774.
2. Bartol FF, Wiley AA, Floyd JG, Ott TL, Bazer FW, Gray CA, Spencer TE. Uterine differentiation as a foundation for subsequent fertility. *J Reprod Fertil Suppl* 1999; 54:287-302.
3. Bartol FF, Johnson LL, Floyd JG, Wiley AA, Spencer TE, Buxton DF, Coleman DA. Neonatal exposure to progesterone and estradiol alters uterine morphology and luminal protein content in adult beef heifers. *Theriogenology* 1995; 43:835-844.
4. Hancock RF, Deutscher GH, Nielsen MK, Colburn DJ. Effects of Synovex C implants on growth rate, pelvic area, reproduction, and calving performance of replacement heifers. *J Anim Sci* 1994; 72:292-299.
5. Gray CA, Bazer FW, Spencer TE. Effects of neonatal progestin exposure on female reproductive tract structure and function in the adult ewe. *Biol Reprod* 2001; 64:797-804.
6. Carpenter KD, Gray CA, Bryan TM, Welsh TH, Jr., Spencer TE. Estrogen and antiestrogen effects on neonatal ovine uterine development. *Biol Reprod* 2003; 69:708-717.
7. Masters RA, Crean BD, Yan W, Moss AG, Ryan PL, Wiley AA, Bagnell CA, Bartol FF. Neonatal porcine endometrial development and epithelial proliferation affected by age and exposure to estrogen and relaxin. *Domest Anim Endocrinol* 2007; 33:335-346.

8. Bartol FF, Wiley AA, Spencer TE, Vallet JL, Christenson RK. Early uterine development in pigs. *J Reprod Fertil Suppl* 1993; 48:99-116.
9. Bagnell CA, Yan W, Wiley AA, Bartol FF. Effects of relaxin on neonatal porcine uterine growth and development. *Ann N Y Acad Sci* 2005; 1041:248-255.
10. Bartol FF, Wiley AA, Coleman DA, Wolfe DF, Riddell MG. Ovine uterine morphogenesis: effects of age and progestin administration and withdrawal on neonatal endometrial development and DNA synthesis. *J Anim Sci* 1988; 66:3000-3009.
11. Allison Gray C, Bartol FF, Taylor KM, Wiley AA, Ramsey WS, Ott TL, Bazer FW, Spencer TE. Ovine uterine gland knock-out model: effects of gland ablation on the estrous cycle. *Biol Reprod* 2000; 62:448-456.
12. Bartol FF, Wiley AA, Bagnell CA. Uterine development and endometrial programming. *Soc Reprod Fertil Suppl* 2006; 62:113-130.
13. Wiley AA, Bartol FF, Barron DH. Histogenesis of the ovine uterus. *J Anim Sci* 1987; 64:1262-1269.
14. Hayashi K, Carpenter KD, Spencer TE. Neonatal estrogen exposure disrupts uterine development in the postnatal sheep. *Endocrinology* 2004; 145:3247-3257.
15. Carpenter KD, Gray CA, Noel S, Gertler A, Bazer FW, Spencer TE. Prolactin regulation of neonatal ovine uterine gland morphogenesis. *Endocrinology* 2003; 144:110-120.
16. Walsh SW, Williams EJ, Evans AC. A review of the causes of poor fertility in high milk producing dairy cows. *Anim Reprod Sci* 2011; 123:127-138.
17. Senger PL. Pathways to Pregnancy and Parturition. Redmond, OR: Current Conceptions, Inc.; 2012.

18. Carpenter KD, Hayashi K, Spencer TE. Ovarian regulation of endometrial gland morphogenesis and activin-follistatin system in the neonatal ovine uterus. *Biol Reprod* 2003; 69:851-860.
19. Taylor KM, Gray CA, Joyce MM, Stewart MD, Bazer FW, Spencer TE. Neonatal ovine uterine development involves alterations in expression of receptors for estrogen, progesterone, and prolactin. *Biol Reprod* 2000; 63:1192-1204.
20. Taylor KM, Chen C, Gray CA, Bazer FW, Spencer TE. Expression of Messenger Ribonucleic Acids for Fibroblast Growth Factors 7 and 10, Hepatocyte Growth Factor, and Insulin-Like Growth Factors and Their Receptors in the Neonatal Ovine Uterus. 2001.
21. Gray CA, Taylor KM, Bazer FW, Spencer TE. Mechanisms regulating norgestomet inhibition of endometrial gland morphogenesis in the neonatal ovine uterus. *Mol Reprod Dev* 2000; 57:67-78.
22. Chen C, Spencer TE, Bazer FW. Expression of Hepatocyte Growth Factor and Its Receptor c-metin the Ovine Uterus. 2000.
23. Chen C, Spencer TE, Bazer FW. Fibroblast Growth Factor-10: A Stromal Mediator of Epithelial Functionin the Ovine Uterus. 2000.
24. Tarleton BJ, Wiley AA, Spencer TE, Moss AG, Bartol FF. Ovary-independent estrogen receptor expression in neonatal porcine endometrium. *Biol Reprod* 1998; 58:1009-1019.
25. Tarleton BJ, Wiley AA, Bartol FF. Endometrial development and adenogenesis in the neonatal pig: effects of estradiol valerate and the antiestrogen ICI 182,780. *Biol Reprod* 1999; 61:253-263.
26. Tarleton BJ, Wiley AA, Bartol FF. Neonatal estradiol exposure alters uterine morphology and endometrial transcriptional activity in prepubertal gilts. *Domest Anim Endocrinol* 2001; 21:111-125.

27. Spencer TE, Wiley AA, Bartol FF. Neonatal age and period of estrogen exposure affect porcine uterine growth, morphogenesis, and protein synthesis. *Biol Reprod* 1993; 48:741-751.
28. Spencer TE, Bartol FF, Wiley AA, Coleman DA, Wolfe DF. Neonatal porcine endometrial development involves coordinated changes in DNA synthesis, glycosaminoglycan distribution, and 3H-glucosamine labeling. *Biol Reprod* 1993; 48:729-740.
29. Cohen RDH, Nicholson HH, Janzen ED. EFFECT OF REPEATED IMPLANTATION WITH ZERANOL FROM BIRTH OR WEANING ON GROWTH AND REPRODUCTION IN BEEF HEIFERS. *Canadian Journal of Animal Science* 1987; 67:37-42.
30. King BD, Kirkwood RN, Cohen RDH, Bo GA, Lulai C, Mapleton RJ. Effect of zeranol implants on age at onset of puberty, fertility and embryo fetal mortality in beef heifers. <http://dx.doi.org/10.4141/cjas95-033> 1995.
31. Moran C, Prendiville DJ, Quirke JF, Roche JF. Effects of oestradiol, zeranol or trenbolone acetate implants on puberty, reproduction and fertility in heifers. 1990.
32. Gray CA, Taylor KM, Ramsey WS, Hill JR, Bazer FW, Bartol FF, Spencer TE. Endometrial glands are required for preimplantation conceptus elongation and survival. *Biol Reprod* 2001; 64:1608-1613.
33. Gray CA, Burghardt RC, Johnson GA, Bazer FW, Spencer TE. Evidence that absence of endometrial gland secretions in uterine gland knockout ewes compromises conceptus survival and elongation. *Reproduction* 2002; 124:289-300.
34. Walker CL. Epigenomic reprogramming of the developing reproductive tract and disease susceptibility in adulthood. *Birth Defects Res A Clin Mol Teratol* 2011; 91:666-671.
35. Cooke PS, Buchanan DL, Lubahn DB, Cunha GR. Mechanism of Estrogen Action: Lessons from the Estrogen Receptor- $\alpha$  Knockout Mouse. 1998.

36. Kurita T, Lee K-j, Cooke PS, Taylor JA, Lubahn DB, Cunha GR. Paracrine Regulation of Epithelial Progesterone Receptor by Estradiol in the Mouse Female Reproductive Tract. 2000.
37. Kurita T, Lee K-j, Saunders PTK, Cooke PS, Taylor JA, Lubahn DB, Zhao C, Mäkelä S, Gustafsson J-Å, Dahiya R, Cunha GR. Regulation of Progesterone Receptors and Decidualization in Uterine Stroma of the Estrogen Receptor- $\alpha$  Knockout Mouse. 2001.
38. Cooke PS, Ekman GC, Kaur J, Davila J, Bagchi IC, Clark SG, Dziuk PJ, Hayashi K, Bartol FF. Brief exposure to progesterone during a critical neonatal window prevents uterine. Biol Reprod 2012; 86:63.
39. Sato T, Wang G, Hardy MP, Kurita T, Cunha GR, Cooke PS. Role of Systemic and Local IGF-I in the Effects of Estrogen on Growth and Epithelial Proliferation of Mouse Uterus. 2013.
40. Lubahn DB, Moyer JS, Golding TS, Couse JF, Korach KS, Smithies O. Alteration of reproductive function but not prenatal sexual development after insertional disruption of the mouse estrogen receptor gene. 1993.
41. Gartner L, Hiatt J. Color Textbook of Histology. W.B. Saunders Company; 2007.
42. Spencer TE, Dunlap KA, Filant J. Comparative developmental biology of the uterus: insights into mechanisms and developmental disruption. Mol Cell Endocrinol 2012; 354:34-53.
43. Cunha GR. The dual origin of vaginal epithelium. American Journal of Anatomy 1975; 143:387-392.
44. Kobayashi A, Behringer RR. Developmental genetics of the female reproductive tract in mammals. Nat Rev Genet 2003; 4:969-980.

45. Kurita T. Normal and abnormal epithelial differentiation in the female reproductive tract. *Differentiation* 2011; 82:117-126.
46. Masse J, Watrin T, Laurent A, Deschamps S, Guerrier D, Pellerin I. The developing female genital tract: from genetics to epigenetics. *Int J Dev Biol* 2009; 53:411-424.
47. Orvis GD, Behringer RR. Cellular mechanisms of Mullerian duct formation in the mouse. *Dev Biol* 2007; 306:493-504.
48. Carroll TJ, Park JS, Hayashi S, Majumdar A, McMahon AP. Wnt9b plays a central role in the regulation of mesenchymal to epithelial transitions underlying organogenesis of the mammalian urogenital system. *Dev Cell* 2005; 9:283-292.
49. Capel B. The battle of the sexes. *Mech Dev* 2000; 92:89-103.
50. DeFalco T, Capel B. Gonad morphogenesis in vertebrates: divergent means to a convergent end. *Annu Rev Cell Dev Biol* 2009; 25:457-482.
51. Swain A L-BR. Mammalian sex determination: a molecular drama. *Genes Dev*. 1999; 13:755-767.
52. Jordan BK, Vilain E. Sry and the genetics of sex determination. *Adv Exp Med Biol* 2002; 511:1-13; discussion 13-14.
53. Nef S, Parada LF. Hormones in male sexual development. *Genes Dev* 2000; 14:3075-3086.
54. W. MH. Vertebrate Fetal Membranes: Comparative Ontogeny and Morphology; Evolution; Phylogenetic Significance; Basic Functions; Research Opportunities. Rutgers University Press; 1987.
55. Spencer TE, Hayashi K, Hu J, Carpenter KD. Comparative developmental biology of the mammalian uterus. *Curr Top Dev Biol* 2005; 68:85-122.

56. Gray CA, Bartol FF, Tarleton BJ, Wiley AA, Johnson GA, Bazer FW, Spencer TE. Developmental biology of uterine glands. *Biol Reprod* 2001; 65:1311-1323.
57. Bartol FF, Wiley AA, Bagnell CA. Epigenetic programming of porcine endometrial function and the lactocrine hypothesis. *Reprod Domest Anim* 2008; 43 Suppl 2:273-279.
58. Bartol FF, Wiley AA, Bagnell CA. Relaxin and maternal lactocrine programming of neonatal uterine development. *Ann N Y Acad Sci* 2009; 1160:158-163.
59. Crain DA, Janssen SJ, Edwards TM, Heindel J, Ho SM, Hunt P, Iguchi T, Juul A, McLachlan JA, Schwartz J, Skakkebaek N, Soto AM, et al. Female reproductive disorders: the roles of endocrine-disrupting compounds and developmental timing. *Fertil Steril* 2008; 90:911-940.
60. Mericskay M, Kitajewski J, Sassoon D. Wnt5a is required for proper epithelial-mesenchymal interactions in the uterus. 2004.
61. Sassoon D. Wnt genes and endocrine disruption of the female reproductive tract: a genetic approach. *Mol Cell Endocrinol* 1999; 158:1-5.
62. Brody JR, Department of Anatomy and the Center for Reproductive Endocrinology UoC, San Francisco, California 94143, Cunha GR, Department of Anatomy and the Center for Reproductive Endocrinology UoC, San Francisco, California 94143, Cancer Research Laboratory UoC, Berkeley, California 94720. Histologic, morphometric, and immunocytochemical analysis of myometrial development in rats and mice: I. Normal development. *American Journal of Anatomy* 2015; 186:1-20.
63. de Witt F. An historical study on theories of the placenta to 1900. *Journal of the History of Medicine and Allied Sciences* 1959; 14:360-374.
64. Needham J. *A History of Embryology*. In. London: Cambridge University Press; 1959.

65. Cooke PS, Spencer TE, Bartol FF, Hayashi K. Uterine glands: development, function and experimental model systems. *Mol Hum Reprod* 2013.
66. M. SP, J. FMW. Mesenchymal influences on epithelial differentiation in developing systems. 1988.
67. Kurita T, Cooke PS, Cunha GR. Epithelial-stromal tissue interaction in paramesonephric (Mullerian) epithelial differentiation. *Dev Biol* 2001; 240:194-211.
68. Cunha GR. Stromal induction and specification of morphogenesis and cytodifferentiation of the epithelia of the mullerian ducts and urogenital sinus during development of the uterus and vagina in mice. *Journal of Experimental Zoology* 1976; 196:361-369.
69. Li Q, Kannan A, DeMayo FJ, Lydon JP, Cooke PS, Yamagishi H, Srivastava D, Bagchi MK, Bagchi IC. The Antiproliferative Action of Progesterone in Uterine Epithelium Is Mediated by Hand2. 2011.
70. Satterfield MC, Hayashi K, Song G, Black SG, Bazer FW, Spencer TE. Progesterone regulates FGF10, MET, IGFBP1, and IGFBP3 in the endometrium of the ovine uterus. *Biol Reprod* 2008; 79:1226-1236.
71. Bartol FF, Wiley AA, Goodlett DR. Ovine uterine morphogenesis: histochemical aspects of endometrial development in the fetus and neonate. *J Anim Sci* 1988; 66:1303-1313.
72. Zhou H-E, Zhang X, Nothnick WB. Disruption of the TIMP-1 Gene Product Is Associated with Accelerated Endometrial Gland Formation During Early Postnatal Uterine Development. 2004.
73. Hu J, Zhang X, Nothnick WB, Spencer TE. Matrix Metalloproteinases and Their Tissue Inhibitors in the Developing Neonatal Mouse Uterus. 2004.

74. Lenhart JA, Ryan PL, Ohleth KM, Palmer SS, Bagnell CA. Relaxin Increases Secretion of Matrix Metalloproteinase-2 and Matrix Metalloproteinase-9 during Uterine and Cervical Growth and Remodeling in the Pig. 2013.
75. Hayashi K, Yoshioka S, Reardon SN, Edmund B. Rucker I, Spencer TE, DeMayo FJ, Lydon JP, II JAM. WNTs in the Neonatal Mouse Uterus: Potential Regulation of Endometrial Gland Development. 2011.
76. Hayashi K, Spencer TE. WNT Pathways in the Neonatal Ovine Uterus: Potential Specification of Endometrial Gland Morphogenesis by SFRP2. 2006.
77. Daftary GS, Taylor HS. Endocrine Regulation of HOX Genes.  
<http://dx.doi.org/10.1210/er.2005-0018> 2006.
78. Teo R, Mohrlen F, Plickert G, Muller W, Frank U. An evolutionary conserved role of Wnt signaling in stem cell fate decision. *Developmental Biology* 2006; 289:91–99.
79. Lee H-Y, Kléber M, Hari L, Brault V, Suter U, Taketo MM, Kemler R, Sommer L. Instructive Role of Wnt/β-Catenin in Sensory Fate Specification in Neural Crest Stem Cells. *Science* 2004; 303:1020-1023.
80. Moon RT, Brown JD, Torres M. WNTs modulate cell fate and behavior during vertebrate development. *Trends in Genetics* 1997; 13:157-162.
81. Benson GV, Lim H, Paria BC, Satokata I, Dey SK, Maas RL. Mechanisms of reduced fertility in Hoxa-10 mutant mice: uterine homeosis and loss of maternal Hoxa-10 expression. *Development* 1996; 122:2687-2696.
82. Gendron RL, Paradis H, Hsieh-Li HM, Lee DW, Potter SS, Markoff E. Abnormal uterine stromal and glandular function associated with maternal reproductive defects in Hoxa-11 null mice. *Biology of Reproduction* 1997; 56:1097-1105.

83. Miller C, Sasoon DA. Wnt-7a maintains appropriate uterine patterning during the development of the mouse female reproductive tract. *Development* 1998; 125:3201-3211.
84. Matsumoto K, Nakamura T. Emerging Multipotent Aspects of Hepatocyte Growth Factor. 1996.
85. Weidner KM, Hartmann G, Sachs M, Birchmeier W. Properties and Functions of Scatter Factor/Hepatocyte Growth Factor and Its Receptor c-Met.  
<http://dx.doi.org/10.1165/ajrcmb/8.3.229> 1993.
86. Beer H, Florence C, Dammeier J, McGuire L, Werner S, Duan D. Mouse fibroblast growth factor 10: cDNA cloning, protein characterization, and regulation of... - Abstract - Europe PubMed Central. *Oncogene* 1997; 15:2211-2218.
87. Bellusci S, Grindley J, Emoto H, Itoh N, Hogan BL. Fibroblast growth factor 10 (FGF10) and branching morphogenesis in the embryonic mouse lung. 1997.
88. Dailey L, Ambrosetti D, Mansukhani A, Basilico C. Mechanisms underlying differential responses to FGF signaling. 2005; 16:233–247.
89. Sonnenberg E, Meyer D, Weidner KM, Birchmeier C. Scatter factor/hepatocyte growth factor and its receptor, the c-met tyrosine kinase, can mediate a signal exchange between mesenchyme and epithelia during mouse development. 1993.
90. Klotz DM, Hewitt SC, Ciana P, Raviglioni M, Lindzey JK, Foley J, Maggi A, DiAugustine RP, Korach KS. Requirement of Estrogen Receptor- $\alpha$  in Insulin-like Growth Factor-1 (IGF-1)-induced Uterine Responses and in Vivo Evidence for IGF-1/Estrogen Receptor Cross-talk. 2002.
91. Jost A, Vigier B, Prepin J, Perchellet JP. Studies on sex differentiation in mammals. *Recent Progress in Hormone Research* 1973; 29:1-41.

92. Clark JH, Gorski J. Ontogeny of the Estrogen Receptor during Early Uterine Development. 1970.
93. Fisher CR, Graves KH, Parlow AF, Simpson ER. Characterization of mice deficient in aromatase (ArKO) because of targeted disruption of the cyp19 gene. 1998.
94. Maggiolini M, Picard D. The unfolding stories of GPR30, a new membrane-bound estrogen receptor. *Journal of Endocrinology* 2010; 204:105-114.
95. Dahlman-Wright K, Cavailles V, Fuqua SA, Jordan VC, Katzenellenbogen JA, Korach KS, Maggi A, Muramatsu M, Parker MG, Gustafsson J-Å. International Union of Pharmacology. LXIV. Estrogen Receptors. *Pharmacological Reviews* 2006; 58:773-781.
96. Jensen EV, Jordan VC. The Estrogen Receptor: A Model for Molecular Medicine. *Clinical Cancer Research* 2003.
97. Couse JF, Hewitt SC, Bunch DO, Sar M, Walker VR, Davis BJ, Korach KS. Postnatal Sex Reversal of the Ovaries in Mice Lacking Estrogen Receptors  $\alpha$  and  $\beta$ . *Science* 1999; 286:2328-2331.
98. Krege JH, Hodgin JB, Couse JF, Enmark E, Warner M, Mahler JF, Sar M, Korach KS, Gustafsson J-Å, Smithies O. Generation and reproductive phenotypes of mice lacking estrogen receptor  $\beta$ . *PNAS* 1998; 95:15677-15682.
99. GRECO TL, FURLOW JD, DUELLO TM, GORSKI J. Immunodetection of Estrogen Receptors in Fetal and Neonatal Female Mouse Reproductive Tracts\*. *Endocrinology* 2013; 129.
100. Cooke PS, Buchanan DL, Young P, Setiawan T, Brody J, Korach KS, Taylor J, Lubahn DB, Cunha GR. Stromal estrogen receptors mediate mitogenic effects of estradiol on uterine epithelium. 1997.

101. Cooke PS, Ekman GC, Kaur J, Davila J, Bagchi IC, Clark SG, Dziuk PJ, Hayashi K, Bartol FF. Brief Exposure to Progesterone During a Critical Neonatal Window Prevents Uterine Gland Formation in Mice. *Biology of Reproduction* 2012; 86.
102. Korach KS, Horigome T, Tomooka Y, Yamashita S, Newbold RR, McLachlan JA. Immunodetection of estrogen receptor in epithelial and stromal tissues of neonatal mouse uterus. 1988.
103. Branham WS, Sheehan DM, Zehr DR, Ridlon E, Nelson CJ. The postnatal ontogeny of rat uterine glands and age-related effects of 17 beta-estradiol. *Endocrinology* 1985; 117:2229-2237.
104. BASSETT JM, OXBORROW TJ, SMITH ID, THORBURN GD. THE CONCENTRATION OF PROGESTERONE IN THE PERIPHERAL PLASMA OF THE PREGNANT EWE. *Journal of Endocrinology* 1969; 45:449-457.
105. Chew BP, Erb RE, Fessler J, Callahan CJ, Malven PV. Effects of Ovariectomy during Pregnancy and of Prematurely Induced Parturition on Progesterone, Estrogens, and Calving Traits1. *Journal of Dairy Science* 1979; 62:557–566.
106. RICKETTS AP, FLINT APF. ONSET OF SYNTHESIS OF PROGESTERONE BY OVINE PLACENTA. *Journal of Endocrinology* 1980; 86:337-347.
107. Spencer TE, Johnson GA, Burghardt RC, Bazer FW. Progesterone and placental hormone actions on the uterus: insights from domestic animals. *Biol Reprod* 2004; 71:2-10.
108. Filant J, Zhou H, Spencer TE. Progesterone inhibits uterine gland development in the neonatal mouse uterus. *Biol Reprod* 2012; 86:146, 141-149.
109. Kurita T, Young P, Brody JR, Lydon JP, O'Malley BW, Cunha GR. Stromal Progesterone Receptors Mediate the Inhibitory Effects of Progesterone on Estrogen-Induced Uterine

- Epithelial Cell Deoxyribonucleic Acid Synthesis1.  
<http://dx.doi.org/10.1210/endo.139.11.6317> 1998.
110. Stormshak F, Bishop CV. BOARD-INVITED REVIEW: Estrogen and progesterone signaling: Genomic and nongenomic actions in domestic ruminants. 2008.
111. Cooke P, Borsdorff D, Ekman G, Doty K, Clark S, Dziuk P, Bartol F. Uterine gland development begins postnatally and is accompanied by estrogen and progesterone receptor expression in the dog. *Theriogenology* 2012; 78:1787–1795.
112. Lydon JP, DeMayo FJ, Funk CR, Mani SK, Hughes AR, Montgomery CA, Shyamala G, Conneely OM, O'Malley BW. Mice lacking progesterone receptor exhibit pleiotropic reproductive abnormalities. *Genes and Development* 1995; 9:2266-2278.
113. Franco HL, Rubel CA, Large MJ, Wetendorf M, Fernandez-Valdivia R, Jeong J-W, Spencer TE, Behringer RR, Lydon JP, DeMayo FJ. Epithelial progesterone receptor exhibits pleiotropic roles in uterine development and function. *The Journal of the Federation of American Societies for Experimental Biology* 2011; 26:1218-.
114. Li Q, Kannan A, DeMayo FJ, Lydon JP, Cooke PS, Yamagishi H, Srivastava D, Bagchi MK, Bagchi IC. The Antiproliferative Action of Progesterone in Uterine Epithelium Is Mediated by Hand2. *Science* 2011; 331:912-916.
115. Bartol FF. Uterus, Non Human. In: *Encyclopedia of Reproduction*, vol. 4: Academic Press.; 1999: 950-960.
116. Diskin M, Teagasc APRC, Mellows Campus, Athenry, Co. Galway, Ireland, Morris D, Teagasc APRC, Mellows Campus, Athenry, Co. Galway, Ireland. Embryonic and Early Foetal Losses in Cattle and Other Ruminants. *Reproduction in Domestic Animals* 2014; 43:260-267.

117. Thatcher WW, Bartol FF, Kncikerbocker JJ, Curl JS, Wolfenson D. Maternal Recognition of Pregnancy in Cattle1. *Journal of Dairy Science* 1984; 67:2797–2811.
118. Mamo S, Mehta JP, Forde N, McGettigan P, Lonergan P. Conceptus-endometrium crosstalk during maternal recognition of pregnancy in cattle. *Biol Reprod* 2012; 87:6, 1-9.
119. Forde N, Carter F, Spencer TE, Bazer FW, Sandra O, Mansouri-Attia N, Okumu LA, McGettigan PA, Mehta JP, McBride R, O'Gaora P, Roche JF, et al. Conceptus-induced changes in the endometrial transcriptome: how soon does the cow know she is pregnant? *Biol Reprod* 2011; 85:144-156.
120. Forde N, Lonergan P. Transcriptomic analysis of the bovine endometrium: What is required to establish uterine receptivity to implantation in cattle? *J Reprod Dev* 2012; 58:189-195.
121. P. L, N. F. Maternal-embryo interaction leading up to the initiation of implantation of pregnancy in cattle. *Animal* 2013; 8:64-69.
122. Bazer FW. Pregnancy recognition signaling mechanisms in ruminants and pigs. *Journal of Animal Science and Biotechnology* 2013; 4:1-10.
123. Clemente M, de La Fuente J, Fair T, Al Naib A, Gutierrez-Adan A, Roche JF, Rizos D, Lonergan P. Progesterone and conceptus elongation in cattle: a direct effect on the embryo or an indirect effect via the endometrium? *Reproduction* 2009; 138:507-517.
124. Vallet JL, Freking BA. Research on uterine capacity and litter size in swine. In: USDA Agricultural Research Service; 2005.
125. !!! INVALID CITATION !!!

126. Tarleton BJ, Braden TD, Wiley AA, Bartol FF. Estrogen-induced disruption of neonatal porcine uterine development alters adult uterine function. *Biol Reprod* 2003; 68:1387-1393.
127. Nijland MJ, Ford SP, Nathanielsz PW. Prenatal origins of adult disease. *Current Opinion in Obstetrics and Gynecology* 2015; 20:132-138.
128. Nathanielsz PW. Animal Models That Elucidate Basic Principles of the Developmental Origins of Adult Diseases. *ILAR Journal* 2006; 47:73-82.
129. Crews D, McLachlan JA. Epigenetics, evolution, endocrine disruption, health, and disease. *Endocrinology* 2006; 147:S4-10.
130. Bagnell CA, Steinetz BG, Bartol FF. Milk-borne relaxin and the lactocrine hypothesis for maternal programming of neonatal tissues. *Ann N Y Acad Sci* 2009; 1160:152-157.
131. Miller DJ, Wiley AA, Chen JC, Bagnell CA, Bartol FF. Nursing for 48 hours from birth supports porcine uterine gland development and endometrial cell compartment-specific gene expression. *Biol Reprod* 2013; 88:4.
132. Camp ME, Wiley AA, Boulos MB, Rahman KM, Bartol FF, Bagnell CA. Effects of age, nursing, and oral IGF1 supplementation on neonatal porcine cervical development. *Reproduction* 2014; 148:441-451.
133. Rahman KM, Lovich JE, Lam C, Camp ME, Wiley AA, Bartol FF, Bagnell CA. Nursing supports neonatal porcine testicular development. *Domestic Animal Endocrinology* 2014; 48:84-92.
134. Bartol FF, Wiley AA, Miller DJ, Silva AJ, Roberts KE, Davolt ML, Chen JC, Frankshun AL, Camp ME, Rahman KM, Vallet JL, Bagnell CA. Lactation Biology Symposium: lactocrine signaling and developmental programming. *J Anim Sci* 2013; 91:696-705.

135. Stockard CR. Developmental rate and structural expression: An experimental study of twins, "double monsters" and single deformities, and the interaction among embryonic organs during their origin and development. *American Journal of Anatomy* 1921; 28:115-277.
136. Sananès N, Baulieu EE, Le Goascogne C. Treatment of neonatal rats with progesterone alters the capacity of the uterus to form decidiomata. *J Reprod Fertil* 1980; 58:271-273.
137. Mori T, Singtripop T, Kawashima S. Animal model of uterine adenomyosis: Is prolactin a potent inducer of adenomyosis in mice? *American Journal of Obstetrics and Gynecology* 1991; 165:232–234.
138. Ohta Y. Sterility in neonatally androgenized female rats and the decidual cell reaction. *Int Rev Cytol* 1995; 160:1-52.
139. Guillette LJ J, Gunderson M. Alterations in development of reproductive and endocrine systems of wildlife populations exposed to endocrine-disrupting contaminants. 2001.
140. Biswas S, Shapiro CA, Kranz WL, Mader TL, Sheltonm DP, Snow DD, Bartelt-Hunt SL, Tarkalson DD, van Donk SJ, Zhang TC, Ensley S. Current knowledge on the environmental fate, potential impact, and management of growth-promoting steroids used in the US beef cattle industry. 2013.
141. Lesmeister JL, Ellington EF. Effect of steroid implants on sexual behavior of beef calves. *Horm Behav* 1977; 9:276-280.
142. COHEN RDH, NICHOLSON HH, JANZEN ED. EFFECT OF REPEATED IMPLANTATION WITH ZERANOL FROM BIRTH OR WEANING ON GROWTH AND REPRODUCTION IN BEEF HEIFERS. <http://dx.doi.org/10.4141/cjas87-005> 2011.
143. Zobell DR, Chapman CK, Heaton K, Birkelo C. Beef Cattle Implants. In: University US (ed.), vol. Paper 29: All Archived Publications; 2000: 1-9.

144. Martal J, Chene N, Camous S, Huynh L, Lantier F, Hermier P, L'Haridon R, Charpigny G, Charlier M, Chaouat G. Recent developments and potentialities for reducing embryo mortality in ruminants: the role of... - Abstract - Europe PubMed Central. 1997; 9:355-380.
145. Spencer TE, Stagg AG, Joyce MM, Jenster G, Wood CG, Bazer FW, Wiley AA, Bartol FF. Discovery and characterization of endometrial epithelial messenger ribonucleic acids using the ovine uterine gland knockout model. *Endocrinology* 1999; 140:4070-4080.
146. Farnell YZ, Ing NH. Endometrial effects of selective estrogen receptor modulators (SERMs) on estradiol-responsive gene expression are gene and cell-specific. *J Steroid Biochem Mol Biol* 2003; 84:513-526.
147. Riggs BL, Hartmann LC. Selective estrogen-receptor modulators -- mechanisms of action and application to clinical practice. *N Engl J Med* 2003; 348:618-629.
148. Shang Y, Brown M. Molecular Determinants for the Tissue Specificity of SERMs. 2002.
149. Pickar JH, Mirkin S. Tissue-selective agents: selective estrogen receptor modulators and the tissue-selective estrogen complex. 2010.
150. Jordan VC, Fox Chase Cancer Center CA, Philadelphia, PA 19111-2497, U.S.A. Tamoxifen (ICI46,474) as a targeted therapy to treat and prevent breast cancer. *British Journal of Pharmacology* 2006; 147.
151. Lunan CB, Klopper A. Antioestrogens. A review. *Clin Endocrinol (Oxf)* 1975; 4:551-572.
152. Cole MP, Jones CT, Todd ID. A new anti-oestrogenic agent in late breast cancer. An early clinical appraisal of ICI46474. *Br J Cancer* 1971; 25:270-275.
153. EBCTCG EBCTCG. Tamoxifen for early breast cancer: an overview of the randomised trials. *Lancet* 1998; 351:1451-1467.

154. Fischer WH, Keiwan A, Schmitt E, Stopper H. Increased formation of micronuclei after hormonal stimulation of cell proliferation in human breast cancer cells. *Mutagenesis* 2001; 16:209-212.
155. Fisher B, Costantino JP, Wickerham DL, Redmond CK, Kavanah M, Cronin WM, Vogel V, Robidoux A, Dimitrov N, Atkins J, Daly M, Wieand S, et al. Tamoxifen for prevention of breast cancer: report of the National Surgical Adjuvant Breast and Bowel Project P-1 Study. *J Natl Cancer Inst* 1998; 90:1371-1388.
156. Tee MK, Rogatsky I, Tzagarakis-Foster C, Cvoro A, An J, Christy RJ, Yamamoto KR, Leitman DC. Estradiol and Selective Estrogen Receptor Modulators Differentially Regulate Target Genes with Estrogen Receptors  $\alpha$  and  $\beta$ . 2004.
157. Smith CL, O'Malley BW. Coregulator function: a key to understanding tissue specificity of selective receptor modulators. *Endocr Rev* 2004; 25:45-71.
158. Eltabbakh GH, Mount SL. Tamoxifen and the female reproductive tract. *Expert Opin Pharmacother* 2001; 2:1399-1413.
159. MacGregor JI, Jordan VC. Basic guide to the mechanisms of antiestrogen action. *Pharmacol Rev* 1998; 50:151-196.
160. Daniel Y, Inbar M, Bar-Am A, Peyser MR, Lessing JB. The effects of tamoxifen treatment on the endometrium. *Fertil Steril* 1996; 65:1083-1089.
161. Branham WS, Sheehan DM, Zehr DR, Medlock KL, Nelson CJ, Ridlon E. Inhibition of rat uterine gland genesis by tamoxifen. *Endocrinology* 1985; 117:2238-2248.
162. Stewart CA, Fisher SJ, Wang Y, Stewart MD, Hewitt SC, Rodriguez KF, Korach KS, Behringer RR. Uterine gland formation in mice is a continuous process, requiring the ovary after puberty, but not after parturition. *Biol Reprod* 2011; 85:954-964.

163. Robertson JA, Bhattacharyya S, Ing NH. Tamoxifen up-regulates oestrogen receptor-alpha, c-fos and glyceraldehyde 3-phosphate-dehydrogenase mRNAs in ovine endometrium. *J Steroid Biochem Mol Biol* 1998; 67:285-292.
164. van der Loos CM. Immunohistochemistry is not the same as immunocytochemistry. *Biotech Histochem* 2010; 85:325-326.
165. Robertson D, Savage K, Reis-Filho JS, Isacke CM. Multiple immunofluorescence labelling of formalin-fixed paraffin-embedded (FFPE) tissue. *BMC Cell Biol* 2008; 9:13.
166. Di Cataldo S, Ficarra E, Macii E. Computer-aided techniques for chromogenic immunohistochemistry: status and directions. *Comput Biol Med* 2012; 42:1012-1025.
167. Bordeaux J, Welsh A, Agarwal S, Killiam E, Baquero M, Hanna J, Anagnostou V, Rimm D. Antibody validation. *Biotechniques* 2010; 48:197-209.
168. Ramos-Vara JA. Technical aspects of immunohistochemistry. *Vet Pathol* 2005; 42:405-426.
169. Coons AH, Kaplan MH. Localization of antigen in tissue cells; improvements in a method for the detection of antigen by means of fluorescent antibody. *J Exp Med* 1950; 91:1-13.
170. Hayat MA. Microscopy, Immunohistochemistry, and Antigen Retrieval Methods. 2002.
171. Jaskolski F, Mulle C, Manzoni OJ. An automated method to quantify and visualize colocalized fluorescent signals. *J Neurosci Methods* 2005; 146:42-49.
172. van der Loos CM. A focus on fixation. *Biotech Histochem* 2007; 82:141-154.
173. Werner M, Chott A, Fabiano A, Battifora H. Effect of Formalin Tissue Fixation and Processing on Immunoh... : The American Journal of Surgical Pathology. *American Journal of Surgical Pathology* 2015; 24:1016-1019.
174. Dapson RW. Fixation for the 1990's: a review of needs and accomplishments. *Biotech Histochem* 1993; 68:75-82.

175. Arnold MM, Srivastava S, Fredenburgh J, Stockard CR, Myers RB, Grizzle WE. Effects of Fixation and Tissue Processing on Immunohistochemical Demonstration of Specific Antigens. *Biotechnic and Histochemistry* 1996; 71:224-230.
176. D'Amico F, Skarmoutsou E, Stivala F. State of the art in antigen retrieval for immunohistochemistry. *Journal of Immunological Methods* 2008.
177. Shi SR, Key ME, Kalra KL. Antigen retrieval in formalin-fixed, paraffin-embedded tissues: an enhancement method for immunohistochemical staining based on microwave oven heating of tissue sections. *Journal of Histochemistry and Cytochemistry* 1991; 39:741-748.
178. Yamashita S. Heat-induced antigen retrieval: mechanisms and application to histochemistry. *Prog Histochem Cytochem* 2007; 41:141-200.
179. Shi SR, Cote RJ, Taylor CR. Antigen retrieval immunohistochemistry: past, present, and future. *J Histochem Cytochem* 1997; 45:327-343.
180. Volkin DB, Klibanov AM. Mechanism of thermoinactivation of immobilized glucose isomerase. *Biotechnol Bioeng* 1989; 33:1104-1111.
181. Absolom DR, van Oss CJ. The nature of the antigen-antibody bond and the factors affecting its association and dissociation. *CRC Crit Rev Immunol* 1986; 6:1-46.
182. van der Loos CM, van den Oord JJ, Das PK, Houthoff HJ. Use of commercially available monoclonal antibodies for immunoenzyme double staining. *Histochem J* 1988; 20:409-413.
183. van der Loos CM, Becker AE, van den Oord JJ. Practical suggestions for successful immunoenzyme double-staining experiments. *Histochem J* 1993; 25:1-13.

184. Nakane PK. Simultaneous localization of multiple tissue antigens using the peroxidase-labeled antibody method: a study on pituitary glands of the rat. *J Histochem Cytochem* 1968; 16:557-560.
185. van der Loos CM, Das PK, Houthoff HJ. An immunoenzyme triple-staining method using both polyclonal and monoclonal antibodies from the same species. Application of combined direct, indirect, and avidin-biotin complex (ABC) technique. *J Histochem Cytochem* 1987; 35:1199-1204.
186. Levenson RM, Mansfield JR. Multispectral imaging in biology and medicine: slices of life. *Cytometry A* 2006; 69:748-758.
187. Mansfield JR, Hoyt C, Levenson RM. Visualization of microscopy-based spectral imaging data from multi-label tissue sections. *Curr Protoc Mol Biol* 2008; Chapter 14:Unit 14.19.
188. Farkas DL, Du C, Fisher GW, Lau C, Niu W, Wachman ES, Levenson RM. Non-invasive image acquisition and advanced processing in optical bioimaging. *Comput Med Imaging Graph* 1998; 22:89-102.
189. Levenson RM, Fornari A, Loda M. Multispectral imaging and pathology: seeing and doing more. *Expert Opin Med Diagn* 2008; 2:1067-1081.
190. Brownlee J. Antigen-Antibody Interaction. In. Melbourne, Australia: Complex Intelligent Systems Laboratory, Centre for Information Technology Research, Faculty of Information and Communication Technologies, Swinburne University of Technology; 2007.
191. Walker RA. Quantification of immunohistochemistry--issues concerning methods, utility and semiquantitative assessment I. *Histopathology* 2006; 49:406-410.
192. Taylor CR, Levenson RM. Quantification of immunohistochemistry--issues concerning methods, utility and semiquantitative assessment II. *Histopathology* 2006; 49:411-424.

193. Garini Y, Young IT, McNamara G. Spectral imaging: principles and applications. *Cytometry A* 2006; 69:735-747.
194. Multispectral Imaging Systems: Product Note. In. Waltham, MA: PerkinElmer, Inc.; 2013.
195. Dickinson ME, Simbuerger E, Zimmermann B, Waters CW, Fraser SE. Multiphoton excitation spectra in biological samples. *J Biomed Opt* 2003; 8:329-338.
196. Suan D, Hampton HR, Tomura M, Kanagawa O, Chtanova T, Phan TG. Optimizing fluorescence excitation and detection for intravital two-photon microscopy. *Methods Cell Biol* 2013; 113:311-323.
197. Zipfel WR, Williams RM, Webb WW. Nonlinear magic: multiphoton microscopy in the biosciences. *Nat Biotechnol* 2003; 21:1369-1377.
198. Zimmermann T. Spectral imaging and linear unmixing in light microscopy. *Adv Biochem Eng Biotechnol* 2005; 95:245-265.
199. Levenson RM, Lynch DT, Kobayashi H, Backer JM, Backer MV. Multiplexing with multispectral imaging: from mice to microscopy. *IJarl j* 2008; 49:78-88.
200. Van der Loos CM, Das PK, Van den Oord JJ, Houthoff HJ. Multiple immunoenzyme staining techniques. Use of fluoresceinated, biotinylated and unlabelled monoclonal antibodies. *J Immunol Methods* 1989; 117:45-52.
201. Ljosa V, Carpenter AE. Introduction to the quantitative analysis of two-dimensional fluorescence. *PLoS Comput Biol* 2009; 5:e1000603.
202. Riber-Hansen R, Vainer B, Steiniche T. Digital image analysis: a review of reproducibility, stability and basic requirements for optimal results. *Apmis* 2012; 120:276-289.
203. Ghaznavi F, Evans A, Madabhushi A, Feldman M. Digital imaging in pathology: whole-slide imaging and beyond. *Annu Rev Pathol* 2013; 8:331-359.

204. Jones TR, Kang IH, Wheeler DB, Lindquist RA, Papallo A, Sabatini DM, Golland P, Carpenter AE. CellProfiler Analyst: data exploration and analysis software for complex image-based screens. In: BMC Bioinformatics, vol. 9: BioMed Central Ltd; 2012: 482.
205. Spencer TE, Gray CA. Sheep uterine gland knockout (UGKO) model. Methods Mol Med 2006; 121:85-94.
206. Capuco AV, Ellis S, Wood DL, Akers RM, Garrett W. Postnatal mammary ductal growth: three-dimensional imaging of cell proliferation, effects of estrogen treatment, and expression of steroid receptors in prepubertal calves. Tissue Cell 2002; 34:143-154.
207. Burry RW. Controls for immunocytochemistry: an update. J Histochem Cytochem 2011; 59:6-12.
208. Roberts KE, Davolt ML, Miller DJ, Wiley AA, Bartol FF. Identification of Endometrial Cell Compartment-specific Expression of Estrogen Receptor-alpha Using Multispectral Imaging and Digital Image Processing. In, vol. 2. Auburn University: Auburn University Journal of Undergraduate Scholarship; 2013: 3-7.
209. SAS. SAS/Stat User's Guide. In, vol. 8. Cary, NC: Statistical Analysis System Institute; 1999.
210. Carpenter AE, Jones TR. CellProfiler Analyst data exploration software. In: Broad Institue.
211. Carpenter AE, Jones TR. CellProfiler cell image analysis software. In: Broad Institute: Imaging Platform.
212. McCluggage WG, Sumathi VP, Maxwell P. CD10 is a sensitive and diagnostically useful immunohistochemical marker of normal endometrial stroma and of endometrial stromal neoplasms. Histopathology 2001; 39:273-278.

213. Muskhelishvili L, Latendresse JR, Kodell RL, Henderson EB. Evaluation of Cell Proliferation in Rat Tissues with BrdU, PCNA, Ki-67(MIB-5) Immunohistochemistry and In Situ Hybridization for Histone mRNA. *Journal of Histochemistry and Cytochemistry* 2003; 51:1681-1688.
214. Kurita T, Wang YZ, Donjacour AA, Zhao C, Lydon JP, O'Malley BW, Isaacs JT, Dahiya R, Cunha GR. Paracrine regulation of apoptosis by steroid hormones in the male and female reproductive system. *Cell Death Differ* 2001; 8:192-200.
215. Chen JC, Wiley AA, Ho TY, Frankshun AL, Hord KM, Bartol FF, Bagnell CA. Transient estrogen exposure from birth affects uterine expression of developmental markers in neonatal gilts with lasting consequences in pregnant adults. *Reproduction* 2010; 139:623-630.
216. Davolt ML, Wilborn RR, Wiley AA, Ellis SE, Bartol FF. Establishment, Validation, and Application of Multispectral Imaging Technology to Studies of Bovine Reproductive Tract Development. *Biology of Reproduction* 2012:322.
217. KOLIGIAN KB, STORMSHAK F. Progesterone Inhibition of Estrogen Receptor Replenishment in Ovine Endometrium. 1977.

